CRANFIELD UNIVERSITY

ALIYU MUSA ALIYU

VERTICAL ANNULAR GAS–LIQUID TWO-PHASE FLOW IN LARGE DIAMETER PIPES

OIL AND GAS ENGINEERING CENTRE

PhD Thesis
Academic Year: 2012 - 2015

Supervisors: Dr Liyun Lao & Prof Hoi Yeung
September, 2015

CRANFIELD UNIVERSITY

OIL AND GAS ENGINEERING CENTRE

PhD Thesis

Academic Year 2012 - 2015

ALIYU MUSA ALIYU

Vertical Annular Gas–Liquid Two-phase Flow in Large diameter Pipes

Supervisors: Dr Liyun Lao & Prof Hoi Yeung

September, 2015

ABSTRACT

Gas–liquid annular two phase flow in pipes is important in the oil and gas, nuclear and the process industries. It has been identified as one of the most frequently encountered flow regimes and many models (empirical and theoretical) for the film flow and droplet behaviour for example have been developed since the 1950s. However, the behaviour in large pipes (those with diameter greater than 100 mm) has not been fully explored. As a result, the two-phase flow characteristics, data, and models specifically for such pipes are scarce or non-existent such that those from smaller pipes are extrapolated for use in design and operation. Many authors have cautioned against this approach since multiphase pipe flow behaviour is different between small and large pipes. For instance the typical slug flows seem not to occur in vertical upwards flows when the pipe diameter exceeds 100 mm. It is therefore imperative that theoretical models and empirical correlations for such large diameter pipes are specifically developed.

In this thesis, four new empirical correlations have been proposed that exclusively model large diameter annular two-phase flow. They concern interfacial friction factor, entrained droplet fraction in upwards flow; film thickness and interfacial friction factor in downwards flow. In all four cases experimental data obtained from the 101.6 mm diameter Serpent Rig flow loop which consists of both upwards and downwards flowing sections connected by a 180˚ U-bend, was used for model development. In order to screen the data so as to limit to only those in the annular flow region, reconstructed images obtained by a 32 x 32 capacitance wire mesh sensor (WMS) were used to

corroborate visual observations for flow regime identification. In the case of obtaining circumferentially averaged film thickness measurements, conductance probes were used. Comparisons made between these measurements and the predictions of many published models produced unsatisfactory results.

Consequently, physical considerations were used to carefully select groups of dimensionless numbers that capture the features of the flow and nonlinear regression used to find the relationship between them. Statistical analyses showed that the new correlations outperformed the previous ones in predicting the large diameter data with the least mean errors. Therefore, the new correlations can provide better closure relationships in numerical simulators used for the design and operation of two-phase flow systems. This ensures that better predictions of pressure drop/pumping requirements are made and for heat transfer processes, boiling crisis or dryout is prevented.

Keywords:

Adiabatic two-phase flow, entrained droplet fraction, falling films, interfacial friction factor, multiphase flow, pressure gradient.

ACKNOWLEDGEMENTS

First and foremost, I would like to thank the Almighty Allah for the opportunity to start and finish my PhD studies. His abundant mercies and favour are boundless.

Appreciation also goes to my sponsors PTDF Nigeria for the full scholarship awarded to me to come to Cranfield University to pursue a doctorate degree. Without this support, it would have been an impossible endeavour.

Special thanks also go to my supervisors: Dr Liyun Lao and Prof Hoi Yeung. I appreciate the hundreds of hours of their time, going through the finer details of multiphase flow with me, the late nights reading my material, hours in the Oil and Gas Laboratory, and indeed general advice. I can only wish you the best life has to offer because repaying you for the knowledge imparted is just not possible.

I will like to recognise the support my family has offered, my wife and daughter for enduring many days without me while I am studying or in the lab or travelling. My mother, siblings, and extended family back home in Nigeria have been immense too. I am truly blessed indeed.

Mrs Sam Skears cannot go without mention. Her patience with all the varied needs of the many PhD students in the department is exemplary; a big thank you goes to her. Singular thanks also go to Mr Stan Collins in the PSE Lab, together with his team of able technicians over the years.

Lastly, but by no means the least, I extend my thanks to colleagues and fellow students in the Energy Division of Cranfield University for all the great times and insightful conversations. The memories will forever linger in my heart.

PUBLICATIONS AND SEMINARS

Aliyu, A. M. (2014). Empirical modelling of vertical up and down two-phase flows in large pipes, a poster presented at E&A DTC Poster Conference, School of Engineering, 4 March 2014.

Aliyu, A. M. (2014). Interfacial shear in downwards annular two-phase flow in large diameter vertical pipes, Research Student presentation at the weekly Energy and Power Division (School of engineering) Research Programme Seminar, 29 April, 2014

Aliyu, A.M., Lao, L., Yeung, H., Almabrok, A.A., 2015. A Comparative Analysis of Interfacial Friction Factor Correlations for Adiabatic Co-Current Gas–Liquid Annular Two-Phase Flow in Large Diameter Pipes, in: Proceedings of the World Congress on Mechanical, Chemical, and Material Engineering (MCM 2015). Avestia Publishing, July 20-21, Barcelona, Spain, Online: http://avestia.com/MCM2015_Proceedings/files/papers/HTFF280.pdf, pp. 280–1–9.

Aliyu, A.M., Lao, L., Yeung, H., 2015. A New Empirical Correlation for Entrained Droplet Fraction Prediction in Co-current Gas–Liquid Annular Two-phase Flow in Large Diameter Pipes, in: APCChE 2015 Congress Incorporating Chemeca 2015. September 27- October 1, Melbourne, Australia. (Awarded best student paper)

Aliyu M. Aliyu, Liyun Lao, Almabrok A. Almabrok, Hoi Yeung, (2016), Interfacial shear in adiabatic downward gas/liquid co-current annular flow in pipes, Experimental Thermal and Fluid Science, Volume 72, Pages 75-87, ISSN 0894-1777, http://dx.doi.org/10.1016/j.expthermflusci.2015.10.025.

Almabrok A. Almabrok, Aliyu M. Aliyu, Liyun Lao, Hoi Yeung, (2016), Gas/liquid flow behaviours in a downward section of large diameter vertical serpentine pipes, International Journal of Multiphase Flow, Volume 78, Pages 25-43, ISSN 0301-9322, http://dx.doi.org/10.1016/j.ijmultiphaseflow.2015.09.012

Aliyu, A. M. (2016). Pressure gradient variations in gas-liquid downward flows in a vertical large diameter pipe, International Conference on Multiphase Flow, May 22 – 27, Florence, Italy. (*Accepted*)

TABLE OF CONTENTS

LIST OF FIGURES

LIST OF TABLES

NOMENCLATURE

A. Symbols

Symbol	*Units*	*Description*
D	[m]	Pipe internal diameter
e	[-]	Entrained liquid fraction
E	[kg/s-m^2]	Entrainment rate
F	[-]	Modified Martinelli flow parameter
Fr_g	[-]	Gas Froude number
Fr_l	[-]	Liquid Froude number
f_i	[-]	Interfacial friction factor
f_s	[-]	Single phase friction factor
g	[m/s^2]	Acceleration due to gravity
H_l	[-]	Liquid holdup
$\dot{m}_g$	[kg/s-m^2]	Gas core mass flux
$\dot{m}_{lf}$	[kg/s-m^2]	Liquid film mass flux
Oh_l	[-]	Liquid Ohnesorge number
P	[bar]	Local pressure
ΔP	[bar]	Differential pressure
Re_g	[-]	Gas Reynolds number
Re_{lf}	[-]	Liquid film Reynolds number
Re_l	[-]	Liquid Reynolds number
S	[m]	Interface or pipe perimeter
t	[m]	Film thickness
t^+	[-]	Dimensionless film thickness defined as a frictional distance parameter: $t_g^+ = t/\nu_g\sqrt{\tau_i/\rho_g}$
t^*	[-]	Nusselt's dimensionless film thickness defined as: $t^* = t(g/\nu_l^2)^{1/3}$
u^*	[-]	Friction velocity: $u^* = \sqrt{\tau_i/\rho_g}$
u_{sg}	[m/s]	Superficial gas velocity
u_{lf}	[m/s]	Liquid film velocity
u_{sl}	[m/s]	Superficial liquid velocity
We_c	[-]	Core flow Weber number
We	[-]	Weber number
x	[-]	Vapour quality
z	[m]	Axial distance along pipe

B. Greek Letters

Symbol	*Units*	*Description*
Γ_k	[kg/m^3-s]	Mass generation rate of phase k per unit volume
ε	[-]	Void fraction

γ	[-]	Liquid droplet hold up
μ_c	[kg/s-m]	Gas core viscosity
μ_g	[kg/s-m]	Gas viscosity
μ_l	[kg/s-m]	Liquid viscosity
ρ_c	[kg/m^3]	Gas core density
ρ_g	[kg/m^3]	Gas density
ρ_l	[kg/m^3]	Liquid density
σ	[N/m]	Liquid surface tension
τ_c	[Pa]	Characteristic shear stress: $\tau_c = \frac{2}{3}\tau_w + \frac{1}{3}\tau_i$
τ_i	[Pa]	Interfacial shear stress
τ_w	[Pa]	Wall shear stress

Chapter One

INTRODUCTION

1.1 Background

Annular two-phase flow in pipes has been identified as one of the most frequently encountered flow regimes in practical applications that involve gas–liquid two-phase flow. It is characterised by the occurrence of a continuous liquid film flowing on the pipe periphery enclosing a central gas core carrying entrained liquid droplets. Properly predicting the flow behaviour is crucial for the safe and efficient design and operation of industrial heat transfer, oil and gas pipelines and other process transport equipment. Common examples of applications where annular two-phase flows are encountered include heat exchangers, deep-water risers in hydrocarbon production, gas condensate transport pipes, air conditioners, and steam boilers used in thermal and nuclear power plants.

Due to a number of competing forces influencing its hydrodynamics, theoretical analysis of annular two-phase flow is highly complex. The presence of inertial, viscous, and gravity forces heavily influence the liquid film flow, while surface tension forces and interfacial drag by the flowing gas flow affect the structure of the gas–liquid interface. Entrained liquid droplets swept into the gas core distort the hydrodynamics of the gas core since these droplets flow at a different velocity than the surrounding gas and there is a drag exerted on them. Also, re-deposition of these droplets can occur. Under steady state or equilibrium conditions, the rate of droplet entrainment balances the rate of deposition

resulting in zero net mass transfer but not momentum transfer. These are further complicated by the flow direction: co-current or counter-current upwards or downwards flows. As shown schematically in Figure 1-1, the velocity of the droplet laden gas core in upwards two-phase flow is always greater than that of the liquid flowing along the pipe wall. This is due to the liquid being the denser phase flowing against gravitational forces and can give rise to a highly irregular interface in the churn–annular flow regime. Conversely, in co-current downwards flow; either phase can have the higher velocity. In cases of high pressure systems, the compressible gas phase tends to travel at a faster velocity thereby reversing the direction (and sign) of the interfacial shear forces. All these considerations are the reasons why annular two-phase flows does not easily lend itself to theoretical modelling (Levy, 1999; Tong & Tang, 1997) and as such Cioncolini et al. (2009a) noted that investigators have resorted to empirical modelling instead.

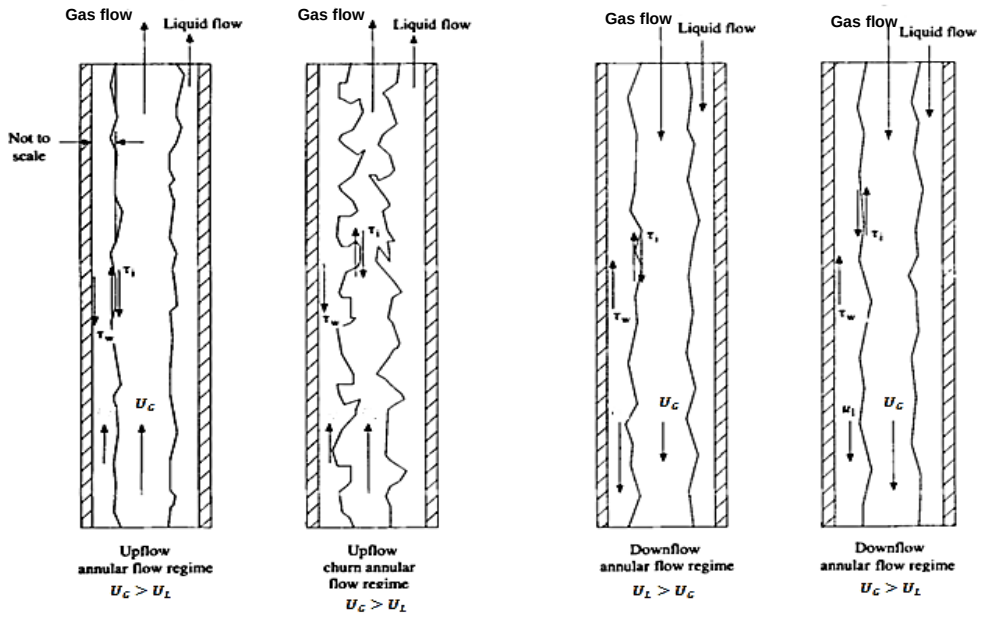

Figure 1-1: Structure of annular two-phase flow in upwards and downwards directions in vertical pipes (from Klausner et al. 1991).

Over the past five or so decades, there has been an enormous amount of work carried out on upwards and downwards two-phase annular flow with air – water being the two most studied gas–liquid combination, mostly using circular pipes of diameter less than 100 mm. However, over the past two decades, several investigators ((Oliemans et al. 1986); Kataoka & Ishii 1987;Omebere-Iyari 2006; Kaji & Azzopardi 2010; Lao et al. 2012; Schlegel et al. 2012) have noted that the flow structure of flow in large diameter pipes (pipes with diameter > 100 mm) is different. For example, the conventional slug flow characterised by bullet shaped Taylor bubbles does not manifest and instead, there is a gradual transition from bubbly to churn flow. For such pipe systems, there is dearth of data since the majority of data available and empirical models in the open literature were developed from smaller pipes, which especially in the case where highly turbulent systems are concerned, do not adequately model the conditions in larger pipes of internal diameters greater than 100 mm. It is therefore imperative to expand the knowledge to large pipe systems.

In this thesis, empirical modelling is used to study co-current upwards and downwards air–water two-phase annular flow using data obtained from the Serpent Rig, a 101.6 mm internal diameter flow loop at Cranfield University's Oil and Gas Engineering Centre.

1.2 Aim of study

To improve the understanding of wall film and droplet behaviour in co-current vertical upwards and downwards annular flows in large diameter pipes by performing carefully controlled experiments to collect data and evaluating the accuracy of existing prediction methods.

1.3 Objectives

The above aim of improving knowledge and evaluating the accuracy of existing methods in vertical annular flow will be achieved by (a) collecting data: experimental and secondary from the open literature; both for large and small pipes (b) comparing small pipe correlation predictions with large pipe experimental and literature data (c) deriving new correlations for large pipe data or a combination of large and small pipe data. These will be done for the following:

1. Falling film thickness in downwards annular flow
2. Interfacial friction factor in downwards annular flow
3. Interfacial friction factor in upwards annular flow
4. Entrained droplet fraction in upwards and downwards annular flow
5. Additionally, pressure gradient behaviour in downward co-current annular flow in large pipes will be examined.

1.4 Structure of thesis

The remaining part of this thesis is divided into five chapters in the following structure:

Chapter 2 presents a review of the relevant literature on gas – liquid two-phase flows, particularly focussing on vertical flows. Specific attention was given to the different modelling approaches that have been applied to vertical annular two-phase flows which are theoretical, numerical, and empirical. Additionally, the various empirical models that describe annular flow pressure drop, film

thickness, droplet fraction, and friction factor have been discussed vis-à-vis their application in small and large diameter pipes.

Chapter 3 describes the flow loop facility used to carry out the experiments. Descriptions of installed instrumentation (Wire Mesh Sensor, film thickness probes, pressure sensors, etc.) are provided here, their principles of operation, calibration, and margins of error.

Chapter 4 details the analyses carried out on the experimental data for downwards two-phase flow. Comparisons are presented here for falling film thickness and interfacial friction factor with literature models. Arguments are put forward for the development of new correlations for large diameter pipes, together with the development procedure and statistical analyses of the new correlations. Also presented in this chapter is pressure behaviour in the top and bottom halves of the downcomer.

Chapter 5 concentrates on upwards flow. Here, the data was subjected to comparison also with the literature models and new correlations were proposed for entrained droplet fraction and upwards interfacial friction factor.

Chapter 6 summarises the main conclusions drawn from the research work, based on the analysis of the experimental data. Recommendations for future work follow.

Chapter Two

LITERATURE SURVEY

2.1 Flow regimes in two-phase vertical flows

The study of multiphase flow and indeed two-phase flow over the decades has been done via classification of flow structures otherwise known as flow patterns or flow regimes. Classification into these flow regimes allows separate treatment of each so that more and more accurate phenomenological models can be developed. Historically, classifying two-phase flow regimes has largely been done by visual observation of the flow during experimental campaigns using transparent pipes.

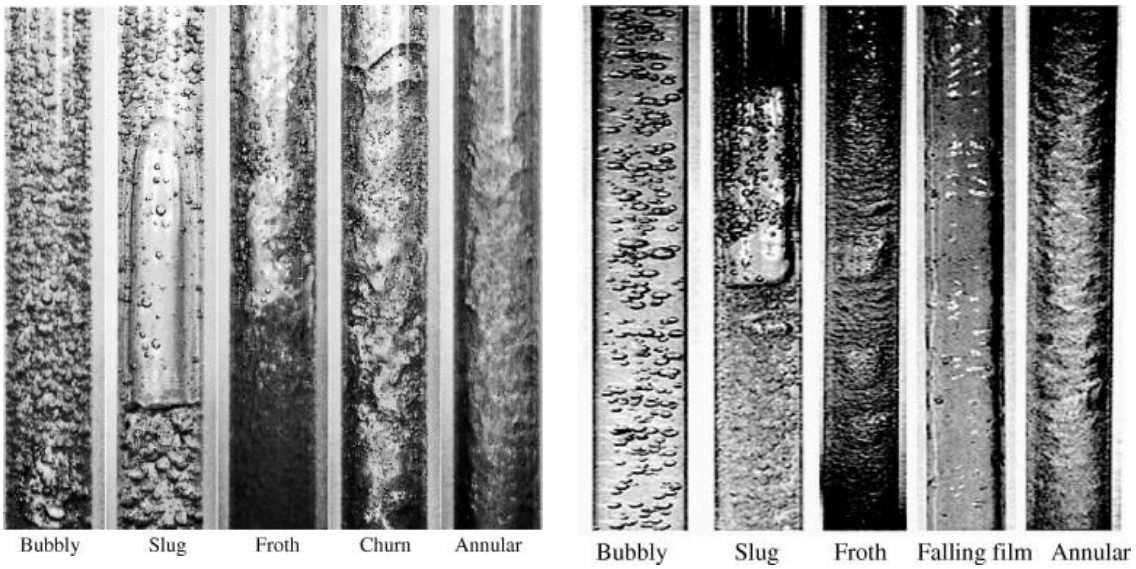

(a) (b)

Figure 2-1: Regimes in gas-liquid two-phase (a) upwards (b) downwards flow (from Bhagwat & Ghajar 2012)

Another way is by measuring and estimating fluctuations of the normal flow variables such as gas void fraction (Jones & Zuber 1975; Barnea et al. 1980; Vince & Lahey 1982; Costigan & Whalley 1997; Tsoukalas et al. 1997) or in

some cases differential pressure (Tutu 1982; Matsui 1984; Matsui 1986) which inherently reflect the in situ flow regime.

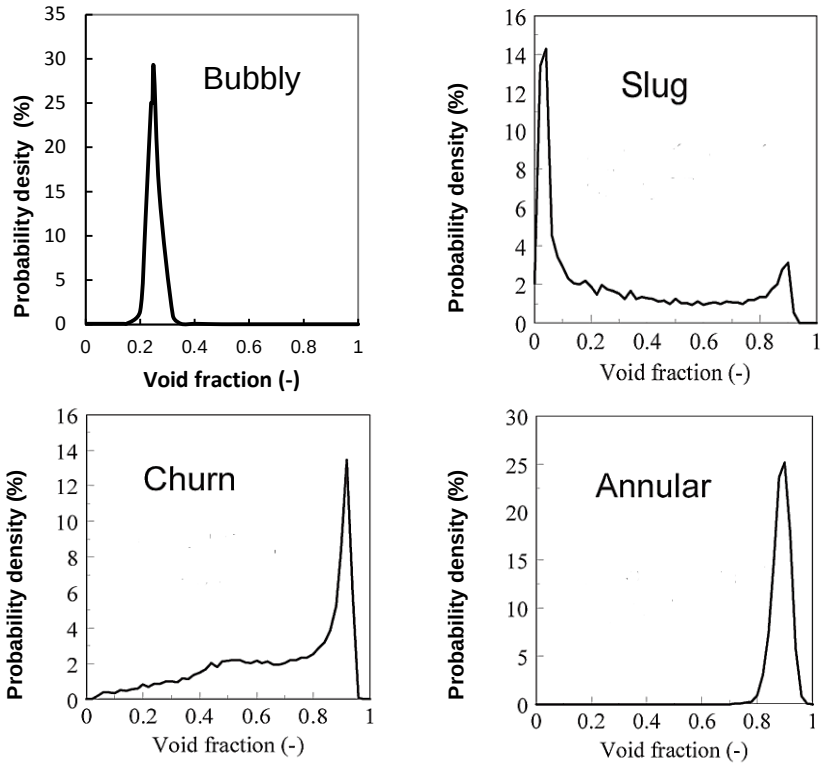

Figure 2-2: Examples of probability density functions of void fraction for bubbly, slug, churn, and annular flow (From Omebere-Iyari & Azzopardi 2007)

These methods make use of the peak values and shape characteristics of the probability distribution function (PDF) and/or power spectral density (PSD) of measured gas void fraction or differential pressure time series. For the PDFs of the time series void fractions, single peaks are obtained for annular and bubbly flows which correspond to the low and high gas void fractions. Bimodal PDFs characterise slug flows such that there exists a high void value as a result of the Taylor bubble and a low void value for the passing of the liquid slug body.

2.1.1 Flow regime maps

A flow regime map is a graphical representation when various known flow rates or superficial velocities of each phase are introduced into the channel and the

flow pattern observed so that boundaries are produced for when one flow configuration transitions to another. Different investigators have in the past come up with various flow regime maps each differing due to the quantities plotted on the axes and the flow direction (upwards, downwards or inclined). Almabrok (2014) noted that not only have superficial velocities been used to produce flow regime maps but also mass flow rates, mass fluxes, or dimensionless numbers such as Reynolds and Froude numbers. Limitations to the use of flow regime maps include the fact that flow regime transitions rather than being sharp are gradual and fluid properties such as viscosity drastically alter where transitions occur.

2.1.1.1 Vertically upwards flow regime maps

For vertical co-current gas–liquid two phase flow, several flow regime maps have been proposed. These plot a variety of quantities on the vertical and horizontal coordinates. While the use of dimensionless quantities is preferable so as to nullify the effect pipe diameter and/or flow conditions, most of the commonly used ones are dimensional, such as that of Hewitt & Roberts (1969) and Taitel et al. (1980) for upwards flow which are in terms of the superficial fluid momentum fluxes and velocities respectively.

a. Griffith and Wallis (1961) flow regime map

Using a 25.4 mm vertical pipe, Griffith & Wallis (1961) invoked a theory to show that the dimensionless numbers $Fr_m = u_m^2/gD$ and u_{sg}/u_{slug} (subscript m denotes mixture) controlled the slug to annular flow transitions. As a result, they arrived at a dimensional flow regime map (Figure 2-3) where the churn and annular flow regimes are lumped together.

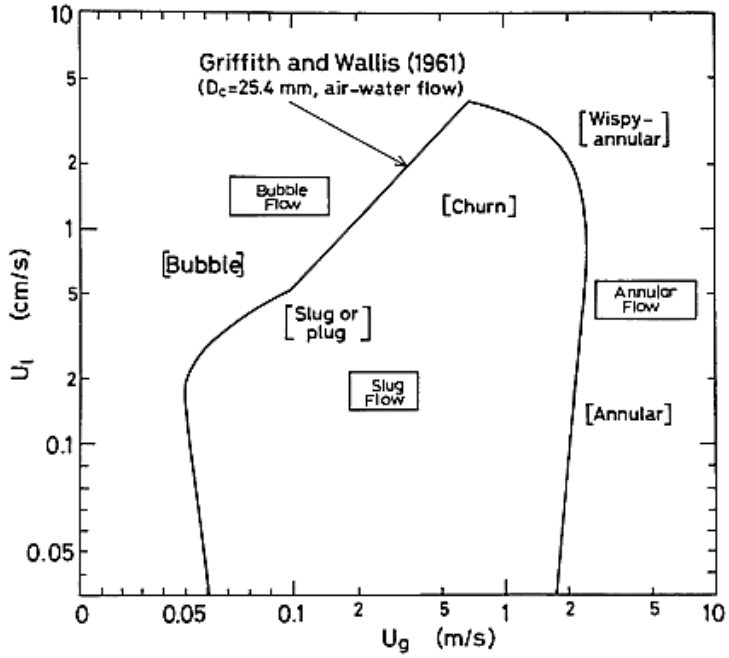

Figure 2-3: Griffith and Wallis flow regime map

Taitel et al. (1980) noted that the theory is not complete in that no analytical expression was derived for the transition curve such that the use of Griffith & Wallis' method for other regime transitions (e.g. bubbly to slug) is open to question.

b. Hewitt and Roberts (1969)

The Hewitt & Roberts (1969) flow regime map was developed at the UK Atomic Energy Authority at Harwell, using observations made in the 23.5 m long LOTUS (LOng TUbe System) a 31.25 mm internal diameter vertical flow loop for air–water studies. Simultaneous X-ray radiography and high speed flash photography complemented visual observations for flow regime identification. They also used previous data obtained using steam–water flow to arrive at a flow regime map in terms of the superficial momentum fluxes of the phases $\rho_g u_{sg}^2$ and $\rho_l u_{sl}^2$, shown in Figure 2-4. Hewitt & Roberts remarked that the flow

regime map is limited in scope due to the small number of fluids used and the flow conditions and that extension over a wider range of parameters will improve its areas of application.

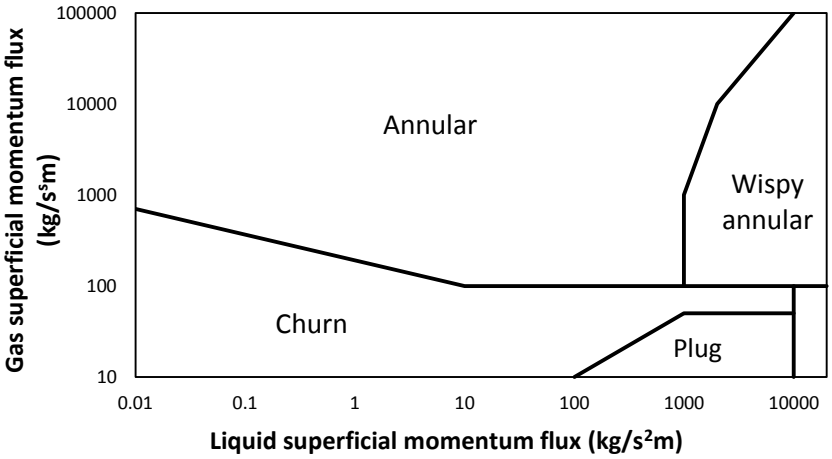

Figure 2-4: Hewitt and Roberts flow regime map

Nevertheless, there seem to be little in the literature to suggest this has been done and the original 1969 flow regime map is still very much in wide use.

c. Yamazaki and Yamaguchi (1979)

Yamazaki & Yamaguchi (1979) carried out experiments in both upwards and downwards air–water two-phase flow using a 2-m long 25 mm internal diameter glass tube. They produced flow regime maps for both orientations in terms of the fluid mass flow rate per unit area (Figure 2-5). As expected, the bubbly flow region is small which is consistent with that of other maps. Their flow regime map never gained widespread use.

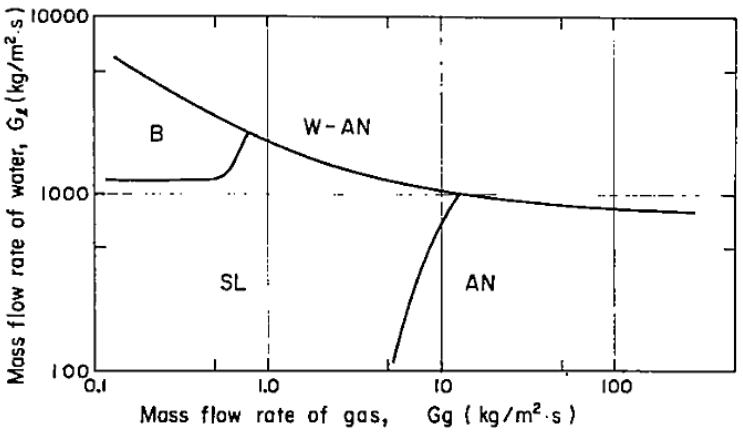

Figure 2-5: Yamazaki & Yamaguchi (1979) upwards flow regime map

d. Taitel et al. (1980)

(Taitel et al. 1980) observed that previous flow regime maps were arrived at arbitrarily without recourse to any theoretical basis. They noted the existence of dimensional and dimensionless regime maps further stating a common problem from previous maps is their empirical nature with the absence of sound physical models. Based on some theoretical arguments, they obtained flow regime transition criteria for bubbly-slug, slug–churn, and churn–annular transition from which they developed the flow pattern map (otherwise known as the Taitel & Dukler flow regime map) shown in Figure 2-6.

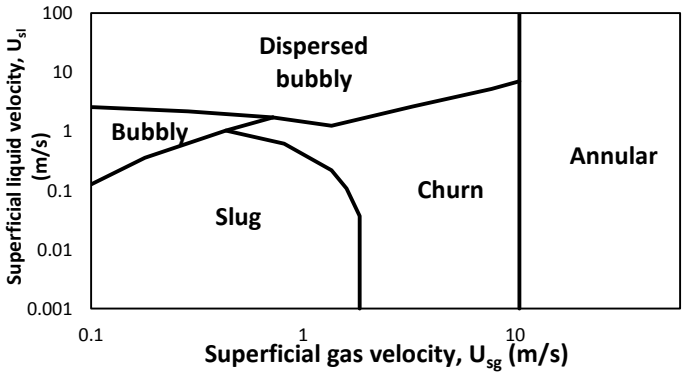

Figure 2-6: Taitel et al. (1980) flow regime map

It is one of the most frequently used, the Taitel et al flow regime map is in terms of the superficial velocities of both phases. They showed that experimental data of other researchers carried out for 25 and 50 mm pipes were in good agreement with their flow regime map.

2.1.1.2 Vertically downwards flow regime maps

a. Oshinowo (1971)

Oshinowo (1971) obtained a flow regime map for vertically upwards two-phase flow in a 25 mm pipe with air and water as the working fluids. Liquid mass flow rate was plotted against the gas mass flow rate on the horizontal axis.

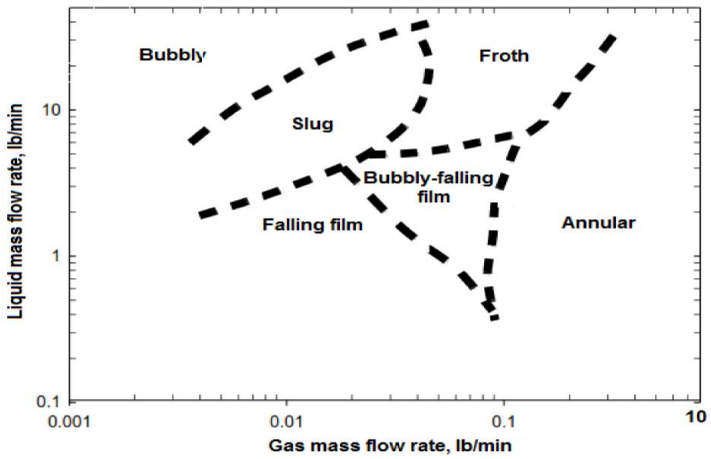

Figure 2-7: Oshinowo (1971) flow regime map

As shown in Figure 2-7 Oshinowo identified six regimes including coring-bubble, bubbly-slug, falling film, falling bubbly-film, froth and annular flow regimes for downflow. A deficiency of the flow regime map is the lack of a clear boundary separating annular and falling film regimes at low liquid loading.

b. Yamazaki & Yamaguchi (1979) flow regime map

As stated earlier Yamazaki & Yamaguchi (1979) produced their (upwards and downwards) flow regime maps in terms of fluid mass flow rate per unit area. An

important feature of the map is the non-existence of bubbly flow. They explained this on basis of bubble coalescence being rapid since flow and buoyancy directions are opposite. Flow regimes observed are slug, wispy annular, annular, and wetted wall flow in other words falling film flow.

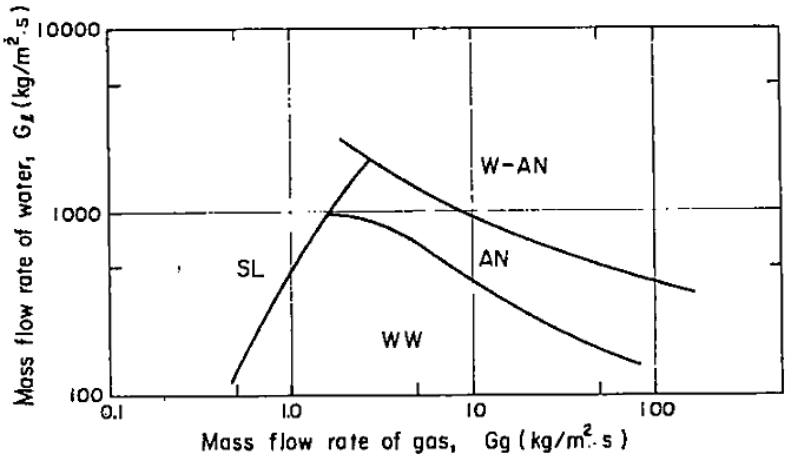

Figure 2-8: Yamazaki & Yamaguchi (1979) downwards flow regime map. Key: AN – annular flow, SL – slug flow, W-AN – wispy annular, WW – wetted wall flow

Jiang and Rezkallah (1993) flow regime map

A downwards flow regime map was produced for vertical downward flow in a 9.25 mm diameter pipe by Jiang & Rezkallah (1993). For flow regime identification, measurements of void fraction using a single beam gamma densitometer calibrated against hold up from a quick shutting valve. Since they carried out their experiments for both up and downflow, they were able to observe that the latter expectedly produced larger void fractions.

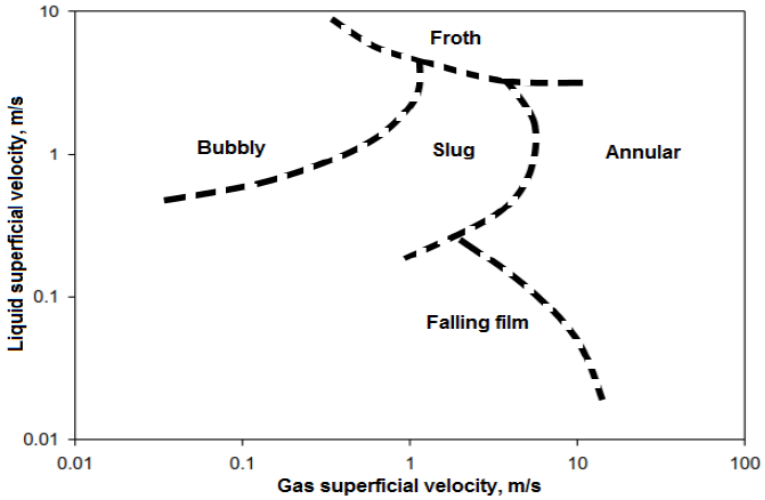

Figure 2-9: Downwards flow regime map of Jiang & Rezkallah (1993)

a. Bhagwat et al. (2012)

The flow pattern map of Bhagwat et al. (2012) was produced using observations for air–water downwards flow in a 12.52 mm ID pipe. As can be seen from the map illustrated in Figure 2-10, there is a large region for annular flow signifying that annular dominates downward two-phase flow.

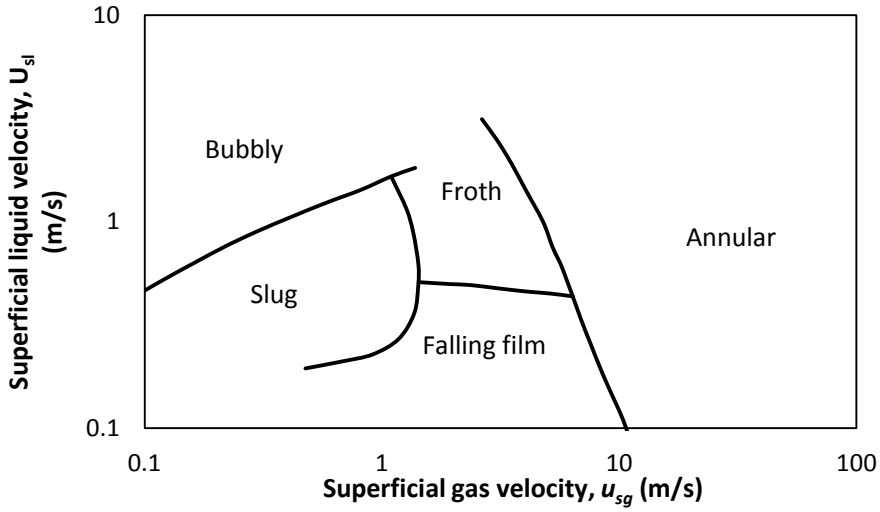

Figure 2-10: Bhagwat et al. (2012) flow pattern map

2.1.2 Evidence of difference in flow regime transitions in small and large diameter pipes

The flow regime maps of the various authors outlined in the previous section are obtainable in pipes of ID < 100 mm, the so called “small diameter pipes”. Therefore their use for typical field applications where the pipes are at least 150 mm in diameter presents severe challenges since evidence suggests that flow patterns and other parameters differ in small and large pipes.

Kataoka & Ishii (1987) studied experimental data for steam–water at various pressures in large diameter 96 and 456 mm vertical tubes and observed distorted bubbles which are not the conventional Taylor bubbles at conditions where they occur in 22–75 mm pipes. They then proceeded to derive a drift flux relationship for pool boiling void fraction in large channels. Cheng et al. (1998) performed tests in a vertical air–water 150-mm diameter pipe in order to study the churn –slug transition region. Their findings indicated that conventional slugs did not exist in the fluid velocity ranges they would normally appear during steady state operations. As a result, there was a gradual transition from bubbly to churn flow. Ohnuki & Akimoto (2000) examined upward air–water two-phase flow at axial L/D positions of 60 in a 200-mm diameter pipe and reported that churn flow is the dominant flow regime under the conditions that slug flow exist in small diameter pipes. Based on their observations, they categorised the observed flow regimes to be bubbly, churn–bubbly, churn–slug and churn–froth. Detailed wire mesh sensor visualisation studies by Prasser et al. (2003) in their 194-mm diameter TOPFLOW facility corroborates the absence of traditional slug flow as previously observed. The works of Ali (2009) and Ali & Yeung

(2014) were conducted in a 254-mm pipe and a distinct shift in the flow regime map was established for the bubbly–churn transition as compared to previous studies.

Other works (Kobayashi et al. 2004; Omebere-Iyari et al. 2007; Ali 2009; Smith et al. 2012; Schlegel et al. 2012; Ali & Yeung 2014) all highlight the differences in flow behaviour between large and small diameter pipes. They have also stressed that there is danger in tenuously extrapolating small diameter results to predict large pipe behaviour because the complex interaction of the phases alter flow regime transitions and result in the wrong use of phenomenological models to for example predict pressure drop and holdup.

The foregoing has therefore led investigators to question the accuracy of existing modelling tools and recommend that additional research to be conducted with larger diameters. Furthermore, the availability of strong experimental evidence has increased the impetus to extend detailed two-phase flow knowledge to larger pipes where understanding and models are scarce or where available, is not fully developed. Nevertheless, to date, very few detailed models (physical and correlational) are available that exclusively apply to large pipe two-phase flow. This is especially so for the annular flow regime where large gas fluxes are required and are as a result expensive experiments to conduct.

2.2 Co-current annular two-phase flow

2.2.1 Churn-annular transition and the Wallis (1962) criterion for annular flow

The churn–annular transition region has been found to be highly complex and a thorough experimental observation by Hewitt et al. (1984) revealed a large amount of interfacial activity and that the liquid film near the pipe wall partly flows upwards and partly downwards under gravity (Owen 1986). As a result it is highly oscillatory. Analysis of air-water data by Owen (1986) using a dimensionless pressure gradient (ΔP*) plot against the dimensionless gas velocity shows that within the churn–annular transition region is a minimum dimensionless pressure gradient as shown in Figure 2-11. The dimensionless gas velocity is given as

$$u_g^* = u_{sg} \Big/ \sqrt{gD(\rho_l - \rho_g)} \qquad \textbf{2-1}$$

which is a modified Froude number, where u_{sg} is the superficial gas velocity, being the velocity of the gas as though it alone flows in the pipe. As can be seen the turning point occurs at $u_g^* = 1$. This is known as the Wallis criterion for annular flow. (Wallis 1962b) carried out experiments in a 12.7 mm diameter pipe with an air–water fluid combination and observed the churn–annular transition to occur at $u_g^* = 1$ in both upwards and downward flow conditions. (Hewitt 1986) explained that the change in slope of ΔP* in churn–annular flow is as a result of a switch from a gravity dominated churn flow to a friction dominated annular flow. Therefore u_g^* is a ratio of frictional (or inertial) to gravitational forces and the minimum in Figure 2-11 occurs when these two forces are equal.

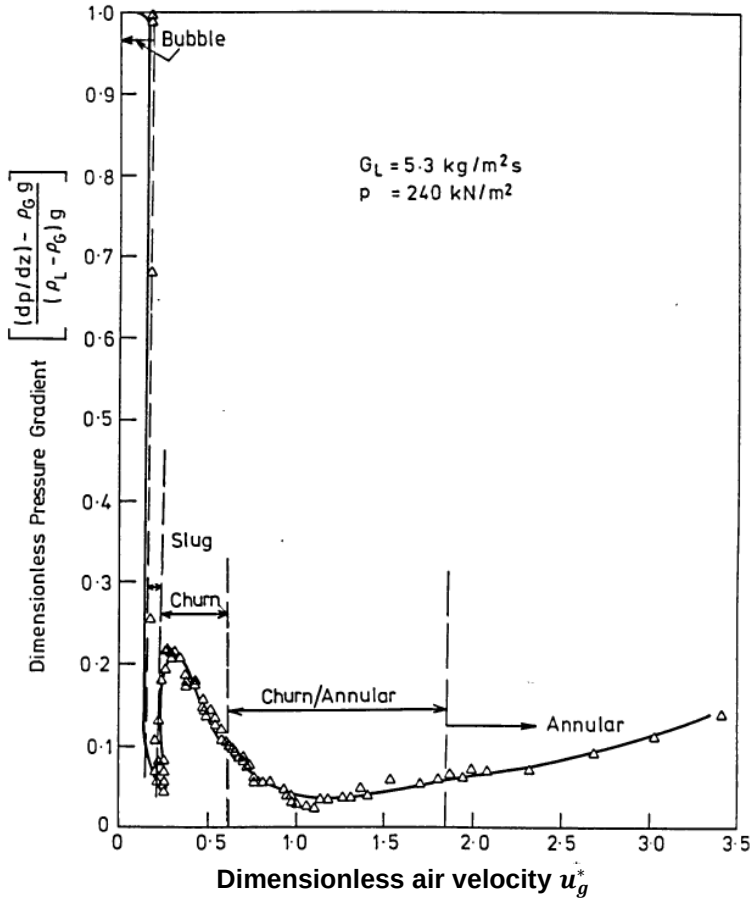

Figure 2-11: Variation of dimensionless pressure gradient with dimensionless gas velocity for gas – liquid flow in vertical pipes (from Owen 1986)

Pressure gradient minimum has also been found by (Hewitt et al. 1965; Govan et al. 1991) as indicative of the churn–annular transition. Hewitt et al. (1965) have gone further to show that the minimum pressure gradient closely corresponds to the condition of zero wall shear stress ($\tau_w = 0$). Also, they showed that the film shear stress can be calculated using the universal velocity profile using a representative average shear stress τ_{avg} rather than τ_w on the assumption that all the liquid in the pipe flows as a film at the minimum pressure gradient. Additionally, Wallis (1962) and Barbosa et al. (2002) using similar sampling probes for entrained droplet fraction measurement found out that a strikingly similar profile is obtainable for the entrained fraction within the same

transition region for air–water flows. It is therefore clear that different hydrodynamics play out as churn flow transits to annular flow and as a result accurate detection of this transition is imperative so the correct phenomenological models are applied for property prediction. This is more so for large diameter pipes where the location of this transition point has been shown in the previous section, to differ from those of smaller pipes. However, no indication in the literature has been found on whether the pressure gradient minimum also occurs at $u_g^* = 1$ for large diameter pipes.

2.2.2 Annular flow, flooding and flow reversal

Flooding is a phenomenon in vertical pipes that occurs for counter-current flow of gas and liquid where the liquid flows downward and the gas upward sweeping chunks of liquid along. This kind of flow configuration is encountered in oil and gas risers associated with declining reservoir pressure that does not provide enough head to transport the denser liquid phase. Such a situation is depicted by (Hewitt & Hall-Taylor 1970) in Figure 2-12 where an initial falling film under gravity is counteracted by an upward flowing gas. Gradually increasing the gas flow causes waves to appear on the liquid surface, which are carried upwards together with the gas. Consequently, this results in liquid flowing beyond the injection point so that simultaneous climbing and falling film flow occurs. Sufficiently high gas flow results in no falling film flow. Now reducing the gas flow causes a point to be reached where partial downflow occurs along the tube as well as maintaining the upflow. This point is known as the flow reversal point.

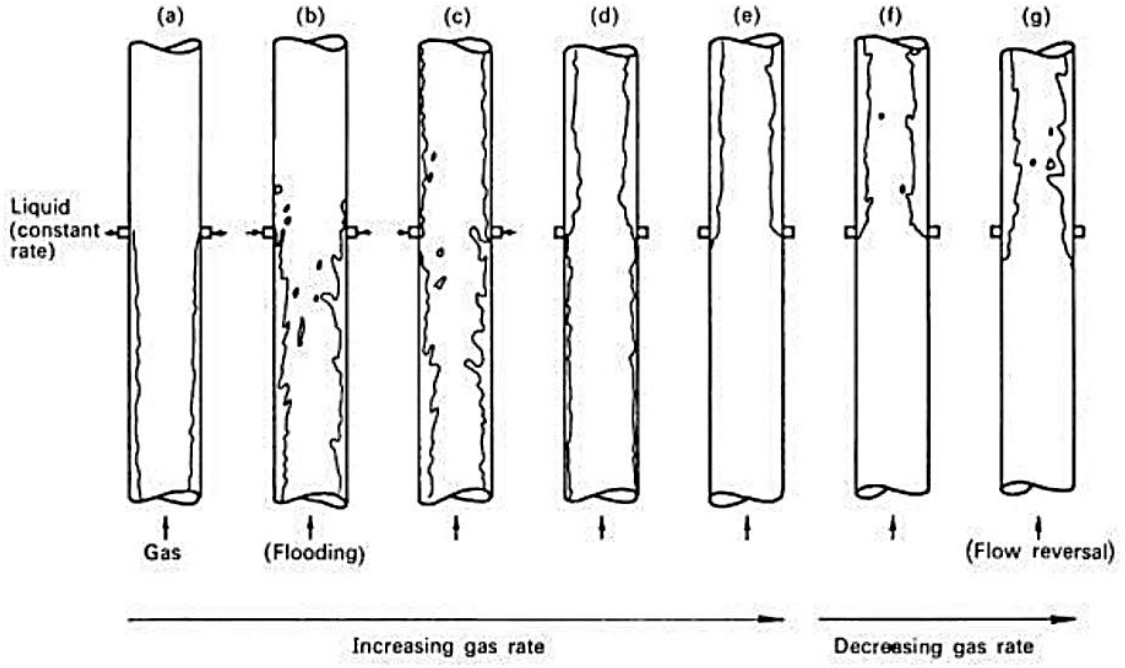

Figure 2-12: Flooding and flow reversal (from Hewitt & Hall-Taylor 1970)

Three probable mechanisms of flooding have been postulated in the past namely: wave, droplet and film dynamics (No & Jeong 1996; Guo & Jeong 2014) . Alekseenko et al. (1985) explained that drop dynamics and film flow dynamics mechanisms depend on local phenomena independent of channel length and entrance geometry while wave instability has been experimentally shown to be independent on those conditions. Thus wave instability is the more plausible flooding mechanism such that small amplitude sine waves with varying frequencies flowing downwards on the pipe walls compete to absorb the kinetic energy of the flowing gas. Peng et al. (2010) suggested that the waves with the quickest growth rates are converted to large roll waves. On the other hand, No & Jeong (1996) remarked that the appearance of huge roll waves are not always indicative of the onset of flooding, but their instability is.

Flooding has been analysed using many models including empirical correlations with the most widely used group of correlations being either of Wallis or Kutateladze-type. The Wallis-type are as follows:

$$u_g^{*1/2} + C_1 \cdot u_l^{*1/2} = C_2 \quad \textbf{(2-2)}$$

where

$$u_g^* = u_{sg}\left[\frac{\rho_g}{gD(\rho_l - \rho_g)}\right]^{1/2} \quad \textbf{(2-3)}$$

$$u_l^* = u_{sl}\left[\frac{\rho_l}{gD(\rho_l - \rho_g)}\right]^{1/2} \quad \textbf{(2-4)}$$

and the Kutateladze-type taking the form:

$$Ku_g^{*1/2} + C_3 \cdot Ku_l^{*1/2} = C_4 \quad \textbf{(2-5)}$$

where

$$Ku_g^* = u_{sg}\left[\frac{\rho_g^2}{g\sigma(\rho_l - \rho_g)}\right]^{1/4} \quad \textbf{(2-6)}$$

$$Ku_l^* = u_{sl}\left[\frac{\rho_l^2}{g\sigma(\rho_l - \rho_g)}\right]^{1/4} \quad \textbf{(2-7)}$$

In the equations **(2-2)**–**(2-7)**, u_{sg} and u_{sl} are the superficial gas and liquid velocities with ρ_g and ρ_l being their respective densities, σ the surface tension, D the pipe diameter, and g acceleration due to gravity. The constants C_1 – C_4 are found by regression of flooding data and (Jayanti et al. 1996) note that the constants are dependent on inlet/outlet conditions and pipe length. A large majority of flooding investigators working with vertical tubes have correlated

their data based on the Wallis-type correlation (Equation **(2-2**)) while others working with tube bundles used the Kutateladze-type model. The former type of correlation involves the use of pipe diameter while the latter does not. As shown in Figure 2-13 for representative liquid velocities, both correlations seem to give close predictions with data from a pipe of 50 mm diameter. Values for C_1 and C_2 are 1 and 0.88 respectively as obtained by Hewitt & Wallis (1963); and C_3 and C_4 values of 1 and 1.79 obtained by Sun (1979).

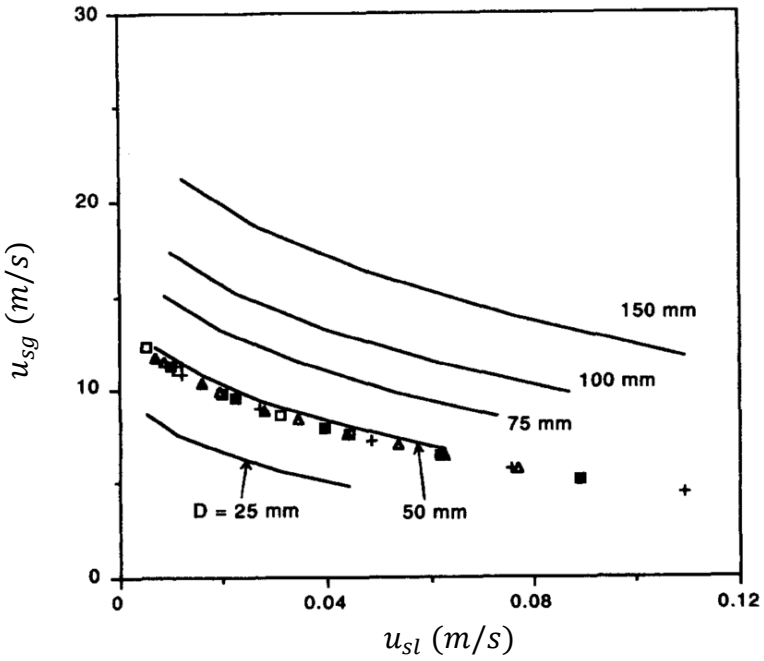

Figure 2-13: A comparison of required gas velocity for flooding as predicted by the Wallis-type correlation (lines) and Kutateladze-type correlation (points) for various pipe diameters. As can be seen there is agreement at a pipe diameter of 50 mm (from Jayanti et al. 1996)

Using the physical observations of the occurrence of incoherent waves in large diameter pipes, Jayanti et al. argued that the wave mechanism cannot be responsible for flooding in large pipes. This is due to the fact that as incoherent waves do not occupy the whole pipe periphery, gas flow cannot exert as much form drag on the wave as when coherent ring-type waves are formed all-round the pipe circumference. However, in such large tubes, large amplitude waves

that form over parts of the circumference would be sources of droplets which are usually ripped off the peaks of the waves thus causing flooding. As a result, the droplet mechanism may be responsible for flooding in large diameter pipes.

2.3 Droplet entrainment in annular two phase flow

2.3.1 Entrainment mechanisms

A distinctive feature of annular two-phase flow is the complex pattern of gas–liquid interfacial waves which in certain flow conditions are presented as so-called disturbance waves. These disturbance waves have long been considered to be a source of droplet entrainment though the behaviour is still not fully understood. However, based on visual observations, several mechanisms have been proposed by which this occurs (Hewitt & Hall-Taylor 1970); these include : disturbance wave breakdown by way of “undercutting”, “rolling”, and bubble breakup. In Figure 2-14a, flowing gas undercuts the wave such that a round liquid bead begins to form. The neck of the developed bead elongates to a point where it breaks up into droplets. Droplet entrainment by roll wave breakup on the other hand occurs when a large disturbance wave on a shallow liquid film becomes steep along the gas flow direction forming a tip which breaks up into droplets as shown in Figure 2-14b. Liquid breakup leading to entrainment may also occur by a release of bubbles on the gas–liquid interface Figure 2-14c. Pioneering work on this phenomenon was carried out by (Garner et al. 1954; Newitt et al. 1954) in that bubble breakup can occur in one of two ways: gas jet breakdown for small bubbles and bubble collapse for larger bubbles. Low surface tension; and liquid viscosity give rise to smaller bubbles being formed.

The presence of wetting agents reduces the amount liquid droplets entrained by bubble breakup as well as the production of smaller droplet sizes.

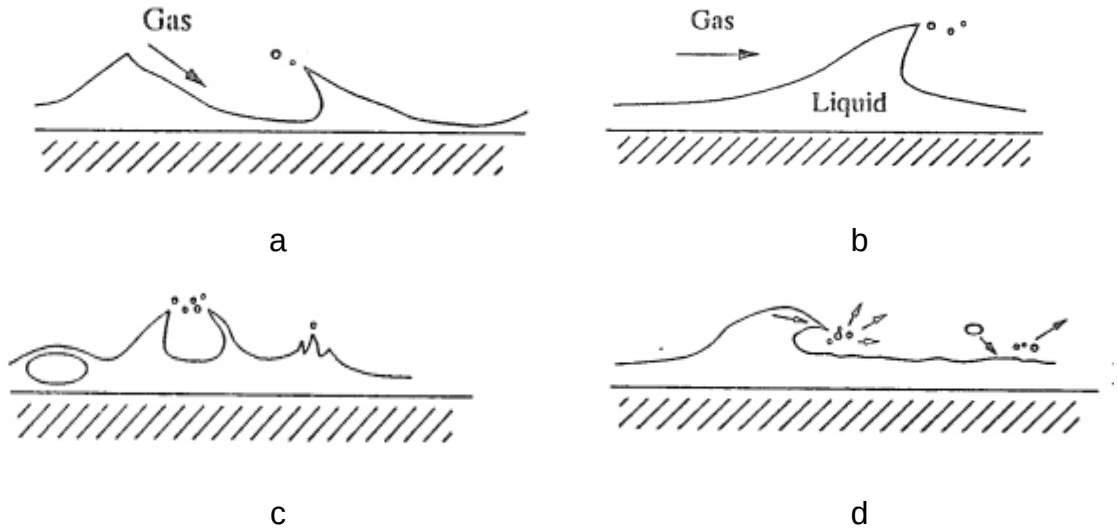

Figure 2-14: Entrainment mechanisms a. Roll wave b. Wave undercutting c. Bubble burst d. Liquid impingement (Kuo & Cheung 1995)

Lastly, droplet entrainment by liquid impingement occurs when comparatively large liquid droplets impinge on the surface of the liquid interface resulting in further entrainment of lesser droplets (Figure 2-14d). (Kuo & Cheung 1995) also note that an advancing roll wave may also cause the production of smaller droplets by impingement.

These mechanisms of entrainment lead to a decrease in amplitude of the disturbance wave as the gas flow increases, therefore resulting in a reduction in the thickness of the liquid film as the droplets are entrained. Also, for a given gas flux, droplet deposition occurs from the gas core to the liquid film and a dynamic equilibrium is established between droplet entrainment and deposition hence keeping the liquid film flow rate fairly constant at the specified gas flow.

2.3.2 Onset of droplet entrainment

The onset or inception of droplet entrainment is the point at which the first liquid droplet tears from the surface of the liquid after a small change in gas or liquid flow rate (Hewitt & Hall-Taylor 1970). When the gas phase flows over the liquid film, the interface becomes unstable with increasing gas velocity due to the Kelvin-Helmholtz Instability. At adequately high gas flow rates, these interfacial waves transition into large amplitude disturbance waves. A point is reached where the shear forces at the gas–liquid interface dominate the competing surface tension forces within the liquid, culminating in droplets being torn off and entrained in the highly turbulent gas flow. Thus, the Weber number is widely used to study this phenomenon since it expresses these competing forces as follows:

$$We = \frac{\rho u^2 D}{\sigma} \quad \textbf{(2-8)}$$

Frohn & Roth (2000) noted that the Weber number is particularly useful where strongly curved surfaces are involved such as in pipes. Experimental observations by (Wicks & Dukler 1960) found that a critical Weber number (We_{cr}) of 22 is required for the inception of droplet entrainment. They developed a correlation based on the Martinelli parameter X and We_{cr} which (Ishii & Mishima 1989) remarked had reasonable agreement with experimental data but noted its limitation of application due to its dimensional nature.

(Ishii & Grolmes 1975) studied the onset of entrainment, reporting a critical liquid Reynolds number ($Re_{l,cr}$) of 160 for horizontal and vertical upflow. By

making a force balance on the crest of a hypothetical liquid roll wave (Figure 2-15) they proposed an inception criterion as follows:

$$\frac{\mu_l u_{sg}}{\sigma}\sqrt{\left(\frac{\rho_g}{\rho_l}\right)} \geq 11.78 N_\mu^{0.8} Re_l^{-1/3} \text{ for } N_\mu \leq 1/15 \quad \textbf{(2-9)}$$

and

$$\frac{\mu_l u_{sg}}{\sigma}\sqrt{\left(\frac{\rho_g}{\rho_l}\right)} \geq 1.35 Re_l^{-1/3} \text{ for } N_\mu > 1/15 \quad \textbf{(2-10)}$$

Where the viscosity number N_μ is defined as

$$N_\mu = \mu_l / \left(\rho_l \sigma \sqrt{\sigma / g\Delta\rho}\right)^{1/2} \quad \textbf{(2-11)}$$

while the superficial liquid Reynolds number is defined as

$$Re_l = \frac{\rho_l u_{sg} D}{\mu_l} \quad \textbf{(2-12)}$$

A point is reached, which they called the “rough turbulent” regime, where the critical gas Reynolds number is independent of the liquid Reynolds number and occurs at $Re_l \leq 1635$. (Ishii & Mishima 1989) noted the good fit with experimental data and also the significant scatter around the criterion. They argued that since there are a lot of droplets along the interface, a modification of the gas core inertia is required so as to take into consideration the droplet inertia.

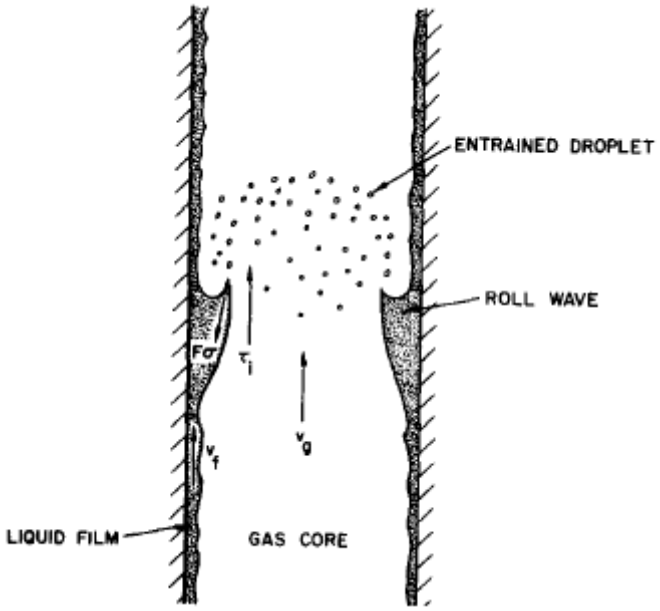

Figure 2-15: Ishii & Grolmes (1975) roll wave entrainment force balance

Despite this shortcoming and the existence of other criteria proposed by other investigators (such as Wallis 1962; Zuber 1962; Jensen 1971; Kutateladze 1972), it however remains the most complete and well tested criterion against a large number of experimental data (Kuo & Cheung 1995; Sawant et al. 2009).

2.3.3 Existing empirical models for entrained droplet fraction

2.3.3.1 Paleev and Filippovich (1967) model

One of the earliest published correlations for entrainment fraction is that of (Paleev & Filippovich 1966). They indirectly measured the entrainment rate by withdrawing the liquid film in a 40 mm pipe through an "absorbing surface" of 33 mm ID, and measuring the resulting amount of liquid collected. The fraction of liquid withdrawn ($\dot{m}_{lf}/\dot{m}_l$) was then correlated with the dimensionless group $\frac{\bar{\rho}}{\rho_l}\left(\frac{\mu_l u_{sg}}{\sigma}\right)^2$ which is a product of the Ohnesorge and gas Weber numbers,

dimensionless numbers that describe the interaction between gas and liquid droplets in a spray nozzle.

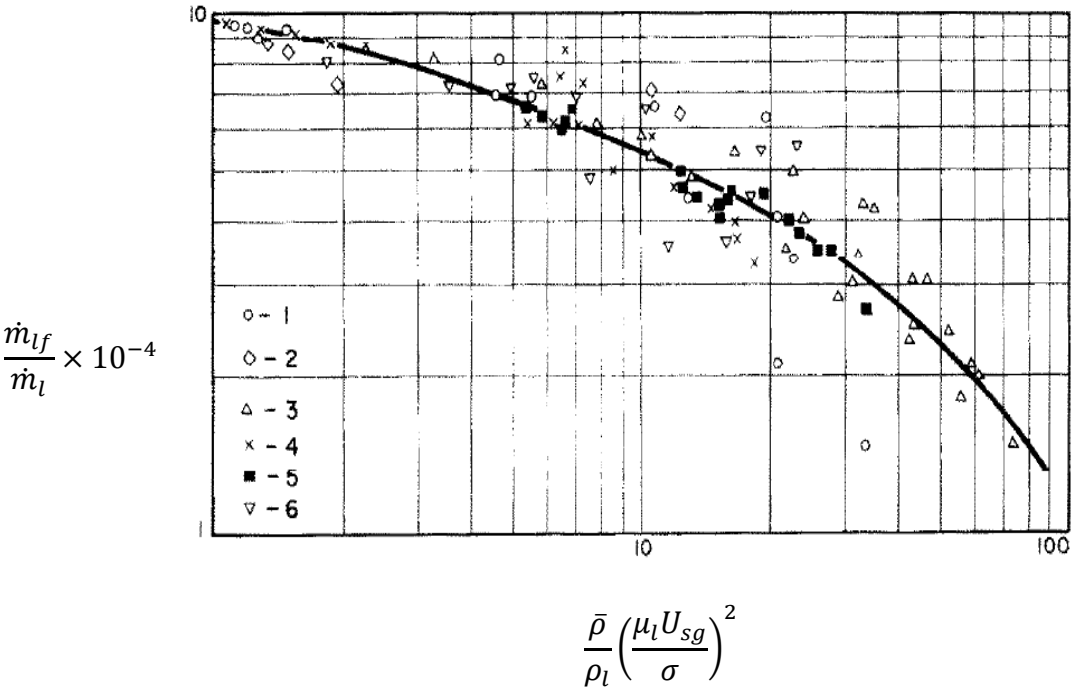

Figure 2-16: Paleev and Fillipovich (1967) correlation between $\dot{m}_{lf}/\dot{m}_l$ and $\bar{\rho}/\rho_L\left(\mu_l u_{sg}/\sigma\right)^2$ (Data: 1-Armand 1964; 2-Hujghe & Mondin 1961; 3-Collier & Hewitt 1961; 4,5-Paleev & Filippovich 1966 (16mm, 27.7mm ID pipe); 6-Magiros & Dukler 1961)

Paleev and Filippovich obtained the following correlation which corresponds to the line in Figure 2-16:

$$\frac{\dot{m}_{lf}}{\dot{m}_l} = 0.985 - 0.44 \log\left[\frac{\bar{\rho}}{\rho_L}\left(\frac{\mu_L u_{sg}}{\sigma}\right)^2 \times 10^4\right] \quad \textbf{(2-13)}$$

Where $\bar{\rho} = \rho_g\left[1 + \frac{\dot{m}_l(1-\dot{m}_{lf}/\dot{m}_l)}{F\rho_g u_{sg}}\right]$ **(2-14)**

Where $\dot{m}_{lf}$ and $\dot{m}_l$ are the liquid film and total liquid flow rates while F is the pipe cross-sectional area. They noted the large amounts of scatter in their plot and attributed it to possible complexities in the different methods the various data were obtained, and that the data comprises of both horizontal and vertical

flow. Figure 2-16 shows fairly good agreement with the data, however, the effects of pipe diameter and liquid Reynolds number have been neglected. Wallis (1968) however found that the scatter can be greatly reduced by correlating with $\rho_g/\rho_l\left(\mu_g u_{sg}/\sigma\right)^2$ instead of $\bar{\rho}/\rho_l\left(\mu_l u_{sg}/\sigma\right)^2$. Nevertheless, Ishii & Mishima (1989) noted that the dimensionless gas flux Wallis used for the onset of entrainment suggested that the effect of liquid viscosity is more complicated than that predicted by their correlation.

2.3.3.2 Oliemans et al (1985) model

(Oliemans et al. 1986) developed a correlation, Equation (2-15) using 727 data points from the Harwell Databank. The model contains 10 regression constants $\beta_0 - \beta_9$ as shown in Table 2-1 such that the estimate for each constant is given based on the liquid film Reynolds number interval.

$$\frac{e}{(1-e)} = 10^{\beta_0}\rho_l^{\beta_1}\rho_g^{\beta_2}\mu_l^{\beta_3}\mu_g^{\beta_4}\sigma^{\beta_5}D^{\beta_6}u_{sl}^{\beta_7}u_{sg}^{\beta_8}g^{\beta_9} \quad \textbf{(2-15)}$$

A restriction on the values of the parameters of the correlation is that the right hand side constitutes a dimensionless group. The liquid film Reynolds number is defined as:

$$Re_{lf} = (1-e)(1-x)\dot{m}_l D/\mu_l \quad \textbf{(2-16)}$$

Where $\dot{m}_L$ is the liquid mass flow rate. Since the values of each parameter depends on the liquid Reynolds number (itself a function of the entrained fraction *e*) an iterative procedure is required to calculate *e.* To achieve this, a first order estimate for e is obtained using the values of $\beta_0 - \beta_9$ for all data points independent of Reynolds number.

Table 2-1: Parameter estimates for Oliemans et al correlation

Parameter	Corresponding physical quantity	All data points		Parameter estimates film Reynolds number intervals					
		Parameter estimate	Standard error	100–300	300–10^3	10^3–3×10^3	3×10^3–10^4	10^4–3×10^4	3×10^4–10^5
β_0	Intercept	−2.52	0.40	−0.69	−1.73	−3.31	−8.27	−6.38	−0.12
β_1	ρ_L	1.08	0.05	0.63	0.94	1.15	0.77	0.89	0.45
β_2	ρ_G	0.18	0.06	0.96	0.62	0.40	0.71	0.70	0.25
β_3	μ_L	0.27	0.04	−0.80	−0.63	−1.02	−0.13	−0.17	0.86
β_4	μ_G	0.28	0.11	0.09	0.50	0.46	−1.18	−0.55	−0.05
β_5	σ	−1.80	0.08	−0.88	−1.42	−1.00	−0.17	−0.87	−1.51
β_6	D	1.72	0.05	2.45	2.04	1.97	1.16	1.67	0.91
β_7	V_{SL}	0.70	0.03	0.91	1.05	0.95	0.83	1.04	1.08
β_8	V_{SG}	1.44	0.05	−0.16	0.96	0.78	1.45	1.27	0.71
β_9	g	0.46	0.03	0.86	0.48	0.41	−0.32	0.07	0.21
No. of points		727		40	206	224	76	102	74

This estimated *e* is then used to calculate the Reynolds number, the values of the parameters are then obtained from Table 2-1 and *e* updated. This is converges in 2 or 3 steps. The iterative nature of the correlation may make it cumbersome for use in some flow codes.

2.3.3.3 Ishii & Mishima (1989) model

A correlation was developed by (Ishii & Mishima 1989) in terms of the superficial liquid Reynolds number a modified Weber number $(\rho_g u_{sg}^2 / D)(\Delta\rho/\rho_g)^{1/3}$ which they termed an "effective Reynolds number for entrainment" as follows:

$$e = \tanh(7.25 \times 10^{-7} We^{1.25} Re_l^{0.25}) \quad \textbf{(2-17)}$$

They identified two different regions of entrainment namely the entrance and the quasi-equilibrium regions. Equation (2-17) applies to the latter region where the entrainment rate is balanced by the droplet deposition rate back to the liquid film. In deriving the correlation, they used an exponential relaxation function to determine the axial distance from entrance where this occurs.

2.3.3.4 Hewitt and Govan (1990) model

A non-equilibrium phenomenological model for annular flow was developed by Hewitt & Govan (1990) using air–water, air–hydrocarbon and steam–water data. This model can be used for phase change systems and also applies to developing flow near the entrance region:

$$\dot{E} = 5.75 \times 10^{-5} \dot{m}_g \left[(\dot{m}_{lf} - \dot{m}_{lfc})^2 \frac{D\rho_L}{\sigma \rho_g^2} \right]^{0.316} \text{ for } \dot{m}_{lf} > \dot{m}_{lfc} \quad \textbf{(2-18)}$$

Where $\dot{E}$ is the entrainment mass flux (in kg/m^{2}s), $\dot{m}_{LF}$ the liquid mass flux and $\dot{m}_{LFC}$ the critical liquid mass flux at the onset of entrainment. They obtained a relationship for $\dot{m}_{LFC}$ as follows:

$$\dot{m}_{LF} = \frac{\mu_l}{D} \exp\left(5.8504 + 0.4249 \frac{\mu_g}{\mu_l} \sqrt{\frac{\rho_l}{\rho_g}} \right) \quad \textbf{(2-19)}$$

2.3.3.5 Pan & Hanratty (2002)

Using the air–water data of (Andreussi & Zanelli 1979; Schadel et al. 1990; Lopez de Bertodano 1998) in 24, 25.4, 42 and 95.3 mm pipes, (Pan & Hanratty 2002) developed a linear relationship between the entrained fraction and a dimensionless parameter as follows:

$$\frac{e/e_M}{1 - e/e_M} = 6 \times 10^{-5} \left(u_{sg} - u_{gc}\right)^2 \left(\rho_g \rho_l\right)^{0.5} D/\sigma \quad \textbf{(2-20)}$$

Where u_c is the gas core velocity. $e_M = 1 - \dot{m}_{lfc}/\dot{m}_{lf}$ such that $\dot{m}_{lfc}$and $\dot{m}_{lf}$ are the critical liquid film flow rate above which entrainment occurs and the liquid film flow rate. It should be noted that e = 0 when $u_{sg} < u_c$ or $\dot{m}_{lf} < \dot{m}_{lfc}$.

2.3.3.6 Barbosa et al (2002)

Barbosa et al. (2002) observed that there is a scarcity of data on flow parameters in the transition region between churn and annular flow. In order to address this deficiency they carried out adiabatic air–water experiments in a vertical tube 10.8 m long having ID of 31.8 mm. An isokinetic probe was used to measure the entrained liquid droplet fraction at system pressures between 1.7 and 5 bara. The range of U_{sl} values covered is 0.012–0.33 m/s. With the measurements they carried out, an empirical correlation was proposed for the prediction of entrained liquid fraction at the onset of annular flow. It is as follows:

$$e = 0.95 + 342.5\sqrt{\frac{\rho_l \dot{m}_l}{\rho_g \dot{m}_g}}D^2 \quad \textbf{(2-21)}$$

The validity of Equation (5-16) is for $0.9 < u_g^* < 1.3$ where $u_g^* = u_{sg}\sqrt{\frac{\rho_g}{gD(\rho_g - \rho_g)}} \approx 1$ at the onset of annular flow; $11 < \dot{m}_l < 334$ kg m^{-2} s^{-1}. Barbosa et al. noted that data from (Wallis 1962a; Verbeek et al. 1993; Fore & Dukler 1995) from tubes of 50.8, 50.8 and 12.7 mm ID were also well correlated with Equation (5-16).

2.3.3.7 Sawant et al (2008, 2009)

A porous wall feature was used to measure *E* by (Sawant et al. 2008) in a 9.4 m vertical pipe. Building on the work of (Ishii & Mishima 1989), they correlated air–water data using Ishii & Mishima's modified Weber number, the liquid Reynolds number and the "limiting" entrainment fraction:

$$e = e_m \tanh(2.31 \times 10^{-4} Re_l^{-0.35} We^{1.25}) \quad \textbf{(2-22)}$$

Where $e = 1 - Re_{lf,lim}/Re_l$ **(2-23)**

$Re_{lf,lim}$ is the limiting liquid film Reynolds number which is a function of Re_l. As this suggests an iterative solution and the absence of satisfactory relations for $Re_{lf,lim}$, Sawant et al. (2008) correlated it with the superficial liquid Reynolds number Re_l as follows:

$$Re_{lf,lim} = 250\ln(Re_l) - 1265 \quad \textbf{(2-24)}$$

They cautioned the use of Equations (2-22)–(2-24) for fluids with surface tension and viscosities very different from air and water as this could introduce errors with unknown effects on the prediction of the transition criteria.

An improvement was proposed for Equation (2-22) by (Sawant et al. 2009) to include additional data collected for air – water and Freon-113 in 9.4 and 10.2 mm ducts and also to account for minimum liquid film flow rate at the maximum entrainment fraction as follows:

$$e = \left(1 - \frac{13N_{\mu l}^{-0.5} + 0.3\left(Re_l - N_{\mu l}^{-0.5}\right)^{0.95}}{Re_l}\right) \times \tanh\left(2.31 \times 10^{-4} Re_l^{-0.35}(We - We_{cr})^{1.25}\right) \quad \textbf{(2-25)}$$

Where $N_{\mu l}$the viscosity number is defined as $N_{\mu l} = \mu_l / \left(\rho_l \sigma \sqrt{\frac{\sigma}{g\Delta\rho}}\right)^{1/2}$ and We_{cr} is the critical Weber number at the critical velocity preceding entrainment.

2.3.3.8 Cioncolini et al (2010, 2012)

An experimental database containing 1504 data points was utilised by Cioncolini & Thome (2010) for the prediction of entrained liquid fraction in adiabatic gas–liquid annular two phase flow in vertical pipes. The database comprises of 8 different gas–liquid combinations and 19 different pipe diameters ranging from 5 to 57.1 mm. They correlated the entrained droplet fraction with a droplet laden core flow Weber number only and arrived at the following equation:

$$e = (1 + 13.18We_c^{-0.655})^{-10.77} \quad \textbf{(2-26)}$$

Cioncolini & Thome argued that the strong connection of wall shear stress/ associated frictional pressure gradient with We_c makes it a controlling dimensionless group for correlating entrained droplet in dispersed annular two-phase flow. Where

$$W_c = \frac{\rho_c u_c^2 D_c}{\sigma} \quad \textbf{(2-27)}$$

D_c is the core diameter, ρ_c is the core flow viscosity given by

$$\rho_c = (1 - \varepsilon_c)\rho_l + \varepsilon_c \rho_g \quad \textbf{(2-28)}$$

The core void fraction ε_c is given by

$$\varepsilon_c = \frac{\varepsilon}{1 + \gamma(1 - \varepsilon)} \quad \textbf{(2-29)}$$

Where

$$\gamma = E\frac{\varepsilon}{1-\varepsilon}\frac{1-x}{x}\frac{\rho_g}{\rho_l} \quad \textbf{(2-30)}$$

And the core flow velocity

$$U_c = \frac{[x + e(1-x)]\dot{m}_t}{\rho_c}\left(\frac{D}{D_c}\right)^2 \quad \textbf{(2-31)}$$

As can be seen, ρ_c and U_c are functions of *e* hence an iterative solution is required.

Because of the complicated nature of prediction using Equations (2-26)– (2-31), and in order to increase the range of prediction, (Cioncolini & Thome 2012) developed an improved correlation now including data from evaporating flows and non-circular channels. The number of data points used increased to 2293 obtained from 38 different literature sources. They have now defined We_c as follows:

$$We_c = \frac{\rho_c u_{sg}^2 D}{\sigma} \quad \textbf{(2-32)}$$

The new correlation now becomes:

$$e = (1 + 279.6We_c^{-0.8395})^{-2.209} \quad \textbf{(2-33)}$$

And a simple predictor–corrector method was used to implement the calculations required to obtain E, since E and We_c are dependent on each other.

Table 2-2: Summary of literature correlations on entrained droplet fraction

Investigator(s)	Pipe diameter ranges (mm)	Fluids	Pressure (bar)	Re_g range	Re_l range	Minimum L/D	Flow direction*	Number of data points	Correlation
Paleev & Filippovich (Paleev & Filippovich 1966)	33	Air/water				40	↑		$\frac{\dot{m}_{lf}}{\dot{m}_l} = 0.985 - 0.44\log\left[\frac{\bar{\rho}}{\rho_L}\left(\frac{\mu_L U_{sg}}{\sigma}\right)^2 \times 10^4\right]$ where $\bar{\rho} = \rho_g\left[1 + \frac{\dot{m}_l(1-\dot{m}_{lf}/\dot{m}_l)}{F\rho_g u_{sg}}\right]$
Oliemans *et al* (Oliemans et al. 1986)	9.3 – 31.8	Air/water, air/ethanol, steam/water, air/genklene	1–100	72–99600	Laminar/ turbulent	200	↑	727	$\frac{E}{(1-E)} = 10^{\beta_0}\rho_l^{\beta_1}\rho_g^{\beta_2}\mu_l^{\beta_3}\mu_g^{\beta_4}\sigma^{\beta_5}D^{\beta_6}u_{sl}^{\beta_7}u_{sg}^{\beta_8}g^{\beta_9}$ where $\beta_0 - \beta_9$ are regression constants depending on film Reynolds number ranges
Ishii & Mishima (Ishii & Mishima 1989)	9.5 – 15.6	Air/water	1–2.7		318 - 6350	n/a	↑ ↓	n/a	$E = \tanh(7.25 \times 10^{-7} We^{1.25} Re_l^{0.25})$
Hewitt & Govan (Hewitt & Govan 1990)		Air/water, air/hydrocarbon, steam/water				n/a	↑	n/a	$\dot{E} = 5.75 \times 10^{-5}\dot{m}_g\left[(\dot{m}_{lf} - \dot{m}_{lfc})^2\frac{D\rho_L}{\sigma\rho_g^2}\right]^{0.316}$ for $\dot{m}_{lf} > \dot{m}_{lfc}$ where $\dot{m}_{LF} = \frac{\mu_L}{D}\exp\left(5.8504 + 0.4249\frac{\mu_g}{\mu_l}\sqrt{\frac{\rho_l}{\rho_g}}\right)$
Pan & Hanratty (Pan & Hanratty 2002)	10.6 – 57.2	Air/water, Freon/Freon, helium/water, air/genklene	n/a	7580–65340	20 - 12900	n/a	↑	n/a	$\frac{E/E_M}{1-E/E_M} = 6 \times 10^{-5}\left(U_{sg} - U_{gc}\right)^2\left(\rho_g\rho_l\right)^{0.5}D/\sigma$ where $E_M = 1 - \dot{m}_{lfc}/\dot{m}_{lf}$
Barbosa *et al* (Barbosa et al. 2002)	31.8	Air/water	1.3–5	4000–9500	380 - 10500	283	↑	33	$E = 0.95 + 342.5\sqrt{\frac{\rho_l\dot{m}_l}{\rho_g\dot{m}_g}}D^2$ for $0.9 < U_g^* < 1.3$
Sawant *et al* (Sawant et al. 2009)	9.4	Air/water	1.2–4	345 – 2670	110–1140	n/a	↑	66	$E = E_m\tanh(2.31 \times 10^{-4} Re_l^{-0.35} We^{1.25})$ where $E_m = 1 - Re_{lf,lim}/Re_l$ and $Re_{lf,lim} = 250\ln(Re_l) - 1265$

Sawant *et al* (Sawant et al. 2008)		Air/water, helium/water, air/genklene, steam/water, Freon	1.2–69	345–29100	110–1140	400	↑	n/a	$E = \left(1 - \frac{13N_{\mu l}^{-0.5} + 0.3\left(Re_l - N_{\mu l}^{-0.5}\right)^{0.95}}{Re_l}\right) \times \tanh\left(2.31 \times 10^{-4} Re_l^{-0.35}(We - We_{cr})^{1.25}\right)$ Where $N_{\mu l} = \mu_l \Big/ \left(\rho_l \sigma \sqrt{\frac{\sigma}{g\Delta\rho}}\right)^{1/2}$
Cioncolini & Thome (Cioncolini & Thome 2010)	9 – 95	Air/water, steam/water, air/ethanol, R113, R12, He/water, air/genklene	1–70	111–266000	8700–14000	n/a	↑ ↓→	1504	$E = (1 + 13.18We_c^{-0.655})^{-10.77}$ where $W_c = \frac{\rho_c U_c^2 D_c}{\sigma}$, $\rho_c = (1 - \varepsilon_c)\rho_l + \varepsilon_c \rho_g$, $\varepsilon_c = \frac{\varepsilon}{1+\gamma(1-\varepsilon)}$, $\gamma = E\frac{\varepsilon}{1-\varepsilon}\frac{1-x}{x}\frac{\rho_g}{\rho_l}$ and $U_c = \frac{[x + E(1-x)]\dot{m}_t}{\rho_c}\left(\frac{D}{D_c}\right)^2$
	5 to 57.1	Air/water, air/ethanol, He/water, air/genklene						2293	$E = (1 + 279.6We_c^{-0.8395})^{-2.209}$ where $We_c = \frac{\rho_c U_{sg}^2 D}{\sigma}$

2.4 Modelling annular two-phase flow

Multiphase flow modelling approaches are generally classified into three categories namely: Empirical, mechanistic, and numerical (Taitel 1994). Mechanistic models estimate physical phenomena by considering the most important processes and neglecting other less important effects that can introduce complications without necessarily improving accuracy. Numerical methods aim to find rigorous solutions of the multidimensional Navier–Stokes equations, and empirical approaches make use of experimental data to find relationships between dimensionless groups. Numerical methods can give rise to detailed information of the flow such as dynamic and spatial distributions of the respective fluids, flow regime transition and some measures of turbulent effects; they are usually computationally expensive even for simple geometries and solution times can run into days or weeks. As a result, numerical methods are not suitable for day to day engineering operations; rather, they are more amenable for design. Conversely, the use of empirical correlational approaches to multiphase and indeed annular flow is popular. This method involves finding the functional relationship between dimensionless groups such as Reynolds and Nusselt numbers using experimental data. Zhao (2005) noted that excellent results can be obtained using this method, but drawbacks include the validity of correlations being limited to the data range and the fact that this method does not take into account much detail concerning the physics of the flow. The division between the various modelling approaches is not always clear cut as observed by (Taitel 1994). Also, all these methods complement each other for

example, correlations are usually required as closure relationships in mechanistic and numerical models.

2.4.1 Empirical modelling

Many correlations exist for the prediction of pressure drop and liquid holdup in two-phase flow. The most widely used are those of (Hagedorn & Brown 1965), (Duns & Ros 1963), (Aziz et al. 1972) for vertical pipes; (Lockhart & Martinelli 1949) for Horizontal pipes; and (Beggs & Brill 1973) for inclined pipelines. These empirical correlations were derived based on the general momentum equation. The general pressure gradient equation for 1-dimensional steady state flow can be written as (Brill 1987; Brill & Mukherjee 1999):

$$\frac{dP}{dz} = \rho_m g\ sin\theta + \frac{f_m \rho_m v_m^2}{2D} + \rho_m v_m \frac{dv_m}{dz} \qquad \textbf{(2-34)}$$

The right side of the equation consists of three components: the pressure gradient due to potential energy (the static pressure gradient), frictional loss and kinetic energy changes respectively; where the subscript *m* denotes “mixture”. For two-phase flow, the definition of fluids properties causes many problems. If phase “slip” (slip is with regards to the different velocities both phases travel) is taken into account, the liquid holdup should be known initially. This is defined as the volumetric ratio of the pipe segment occupied by liquid to that of the whole pipe segment. Therefore, liquid holdup is a very important parameter in pressure drop estimation, specifically in the case of vertical flow due to the effect of gravity. Usually, the friction factor is calculated using the standard Blasius correlation for single phase flow. In the past, mixture velocity was

calculated using the inlet gas–liquid ratio. Later, in order to improve accuracy, slip and/or flow pattern were also taken into account.

The Lockhart and Martinelli correlation (1949) related the two-phase pressure gradient with the single-phase gradient by a correction factor. This approach was instead of directly evaluating the friction factor. Analytically, (Taitel & Dukler 1976) demonstrated that the holdup and dimensionless pressure drop for stratified flow were unique functions of the Lockhart-Martinelli parameter X under the assumption that the ratio of gas friction factor at the pipe wall to that at the gas–liquid interface was constant. This assumption was shown to be consistent with experimental data. Recently, not many correlations have been developed for liquid holdup prediction, flow regime transition and pressure gradient. Instead, some of the earlier correlations were modified for new applications. A few instances follow.

Chien (1990) collected wet steam flow regime data in horizontal pipes and using Taitel & Dukler's method, predicted regimes for two-phase flow. Abdul-Majeed (1993) developed a new liquid holdup correlation for all pipe inclinations and flow regimes. Bilgesu & Ternyik (1994) developed a new multiphase flow model for vertical, inclined, and horizontal pipes and wellbores using a modified Beggs and Brill (1973) method. Two new correction factors were introduced which were correlations from experimental data in order to modify the holdup correlation. The first equation considers pressure changes along the pipe while the second was developed as a simple function of two-phase Reynolds number. Friction factor is another important parameter that enhances pressure drop predictions. Recent correlations may be classified into those that derive two-

phase friction factor based on homogeneous fluid properties (e.g. Klausner et al. 1991; Dalkilic et al. 2008; Cioncolini et al. 2009b) and those focussed on the interfacial friction factor (e.g. Asali et al. 1985; Fukano et al. 1991; Fukano & Furukawa 1998; Fore et al. 2000). All these were arrived by regressing a lot of experimental data for air/water, steam/water, air/oil, air/glycerol, water/hydrocarbon, and refrigerant mixtures.

Artificial neural network methods are being increasingly applied to a large number of real world problems of substantial complexity including multiphase flow regime identifiers. They are excellent pattern recognition tools and robust classifiers with the ability to come up with generalized descriptions of seemingly random input. Examples of such are (Cai et al. 1994; Ternyik et al. 1995a; Ternyik et al. 1995b; Tsoukalas et al. 1997; Osman 2001; Tambouratzis & Pázsit 2009; Tambouratzis & Pàzsit 2010; Liu & Zhang 2010; Bar et al. 2015). Cai et al. (1994) applied a self-organizing neural network to identify flow regimes in horizontal air-water flow. Ternyik (1995a, 1995b) utilised artificial neural networks for the combined prediction of liquid holdup, flow regime, pressure drop and optimal design of pipelines under multiple circumstances. They maintained that the fundamental problem with conventional approaches is the inherent sequential rather than parallel information processing methods in correlation development. They claimed this method performed better than traditional correlations. Osman (2001) developed a new model for identifying different flow regimes and predicting the holdup of horizontal gas-liquid flow. The model was based on a three-layer back-propagation neural network algorithm. The model well classified slug, annular, and stratified flow. Osman's

showed that removing liquid holdup from the neural network inputs did not bring about a huge loss of accuracy. Tambouratzis & Pázsit (2009, 2010) used ANN by feeding neutron radiography images of coolant two-phase flow for regime identification. Features of the photographs were extracted and fed as input to an ensemble of self-organising maps whose outputs demonstrate quite quickly, accurate regime classification. Artificial neural networks are adaptive; they learn from the data and simplify things learned. They extract the essential characteristics from the numerical data instead of memorizing all of it thereby offering a convenient technique of data reduction in addition to providing an implicit model without having to obtain a conventional, physical model of the fundamental phenomenon. Contrary to traditional models, which are rich in theory but poor in data, the neural networks are rich in data but poor in theory in that little or no previous knowledge of the system is required.

2.4.2 Mechanistic modelling

Mechanistic models for two-phase flow have been constructed for many phenomena such as film thickness in annular flow, bubble translational velocity in bubbly and slug flow, and of course pressure drop. (Kosky 1971) derived an expression for liquid film thickness from Prandtl's 1/7th power law velocity profile:

$$u^+ = 8.74 y^{+\frac{1}{7}} \quad \textbf{(2-35)}$$

Where u^+ is the velocity parameter defined as $u^+ = u\sqrt{\rho/\tau}$, with u and τ being the liquid film velocity at distance y^+ from the wall, and τ the shear stress within the liquid film; y^+ is the friction distance parameter given by $y^+ = (\rho y/\mu)\sqrt{\rho/\tau}$.

The mass flow rate per unit wetted perimeter of the thin liquid film is approximately given by

$$\dot{m}_{lf} = \rho_l \int_0^t u \, dy \qquad \textbf{(2-36)}$$

where t is the liquid film thickness. From definition, the liquid film Reynolds number is given as $Re_{lf} = 4\dot{m}_{lf}/\mu_l$ and combining it with Equation **(2-36**) yields:

$$Re_{lf} = 4 \int_0^t u^+ \, dy^+ \qquad \textbf{(2-37)}$$

Now substituting Prandtl's 1/7th law velocity profile law for turbulent films where $Re_{lf} > 1000$ or $t^+ \equiv \left(\frac{\rho t}{\mu}\right)\sqrt{\frac{\rho}{\tau}} > 25$, into Equation **(2-37**) and integrating gives the model for predicting the dimensionless liquid film thickness explicitly as a function of Re_{lf} as follows:

$$t^+ = 0.0504 \, Re_{lf}^{0.875} \qquad \textbf{(2-38)}$$

It is noted that though Kosky's film thickness model is mechanistic, it is still dependent on an empirical velocity profile.

A common mechanistic model that has been used for pressure and holdup prediction by many investigators is the two fluid model where the liquid and gas flowing in the pipe are treated as two different fluids with focus on average quantities for the parameters. This is a simplified form of the Navier –Stokes momentum equations and in the one-dimensional transient form, it is as follows (Taitel 1994):

Momentum equation for the liquid phase:

$$\frac{\partial}{\partial t}(\rho_l A_l u_l) + \frac{\partial}{\partial z}(\rho_l A_l u_l^2) - \Gamma_l A\widehat{U} = -\tau_l S_l + \tau_i S_i - \rho_l A_l g sin\theta - \frac{\partial}{\partial z}(\rho_l A_l) + P_l \frac{\partial A_l}{\partial z} \quad \textbf{(2-39)}$$

And that for the gas phase:

$$\frac{\partial}{\partial t}(\rho_g A_g u_g) + \frac{\partial}{\partial z}(\rho_g A_g u_g^2) - \Gamma_g A\widehat{U} = -\tau_g S_g + \tau_i S_i - \rho_g A_g g sin\theta - \frac{\partial}{\partial z}(\rho_g A_g) + P_g \frac{\partial A_g}{\partial z} \quad \textbf{(2-40)}$$

Where Γ is the rate of gas or liquid produced per unit volume; $\Gamma > 0$, $\widehat{U} = U_l$ for condensing flows $\Gamma < 0$, $\widehat{U} = U_g$ for evaporating flows such that $\Gamma_l = -\Gamma_g$, and $\Gamma = 0$ in adiabatic conditions. S_i, S_l, and S_g are respectively the perimeters of the gas–liquid interface, liquid–pipe wall, and gas–pipe wall boundary (for stratified flow).

Another approach of the multi-fluid model also exists where a third equation is added to Equations **(2-39**) and **(2-40**) for the droplet phase. This approach is useful where significant amounts of droplets are entrained in the gas core and is the common practice with nuclear reactor core thermal hydraulics modelling. Investigators such as (Stevanovic & Studovic 1995; Alipchenkov et al. 2002; Stevanovic et al. 2007; Alipchenkov et al. 2004; Mikielewicz et al. 2011) used this formulation. (Bendiksen et al. 1991) extended this method for use in the oil and gas industry and is the basis for the flow simulator OLGA.

Despite significant simplification, (Taitel 1994) remarked that the use of the two or three fluid model for the solution of practical problems is difficult. The most severe problem is that it needs as an input geometrical estimations and constitutive relations (empirical correlations) that relate the shear stresses to the

local velocities. These relations depend on the flow regime. Furthermore, other basic mathematical problems with the model exist as the formulation is not always well posed.

Simplifications of the multi-fluid model are in widespread use for annular and stratified flow patterns. (Oliemans et al. 1986; Shoham 2006; Vieira et al. 2015) used a steady state version for the annular flow regime where the time derivative vanishes, inclination angle $\theta\ is\ 90^{\circ}$, $\Gamma = 0$, and single phase gas core flow with no entrainment is assumed. The result is a version of the two-fluid model that has been used by many investigators (Taitel & Dukler 1976; Oliemans et al. 1986; Xiao et al. 1990; Alves et al. 1991; Taitel 1994; Gomez et al. 1999; Petalas & Aziz 2000; Vieira et al. 2015); it is given as:

$$-A_l\left(\frac{\partial P}{\partial z}\right)_l - \tau_l S_l + \tau_i S_i + \rho_l A_l g = 0 \qquad \textbf{(2-41)}$$

$$-A_l\left(\frac{\partial P}{\partial z}\right)_g - \tau_i S_i + \rho_g A_g g = 0 \qquad \textbf{(2-42)}$$

In order to improve the accuracy of pressure drop estimations, other researchers account for droplet entrainment albeit not as a separate phase but as part of a homogeneous core mixture consisting of averaged liquid droplet and gas phase densities. Following this approach, Equation **(2-42**) is replaced with:

$$-A_c\left(\frac{\partial P}{\partial z}\right)_c - \tau_i S_i + \rho_c A_c g = 0 \qquad \textbf{(2-43)}$$

Where $\rho_c = \rho_g \varepsilon + \rho_l(1-\varepsilon)$, with ε being the void fraction, is the form of homogeneous core density favoured by most authors. Others like (Cicchitti et al. 1960; Ghajar 2005) prefer the reciprocal mean homogeneous density:

$\frac{1}{\rho_c} = \frac{\varepsilon}{\rho_g} + \frac{(1-\varepsilon)}{\rho_l}$. A common assumption made is that the pressure drop is constant at each axial cross-section. This equates the gas phase or core pressure drop with that of the continuous liquid phase hence eliminating the pressure term in Equations **(2-41**) and **(2-43**) yielding a combined momentum equation. For annular flow this takes the form:

$$-\tau_i S_i \left(\frac{1}{A_l} + \frac{1}{A_c}\right) + (\rho_l - \rho_c)g - \tau_w \frac{S_l}{A_l} = 0 \qquad \textbf{(2-44)}$$

Where τ_w and τ_i are the wall, and interfacial shear stresses respectively defined as follows:

$$\tau_w = \frac{1}{2} f_l \rho_l u_{lf}^2 \qquad \textbf{(2-45)}$$

$$\tau_i = \frac{1}{2} f_i \rho_c u_c^2 \qquad \textbf{(2-46)}$$

The liquid friction factor f_l is calculated using the correlation of Blasius:

$$f_l = 0.046_l Re_{lf}^{-0.2} \qquad \textbf{(2-47)}$$

Where the liquid film Reynolds number $Re_{lf} = \frac{\rho_l u_{lf}}{\mu_l} \frac{4t(D-t)}{D}$, t being the liquid film thickness assumed uniform. From mass balances, (Vieira et al. 2015) showed that the film velocity can be determined from the superficial liquid velocity, liquid film thickness and droplet entrainment fraction (e) as follows:

$$u_{lf} = \frac{u_{sl} D^2}{4t(D-t)}(1-e) \qquad \textbf{(2-48)}$$

The inferfacial friction factor is also estimated by Blasius equation using a core flow Reynolds number calculated based on the core velocity:

$$f_i = 0.046_l Re_c^{-0.2} \qquad \textbf{(2-49)}$$

Also, the core velocity is similarly calculated:

$$u_c = \frac{(u_{sl} + u_{sg}e)D^2}{(D-t)^2} \quad \textbf{(2-50)}$$

Where the liquid film Reynolds number $Re_c = \frac{\rho_c u_c}{\mu_c}$. In many cases, the gas velocity has been used in place of the core flow velocity, but with the core density and viscosity being averages of the gas and droplet values.

Supplying the shear stresses, together with geometrical relations for S_i and S_l into Equation **(2-44)**, a relation implicit in *t,* the film thickness is obtained which is iteratively solved. Once this is done, the pressure drop is calculated from any of Equations **(2-41)**–**(2-43)**.

2.4.3 Numerical modelling

The basis of numerical modelling approaches in two-phase flow is the two-fluid model established by (Wallis 1969b; Ishii 1975) which is a simplified form of the Navier–Stokes equation applied to the two fluids. The equations are expressed in terms of two sets of governing mass, momentum and energy equations for each phase with appropriate averaging of local instant variables. As the average fields of one phase are dependent on that of the other, interaction terms are also included. For many practical uses, the model advanced by (Ishii 1975) as reported by (Zhao 2005) can be expressed in simplified form as follows, giving the continuity and momentum equations respectively:

$$\frac{\partial \alpha_k \rho_k}{\partial t} + \nabla \cdot (\alpha_k \rho_k \bar{v}_k) = \Gamma_k \quad \textbf{(2-51)}$$

$$\frac{\partial \alpha_k \rho_k}{\partial t} + \nabla \cdot (\alpha_k \rho_k \bar{v}_k \bar{v}_k) = -\alpha_k \nabla P_k + \nabla \cdot \alpha_k (\bar{\bar{\tau}}_k - \bar{\bar{\tau}}_k{}') + \alpha_k \rho_k \vec{g} + \vec{v}_{ki}\Gamma_k + \bar{M}_{ik} - \nabla \alpha_k \cdot \tau_i \quad \textbf{(2-52)}$$

Where Γ_k , $\bar{M}_{ik}$, τ_i , $\vec{v}_{ki}$, α_k , ρ_k , $\vec{v}_{ki}$, P_k , are the mass generation, generalised interfacial drag (i.e. sum of interfacial forces: drag, lift, virtual mass, etc.), interfacial shear stress, void fraction, density, interfacial velocity, and pressure of phase k ; $\bar{\bar{\tau}}_k$ and $\bar{\bar{\tau}}_k{}'$, denote the mean viscous, and turbulent stresses respectively.

Strategies for solving Equations **(2-51)** and **(2-52)** are the subject of Computational Fluid Dynamics (CFD) studies where the numerical solution is achieved by discretising both the space and time derivatives and providing suitable initial and boundary conditions. In the pre-processing stage, the geometry is made first, then meshed into discrete cells. The simulations are performed where an appropriate method (finite difference, finite element, etc.) is used to iteratively solve the problem at the node of each cell. A postprocessor is used to analyse the solution and visualise it.

2.5 Earlier empirical modelling studies on annular two-phase flow

2.5.1 Review of empirical modelling works on downwards flow interfacial friction factor

A large number of studies have been carried out on vertical air–water two-phase annular flow in pipes. This is not surprising considering the huge importance annular two-phase flow plays in the nuclear, chemical and petroleum industries where it is generally agreed to be one of the most frequently encountered flow patterns. To this end, many studies have been commissioned to investigate annular two-phase flow phenomena with the bulk of published works focussing on co-current upward annular flow. In sharp contrast there have been far fewer studies published on co-current downward annular two-phase flows. This is against the backdrop that co-current downward

annular two-phase flow is also often encountered in engineering equipment such as gas absorbers as falling film flow, gas condensate pipelines, refrigeration systems, and in heat transfer equipment like boilers and heat exchangers. What little work is available is dominated by pipes of which the scales are much less than 100 mm in internal diameter. It has been noted that there is no guarantee that the use of models developed for these small pipes will predict large diameter flows well; therefore several reported studies (Oliemans et al. 1985; Kataoka & Ishii 1987; Omebere-Iyari 2006; Omebere-Iyari & Azzopardi 2007; Kaji & Azzopardi 2010; Peng et al. 2010; Lao et al. 2012; Schlegel et al. 2012) have addressed that there is need to expand the knowledge of multiphase flow behaviour to large diameter pipe systems. For example, Oliemans et al. (1985) compared entrainment correlations with large diameter test data and concluded there is not much confidence in the predictive value of the correlations. Kataoka & Ishii (1987) showed that the application of the conventional drift flux model for pool void fraction prediction to relatively large vessels was only limited to low gas fluxes, and thus had to develop a new correlation for such large systems when annular flow for instance occurs at higher gas fluxes. Disturbance waves which greatly contribute to wall shear stress and are a source of entrained droplets were observed by Azzopardi et al. (1982) to be incoherent in large diameter pipes. Careful observations revealed that in large pipes, the waves were not perpendicular to the flow direction but were curved “bow waves”. This is in sharp contrast to what is obtained in smaller tubes where the waves are continuous around the tube circumference. The study by Omebere-Iyari & Azzopardi (2007) on disturbance wave velocity

provided a strong quantitative indication of pipe diameter effect on the gas–liquid interface behaviour. They established that Pearce's coefficient, which is proportional to wave velocity, increases with pipe diameter such that its value of 0.9 remains fairly constant at large pipe diameters.

The interfacial friction factor has been likened to surface roughness in single-phase fluid flow (Bergelin et al., 1949; Hewitt & Hall-Taylor, 1970). In addition to the wall or skin friction in two-phase flow, interfacial friction as a result of slip between the two phases contributes to the frictional pressure loss. Therefore, the contribution of interfacial friction to the two-phase frictional component increases with increasing slip velocity or as the flow pattern moves from bubbly to annular flow. Klausner et al. (1991) pointed out that the correlations of Henstock & Hanratty (1976); Andreussi & Zanelli (1978); and Asali et al. (1985) are the only reported works that proposed relations for determining the downwards interfacial friction factor. Since then, Hajiloo et al. (2001) and Dalkilic et al. (2008) have developed downflow two-phase friction factor correlations, of which the former correlated data obtained from four different tube diameters ranging from 15.6–41.2 mm. The latter used data obtained for refrigerant HFC-134a in an 8.1 mm diameter vertical tube-in-tube heat exchanger and correlated the two-phase friction factor with an equivalent Reynolds number obtained as a function of gas quality and fluid density ratios. The physical correlating parameters used by Hajiloo et al. (2001) using the friction length parameter and gas Reynolds number are similar to that earlier used by Asali et al. (1985). This method will further be extended in the present work using data obtained from a 101.6 mm large internal diameter pipe and it is

envisaged to improve interfacial friction factor predictions for co-current downward air–water annular flow in large vertical pipelines.

A number of empirical friction factor correlations have been put forward by prior investigators. Literature is replete with such correlations proposed for upward gas–liquid flow; however, some recommendations have been made for downward gas–liquid flow systems. The fluid combination used in most cases is air and water. Early downward co-current two-phase friction factor correlations were obtained by Chien & Ibele (1964) and Fedotkin et al. (1979). Hajiloo et al. (2001) noted that the results of the former study show appreciable qualitative agreement of the liquid and gas flow rates such that for a certain pipe diameter, the friction factor, *f* , always increases with increasing liquid flow rate but at some point, there is a decrease with increasing gas flow rate. This is also true when the friction data of Bergelin et al. (1949), Chung & Mills (1974), and Tishkoff et al. (1979) is plotted against Re_G the superficial gas Reynolds number. The correlation of Fedotkin et al. (1979) is not consistent with the others as it shows progressive decrease in the magnitude of *f* with increasing Re_G. Conversely, there is generally poor quantitative agreement between these studies. It might be partly due to that the different tube sizes used by each set of investigators greatly affected any agreement.

Table 2-3: Summary of previous experimental research on downward co-current interfacial friction factor (All test fluids are air/water at near atmospheric system pressures except where stated)

Reference	D (mm)	Re_g range	Re_l range	L/D ratio	Measurement made
Bergelin et al. (1949)	25.4	3100-65000	0-10,000	130	ΔP
Chien & Ibele (1964)	50.8	28000-350000	1250-22000	63	ΔP, t*
Ueda & Tanaka (1974)	28.8	185-13500	6,000-100000	63	ΔP
Tishkoff et al. (1979)	28.6	15800-86400	4040-18600	64	ΔP,t
Chung & Mills (1974)**	20.5	8000-30000	0-8030	77	ΔP
Fedotkin et al. (1979)	30	6000-30000	2000-30000	79	ΔP,t
Henstock & Hanratty (1976) [+]	25.4, 50.8, 63.5	5000-255000	20-15,100	n/a	ΔP, t, E
Asali et al. (1985) [+]	22.9, 42	n/a	20-3000	41-75	ΔP,t
Fukano et al. (1991)	10,16,26	12780-99217	70-2900	269-700	ΔP, H_L*
Hajiloo et al. (2001)	15.6, 20.3, 34.2, 41.2	3400-21600	5100-27200	43-80	ΔP
Present	101.6	8400-187000	11300-113300	49	ΔP, t

*Where ΔP represents pressure drop; t film thickness; and H_L liquid holdup
**Fluids used are water and carbon (IV) oxide
[+] Re_{LF} is based on wetted pipe cross-section not Re_L based entire pipe diameter (superficial)
[†] Fluids used are refrigerant R11 and air-glycerine mixtures
[‡] Fluid used is pure refrigerant HFC-134a during condensation

The correlations found to date factored in the effect of pipe diameter, however, as will be shown later, they do not provide satisfactory enough predictions for pipes of 100 mm and over – the so-called large diameter pipes. The summary in Table 2-3 gives details of previous studies of *f* with the tube diameters given, together with the fluid velocity and Reynolds number ranges.

2.5.2 Review of downwards annular flow pressure behaviour

Pressure gradient is an important parameter in both single and multiphase flows. It quantifies pressure losses along a given length of pipe for a particular fluid or combination of fluids and hence, together with the required head to be

overcome, determines minimum pumping requirements. Therefore, accurate prediction of the pressure gradient is critically important for energy efficient designs of two-phase flow systems and their operation. In annular flow, pressure gradient is directly related to the liquid film flow on the pipe walls, which interacts with the flowing gas at the pipe core. This interaction brings about intricate wave motion at the gas–liquid interface thus complicating exact analytical description of pressure gradient with respect to the liquid film. As a result, the past decades has seen numerous empirical correlations proposed in a wide variety of studies. Nevertheless, these studies were not carried out in pipes for dimensionless hydraulic diameter defined by Schlegel et al. (2012) as:

$$D_H^* = \frac{D_H}{\sqrt{\sigma / g(\rho_l - \rho_g)}} \geq 40 \qquad \textbf{(2-53)}$$

In other words pipes of $D_H^* \geq 40$ (equivalent to about 100 mm internal diameter for water/air flows) considered to be 'large diameter' pipes, been shown in past studies not to be able to maintain large Taylor bubbles that bridge the entire tube cross-section. Kataoka & Ishii (1987) (who observed the transition between large and small pipes occurred at $D_H^* = 30$) noted that large bubbles are highly deformed in bubbling and pool boiling in large diameter vessels. Schlegel et al. (2012) and Smith et al. (2012) explained that responsible for this is the Raleigh–Taylor instability which causes larger bubbles to be broken down into many smaller spherical cap bubbles. Subsequently, additional turbulence is introduced by bubble drag as well as strong flow recirculation.

Hence, as identified by Peng et al. (2010) the hydrodynamics of the flow in such large pipes are completely changed from those of $D_H^* < 40$. They declared that

flow regime transition criteria have to be altered since different physical phenomena in this case dictate the transition mechanisms. Peng and co-workers then showed that the Hewitt & Wallis (1963) and Wallis (1969) criterion for transition to annular flow (i.e. $u_g^* = u_{sg}\sqrt{\rho_g/[gD(\rho_l - \rho_g)]} \approx 1$) is not achieved at the same gas superficial mass flux ($\rho_g u_g^2$) in different pipe scales. Data obtained for a small diameter pipe of 32 mm from the work of Barbosa et al. (2002), $\rho_g u_g^2$ was found to be approximately 600, for 67 mm pipe, it was found to be 1000, while for 100 and 150 mm pipes the value was constant at 1050 suggesting a boundary between large and small pipe behaviour. They went on to demonstrate that flow regime transition can be observed by slope change in dimensionless pressure gradient profiles against dimensionless gas velocity u_g^*.

In fact, as shown previously such pressure drop analysis has previously been used to study flow regime transitions. Hewitt (1986) described that at low gas flows (i.e. low void fractions), the total pressure gradient decreases with gradual increase in gas flow. This decrease in total pressure gradient is as a result of a reduction in the gravitational pressure gradient component. The flow regimes in this situation transit from bubbly to plug or slug flow. However, a minimum is reached at churn flow conditions with increasing contribution of the frictional component to the total pressure gradient. The pressure gradient then passes through a maximum as the flow goes from churn to annular and decreases with increasing gas flow rate in a regime termed “churn – annular flow”. Another minimum is achieved with increasing gas flow with even more contribution of

the frictional pressure gradient. Within the annular flow regime, a second maximum/minimum occurs at very high gas rates.

Flow regime transition associated with pressure gradient slope change has also previously been observed by (Chien & Ibele 1964; Ueda & Tanaka 1974). Chien & Ibele observed this change in annular downflow where there is a transition between annular and annular mist flow. No maximum or minimum occurs, only a noticeable change to a more positive slope occurs.

In the case of Ueda & Tanaka (1974), pressure gradient and flow regime transition were indirectly linked by way of friction factor plots. A maximum is observed at all liquid flow rates (or Reynolds numbers) within a small gas Reynolds number range. This slope change from positive to negative was also observed at the same gas phase Reynolds number range for the disturbed wavy layer film thickness.

Overall, in the aforementioned studies, flow regime transition was monitored by pressure gradient slope changes. It is however worthy to note that none of the studies catered for high gas flows in large diameter pipes which are prevalent in transport pipelines for gas condensates and pipes in boiling water reactor (BWR) nuclear power plants.

2.5.3 Review of upwards two-phase flow friction factor modelling

A large number of experimental studies have been carried out on vertical air–water two-phase annular flow in pipes. This is due to the importance annular two-phase flow plays in the nuclear, chemical and petroleum industries where it is generally agreed to be one of the most frequently encountered flow patterns.

In investigating annular two-phase flow, the bulk of published works focussed on co-current upward annular flow in small diameter pipes, mostly less than 50 mm in internal diameter. In sharp contrast there have been far fewer studies published on annular two-phase flow in large diameter pipes. This is against the backdrop that annular two-phase flow in large pipes is often encountered in engineering equipment such as gas absorbers, gas condensate pipelines, and in heat transfer equipment like boilers and heat exchangers. It has been noted that there is no guarantee that the use of models developed for these small pipes will accurately predict large diameter flows; and several authors (Oliemans et al. 1985; Kataoka & Ishii 1987;Omebere-Iyari 2006; Kaji & Azzopardi 2010; Peng et al. 2010; Lao et al. 2012; Schlegel et al. 2012) have addressed the need to expand the knowledge to large diameter pipe systems. The contribution of interfacial friction to the two-phase frictional component increases with increasing slip between the phases. Early studies correlated the interfacial friction factor to the ratio of the average wave height to pipe diameter, which has been likened to surface roughness in single-phase flow (e.g. Bergelin et al., 1949; Hewitt & Hall-Taylor, 1970). The interfacial friction factor correlations of Wallis (1969); Moeck (1970); Asali et al. (1985); Fukano & Furukawa (1998); Wongwises & Kongkiatwanitch (2001) among others are based on data from small pipes. It will be shown that these do not sufficiently model interfacial friction factor data in pipes greater 100 mm internal diameter. Hence a new correlation of upflow friction factor will be proposed based on data from pipes of 101.6 mm and 127 mm which improves interfacial friction factor predictions for co-current air–water annular flow in large vertical pipelines.

2.5.4 Review of previous studies on large diameter annular two-phase flow

As earlier stated, studies conducted on gas–liquid annular two-phase flow in large diameter pipes is scarce. Most of the previous reported works (using pipes of diameter between 101–480 mm) were conducted for bubbly to churn flow regimes, i.e. low gas flow rates. This may not be unconnected to the fact that gas–liquid annular two-phase flow experiments require high gas fluxes in large tube, hence a massive air delivering capability. Of the few studies found, bubbly flow dominates. Only a handful were for vertical upwards annular flow (as shown in Table 2-4), with vertical downwards annular flow works in large diameter pipes not reported in the open literature.

Studies found for upwards annular flow are for diameters between 101.6 and 127 mm for Zangana (2011) and Skopich et al. (2015) who worked on air/water upflow annular flow in vertical pipes of 127 and 101.6 mm internal diameters respectively. Their experiments fall in the annular flow regime. Zangana made simultaneous measurements of wall shear stress, liquid film thickness, and pressure gradient. He observed that the onset of annular flow occurred at the same dimensionless gas velocity as in smaller pipes and that the total pressure gradient for given liquid and gas superficial velocities fall as the pipe diameter increases.

Similarly, Skopich et al. (2015) measured time averaged pressure gradient, and cross-sectionally averaged liquid film thickness for liquid loading studies in gas transport pipes. Liquid holdup measurements were made using the quick closing valve method in the middle of the 15.4 m long test section. They

reported that inconsistencies observed between experimental pressure gradient, liquid holdup and mechanistic model predictions are due to inaccurate flow regime predictions resulting from the different regime transitions occurring at different pipe scales.

Table 2-4: Summary of annular flow large diameter works

Study	D (mm)	L/D to sensor (s)	Flow Regime	Measurement (s)	P (bara)	Re_g range	Re_l range	Flow direction	No. points
Hills (1976)	150	70	Bubbly–Churn	*α (void fraction)*	1	5500–34000	80000–440000	↑	n/a
Azzopardi et al. (1982)	125	40	Annular	*E*	1.30	195000–336000	700–2880	↑	19
Hashemi et al. (1986)	305	9.4	Bubbly–churn	*α*	1	n/a	n/a	↑	n/a
Ohnuki et al. (1995 – 2001)	200, 480	60	Bubbly–churn	*α*	1–2	129–62000	22000–1000000	↑	58
Shoukri et al. (2003)	200	43	Bubbly	*α, ΔP*	1	258–1290	0–89000	↑	24
Ali (2009)	254		Bubbly	*α, ΔP*	1	2900–36500	50000–312000	↑	130
Zangana (2011)	127	60, 62	Churn–Annular	τ_w, *t, ΔP*	3	48460–399800	1536–16452	↑	110
Smith et al. (2012)	102, 152	5– 30	Bubbly–Churn	*α*	1–5	980–900000	16000–800000	↑	95
Schlegel et al. (2012)	102, 152	34	Bubbly–Churn	*α, ΔP*	1–5	980–900000	16000–800000	↑	33
Van der Meulen (2012)	127	83	Churn–Annular	*E, t*	1.15	67000–147500	637–2861	↑	31
Skopich et al. (2015)	101.6	58–92	Annular	H_L, *ΔP*	1.2	55570–164780	877–4300	↑	20

Azzopardi and co-workers carried out their measurements in a 125 mm diameter vertical tube at AERE Harwell with the fluids (air and water) flowing concurrently upwards. Entrained liquid droplet fraction was measured indirectly by extracting the liquid film through a porous wall feature thereby obtaining the liquid film flow rate.

Van der Meulen (2012) performed experiments at 2 bar pressure in the vertical 127 mm internal diameter pipe at the University of Nottingham. Measurements were made for the liquid film thickness using conductance ring probes.

Measured liquid film velocities at different superficial liquid velocities were also obtained from which entrained droplet fraction calculations were made.

Based on the literature review conducted above, studies/data on bubbly–churn flow in large pipes are in relative abundance in comparison to annular flow. In fact no published study was found that explicitly treated theoretical or empirical modelling for large diameter pipe film thickness, or friction factor prediction. This is despite ample experimental evidence revealing a difference in behaviour between the different pipe scales.

2.6 Summary of the literature review

From the foregoing, the following could be adduced from the literature reviewed:

- Flow pattern maps in existence are mainly based on observations of flow in small diameter pipes, and it is unclear if their regime transitions are representative of larger pipe behaviour
- Reported studies for annular flow in large pipes are scarce in the open literature and more work needs to be done to improve understanding including mechanisms involved and ameliorate the unavailability of data for design and operation
- While mechanistic and CFD approaches capture the physics of the flows, correlational or empirical methods provide quite accurate results on flow behaviour and is still a widely used approach.

Chapter Three

EXPERIMENTAL

3.1 Description of Serpent Rig flow loop facility

3.1.1 Test sections and metering

The experimental apparatus is schematically shown in Figure 3-1. Air and water are the test fluids. Air filtered and chilled, is supplied via an 8-m^3 receiver tank to the test section by two compressors GA55 and GA75 connected in parallel to deliver a maximum 1200 Sm^3/h at 7.5 barg pressure. The air flow rate is regulated by automated pneumatic valves controlled at the DeltaV Plant Automation system. Water is supplied to the test rig from a 1.2 m^3 storage tank and pumped using a Grundfos CRE3-26 variable speed pump delivering a maximum flow rate 10 litre/s at 6 barg. After mixing both phases flow into the test section of the flow loop through two inverted U bends on either side of an upright U-bend before being separated so that the water is recirculated while the air is vented off. A detailed description of the Serpent Rig facility is given in (Almabrok 2014). The key components of the rig with respect to this study are the downward flowing section to the right of the upright U-leg, and the upwards section to the left.

Each of these test sections include a liquid film sensor spool used for measuring liquid film thickness at four different circumferential positions, and a clear section for visual flow observation. All straight sections in the test facility were made from ABS plastic. The test facility is rated at 10 barg at the ambient temperature conditions. In addition two PT100 temperature sensors, T_1 and T_2,

with an accuracy of within ±0.5% are used to measure the water and air/water mixture temperatures, respectively.

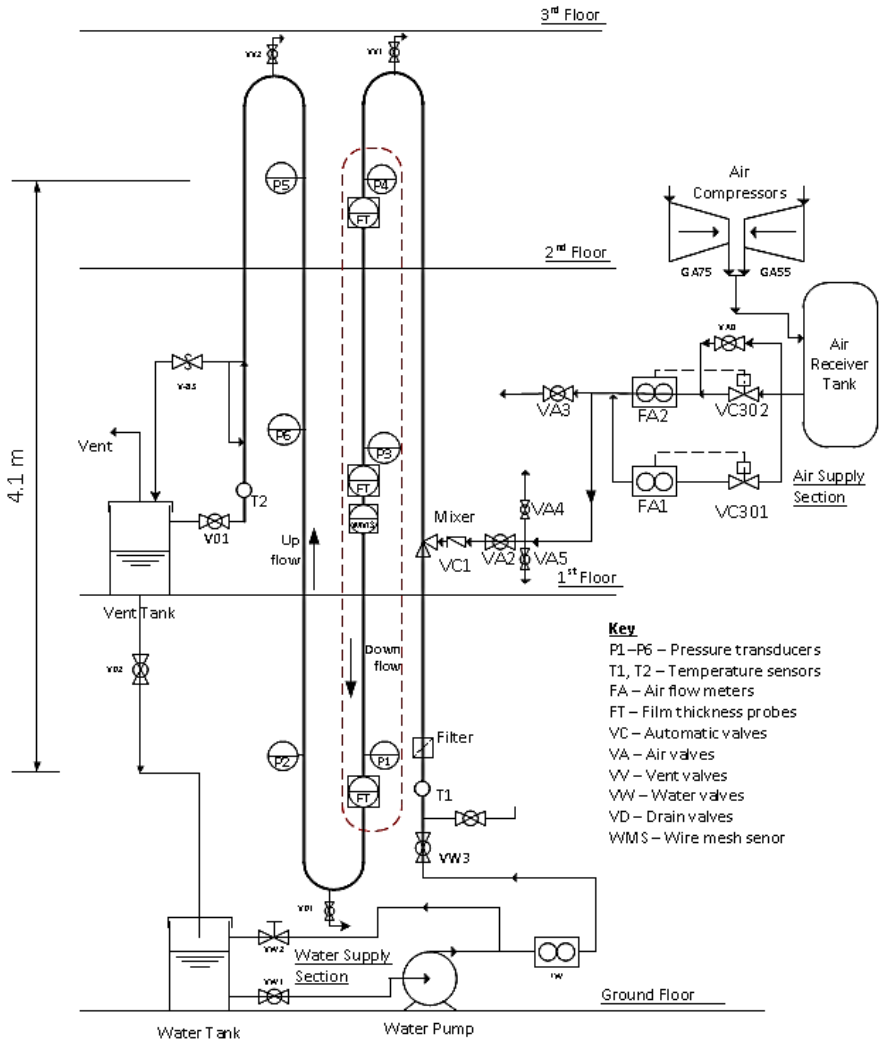

Figure 3-1: Experimental serpent rig flow loop

3.1.2 Instrumentation

3.1.2.1 Pressure transducers

Three UNIK 5000 GE Sensing pressure transducers are installed namely P_1 to P_5 along the upwards and downward flow sections as shown in which measure with a range of 0–1.5 barg and an accuracy of ± 0.02%.

3.1.2.2 Conductance film thickness probes

Four film thickness probes are mounted on a probe spool is shown in Figure 3-2 (a) and (b). The spool consists of four film conductivity sensors which are spaced 90° from each other to measure the circumferential distribution of the liquid film thickness at the pipe axial location where the spool is installed.

As shown in Figure 3-2 (c), the sensing part of the conductivity film thickness probe comprises a 10 mm diameter stainless steel rod and a stainless steel sleeve (18 mm outer diameter by 2 mm wall) arranged concentrically. Between them is a 2 mm thick insulation layer. The end of the sensor is flushed with the inner surface of the spool. Each conductor is in electrical contact with the liquid film as it flows over them, such that a conductive bridge forms. The conductivity between the two conductors changes with the thickness of the water film.

For precise measurements, calibration of the film thickness sensors was carried out by using acrylic blocks of different diameters concentrically inserted into the probe spool to produce a liquid layer of known thickness. The temperature variations against the voltage output were also identified and considered to perform accurate film measurements. The correction of temperature was applied for a range of 10–26°C, covering the range of experimental fluid temperatures. Tests on the repeatability of these liquid film sensors and pressure drop measurements were carried out by Almabrok (2014) and it was showed that an uncertainty of 0.1 mm can be attained for measuring a film thickness up to 3 mm, therefore giving an error margin of ±3.3%.

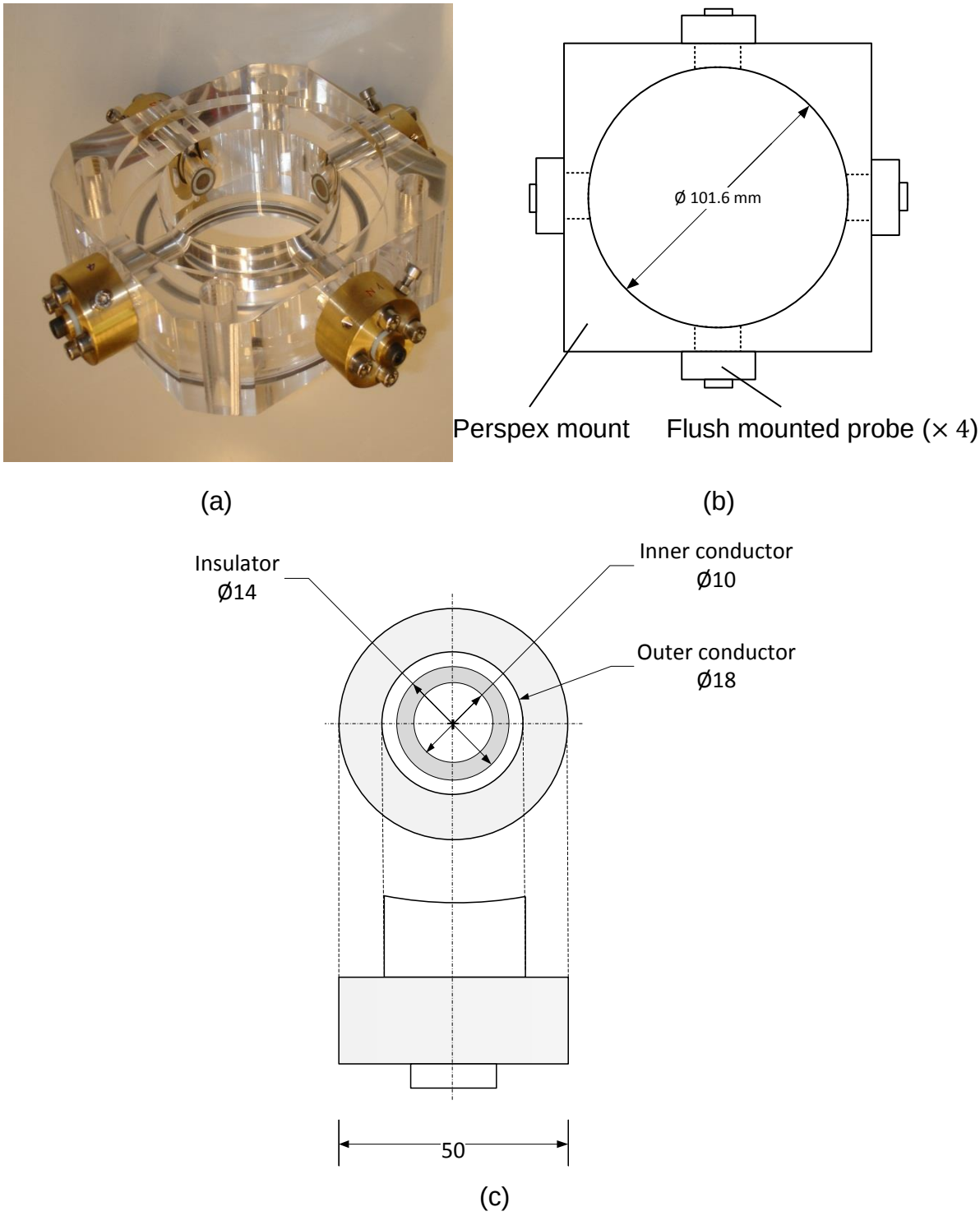

Figure 3-2: Conductivity liquid film thickness sensor (a) Photograph showing sensor spool with four flush mounted probes (b) Schematic of sensor spool (c) Details of individual probe design (All dimensions in mm)

3.1.2.3 Capacitive Wire Mesh Sensor

A 32×32 WMS, as shown in Figure 3-3, is used for air-water cross-sectional void distribution measurement at different locations along the pipe axis. The sensor, accompanying electronics and data processing software were provided by Helmholtz–Zentrum Dresden–Rossendorf, Germany. The method of phase fraction distribution measurement in air/water flows using similar WMS systems has been validated by a number of studies, for example Prasser et al. (2007), and Da Silva et al. (2010). In the sensor assembly, wire electrodes are stretched across the flow cross-sectional area with the two sets of wire electrodes being perpendicular to each other. One set acts as a sender while the other acts as a receiver.

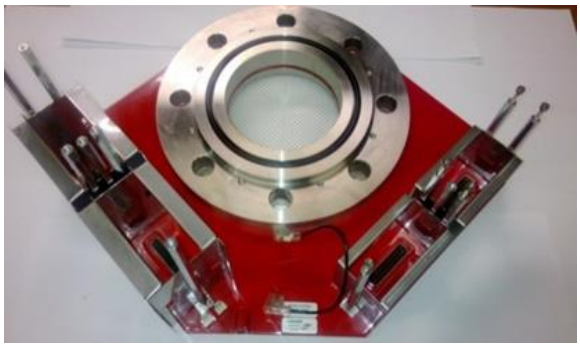

Figure 3-3: Wire mesh sensor used for study

The wire mesh sensor electronics measures the local permittivity of the fluid in the gaps of each crossing point by successively applying an excitation voltage to each one of the sender electrodes while keeping all other sender electrodes at ground potential and measuring, respectively, the AC electrical current flow to all receiver electrodes synchronously. Based on these measurements the cross-sectional fluid distribution across the pipe the sensor is able to be estimated. More details about WMS can be found in Da Silva et al. (2007). For

the sensor used in this study, the separation between the sender and receiver planes of wires is 2.5 mm. The spacing between two wires in parallel is 3.2 mm. A sampling rate of 1000 frames cross-sectional images per second is used for the measurement. On the straight upwards section of the Serpent rig, void fraction measurements by other methods were compared with the time and cross-sectionally averaged void fraction values obtained from the WMS. The upwards section was chosen as the flow regimes in this section cover different vertical flow regimes as the gas flow rate is increased. In the validation tests, a low liquid superficial velocity of 0.1 m/s was used, while the air velocity varied in the range of 0.15-30.0 m/s. At an air velocity up to 6.0 m/s, the flow regimes are bubbly, slug and churn flows. In these flows, the void fraction obtained from the differential pressure ΔP using the pressure transducers P_1 and P_4 were compared with the WMS values obtained at the measurement and visual observation station, which is the middle point between the locations of pressure transducers P_1 and P_4 on the pipe. The distance $\mathrm{L\ between}$ the two transducers is 4.1 m. On the assumption that the frictional pressure drop is negligible, the local time averaged void fraction ε at the can be calculated by:

$$\varepsilon = 1 - \frac{\Delta P/L}{g(\rho_l - \rho_g)} \quad \textbf{(3-1)}$$

where g is the gravitational acceleration, and ρ_l, ρ_g are the densities of water and air respectively. For the superficial air velocity larger than 10.0 m/s, which results in an annular flow regime, film thickness (FT) measurements were used to obtain the void fraction by the equation:

$$\varepsilon = \frac{(D-2t)^2}{D^2} \quad \textbf{(3-2)}$$

where t is the mean liquid film thickness, D the internal diameter of the pipe. Apparently here liquid entrainment in the gas core was ignored in the calculation of the void fraction. Figure 4 (b) shows the comparison of the WMS void fractions with those obtained using Equations **(3-1)** and **(3-2)**.

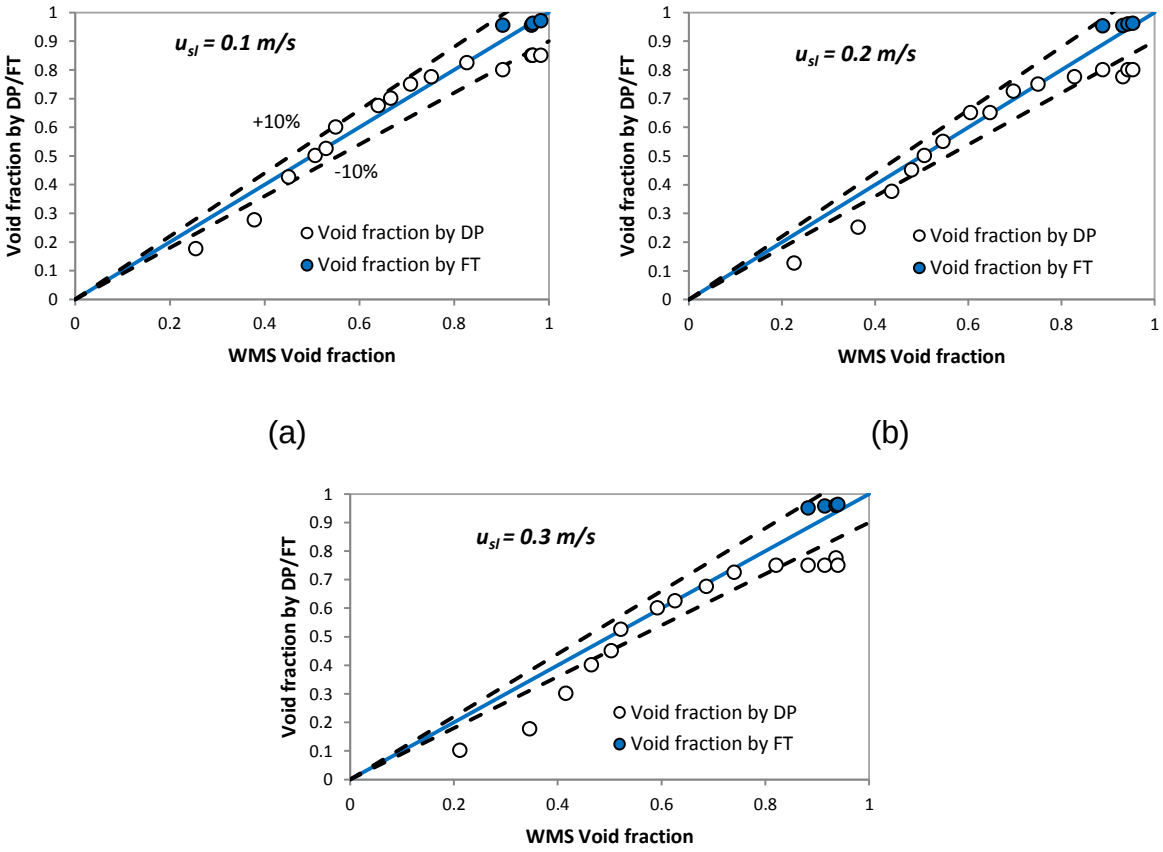

Figure 3-4: comparison of measured WMS void fractions and other methods

As can be seen, in the low void fractions range (<0.4), the WMS is likely to overestimate the void fraction by as much as 12% in a relative error. While in the range of the void fraction between 0.4–0.6, the WMS void fractions can be up to 20% higher in comparing with the referenced void fractions. In the upper half range of the void fraction (>0.5), the differences between the referenced and WMS void fractions are much smaller. As the flow reaches the annular

regime i.e. beyond about 0.8, it can be seen that void fractions are increasingly being underestimated by the DP method, indicating the increasing influence of the ignored frictional pressure gradient. In such cases, it was felt using the measured film thicknesses to estimate the void fraction is more logical given that the measurements are within a 3% error band. However, it is worth noting that the void fractions calculated from the film thickness measurements are themselves only approximations since entrained liquid droplets in the gas core were ignored. Nonetheless the relative uncertainty of WMS measurement for large void fraction (which is the main concern of this study) is estimated to be within ±10%.

Table 3-1 summarises the instrumentation used, their designations as used in Figure 3-1, manufacturer and model, measuring range, and quoted measurement uncertainties. Further details can be found in Almabrok (2014).

Table 3-1: List of instruments and experimental measurement uncertainties

Instrument	Name	Manufacturer & Model	Uncertainty	Range
Air flow meter 1	FA_1	Rosemount Mass Probar $^1/_2$''	±0.5%	0-150 Sm^3/h
Air flow meter 2	FA_2	Rosemount Mass Probar 1"	±0.5%	150-4250 Sm^3/h
Water flow meter	FW	ABB MMSG-Special	±0.1%	0.06-16 l/s
Pressure sensors	P_1 to P_6	GE Sensing UNIK 5000	±0.02%	0-1.5 barg
Temperature sensors	T_1-T_2	PT 100	±0.5%	0°-100°C
Wire mesh sensor	-	Helmholtz-Zentrum Dresden-Rossendorf	±10%*	Void fraction 0-100%
Liquid film thickness probes	FT_1-FT_2	Designed and manufactured by PSE	±0.1 mm (±3.3%)*	0-3 mm

* Experimentally determined rather than as quoted by manufacturer

3.1.3 Data acquisition

A LabView program is developed for recording the pressures, film thickness and fluid temperature. The sampling rate is 100 Hz, which is fast enough to capture

the fluctuation of these parameters during tests. The LabView system also provides an online view of the time traces of these parameters.

The DeltaV system was used to set and record gas flow rates. Its sampling rate was fixed at 1 Hz.

The WMS data acquisition system is exclusively designed for the device to measure phase distribution over the cross section of the pipe. For the experiments in this study, a sampling rate of 1000 Hz was used to capture the void data. Reference permittivities of 80 and 1 were provided for single phase liquid and gas phases respectively in order for the two-phase permittivity to be determined by the WMS.

3.1.4 Test procedure

Prior to starting the tests, the test section is first emptied and blown dry. The air flow is then stopped to record the zero points of the instrumentation. The rig is then filled with water to record full scale output of liquid film sensors and WMS, which will be used for the normalisation of the outputs from the sensors and the WMS, respectively. During the experiments the water flow rate is adjusted for each test run to a predetermined value before air is introduced to the test section. The water flow rate is monitored and adjusted to keep it at the predetermined value while the air flow is slowly increased to the desired value. The data will not be logged until both the water and air flow rates become reasonably stable and steady state conditions are assumed to have been achieved. The recording period for each test run is 120 s for the liquid film and pressure sensors, and WMS. In order to ensure the quality of the data, zero

points of the instrumentation are checked regularly, at least once a day during testing, and the recorded data are offset by the zero points accordingly. The test matrix of the experiments is provided in Appendix A.

Chapter Four

DOWNWARDS ANNULAR FLOW

4.1 Effect of pipe diameter on falling liquid film thickness

4.1.1 Importance of falling liquid film thickness

Thin liquid films falling under the influence of gravity are widely encountered in industries that involve gas-liquid two-phase flow. Instances of this flow structure include flow in nuclear reactor cores, steam condensers, water tube boilers, cooling towers, distillation columns, and evaporators. A reason attributed for the wide range of application may be because this flow regime can deliver high rates of heat and mass transport per unit volume (Zadrazil et al. 2012). In order to design more cost effective systems with greater efficiency, accurate modelling of falling film behaviour is needed.

Falling annular films represent the limiting case of annular two-phase gas–liquid flows. The liquid film descends on the walls and there is zero net flow of gas in the pipe meaning that the gas core is at a constant pressure. For the case of co-current gas flow at low to moderate gas velocities, the shearing effect of the gas core on the liquid film is minimal and the falling liquid film dominates the two fluid hydrodynamics. Falling films can generally be classified into laminar and turbulent film flows. Of greater practical interest is turbulent film flow where there are random fluctuations in the velocity field and therefore do not lend themselves easily to theoretical or mechanistic modelling. Unsteady and non-uniform waves are present on the gas-liquid interface and these enhance the bulk transport properties of the system. Consequently, simplified energy transfer

equations fail to adequately describe the flow process and hence correlational approaches are generally resorted to.

4.1.2 Comparison of the current large pipe downward liquid film thickness with established models

In comparing the measured mean film thicknesses from this study (obtained at 46D axial position downstream of the upright U-bend) with existing models, reference is made to earlier theoretical studies on falling films based on Nusselt's (1916) falling film theory:

$$t = \left[\frac{3{\nu_L}^2 Re_{lf}}{4g}\right]^{1/3} \quad \textbf{(4-1)}$$

Where Re_{lf} the liquid film Reynolds number based on the liquid film mass flux $\dot{m}_{lf}$. Nusselt arrived at the equation by taking a force balance on an elemental liquid film assuming viscous flow and that no shear or waves occur on the liquid surface. Kapitza's (1965) modification to account for these waves and surface tension resulted in the following relation:

$$t = \left[\frac{2.4{\nu_L}^2 Re_{lf}}{4g}\right]^{1/3} \quad \textbf{(4-2)}$$

A large number of empirical and semi-empirical correlations have been proposed with the form of Nusselt's theory such that:

$$t = A({\nu_L}^2/g)^{1/3} Re_{lf}^{n} \quad \textbf{(4-3)}$$

Where *A* and *n* are regression constants. Table 4.1 shows the value of *A* and *n* previously obtained experimentally by several investigators. It should be noted

that differing values of *A* and *n* by the various studies over the years only serve to slightly change the slope or magnitude of the respective dimensionless film thickness curves within the same Re_{lf} range.

Table 4-1: Some falling film relations and flow conditions

Researchers	*A*	*n*	Basis of model	Geometry/flow conditions
Brotz (1954)	0.161	2/3	Empirical	Pipe/Re_{lf} = 100–4300
Brauer (1956)	0.245	8/15	Empirical	Not available
Fiend (1960)	0.532	1/2	Empirical	Not available
Kapitza (1965)	0.843	1/3	Theoretical	Not available
Kosky (1971)	0.136	7/12	Semi-empirical	Pipe/Re_{lf} > 1000
Ganchev et al. (1972)	0.137	7/12	Theoretical	Not available
Takahama and Kato (1980)	0.473	0.526	Empirical	Pipe/Re_{lf} < 8000
Brauner (1987)	0.104	7/12	Theoretical	Flat plate/Re_{lf} > 300
Mudawar and El-Masri (1988)	0.145	0.58	Theoretical	Pipe, Re_{lf} < 10000
Karapantsios and Karabelas (1995)	0.451	0.538	Empirical	Pipe, Re_{lf} = 370–11080

This fact is shown in Figure 4-1 (a) where the current data is plotted together with the models in Table 4-1. It can be seen that only a handful of the predictions (Nusselt, Kapitza, and Brauner) are within the vicinity of the current large pipe experimental film thicknesses. The models of Ganchev (1972), Kosky (1971), Mudawar & El-Masri (1995) have very similar slopes and predictions due to the close values of their respective *A*, *n*; they are in agreement with the current data up to Re_{lf} = 8000 but dramatically lose accuracy beyond that even though their range of application are between Re_{lf} ranges of 1000 and 10000. Kapitza's (1965) theoretical model agrees with the large pipe data up to Re_{lf} =

10000 while Brauner (1987) predicts well within the range Re_{lf} = 10000–14500. In fact, only the model of Karapantsios & Karabelas (1995) caters for Re_{lf} > 10000 up to 11080 only, while the current measured film thicknesses were obtained at Reynolds number ranges of 4000–20200. At high film Reynolds numbers the large deviations produced may be as a result of higher interfacial friction. As Figure 4-1 (b) shows values of *A* = 1.4459 and *n* = 0.3051 fit the large pipe data best. Therefore the relationship that is appropriate for the large pipe downward flow film thickness data is as follows:

$$t^* = t(g/\nu_l^2)^{1/3} = 1.4459\, Re_{lf}^{0.3051} \qquad \textbf{(4-4)}$$

This indicates an increase in intercept and a decrease in slope when compared to the existing relations derived from smaller pipes and is clearly visible in Figure 4-1 (a). Use of Nusselt-type equations such as Equation **(4-4)** for two-phase flow is justified since for downwards flow, gravity ensures that the inertia of the liquid film dominates that of the gas and of course also dominates surface tension forces.

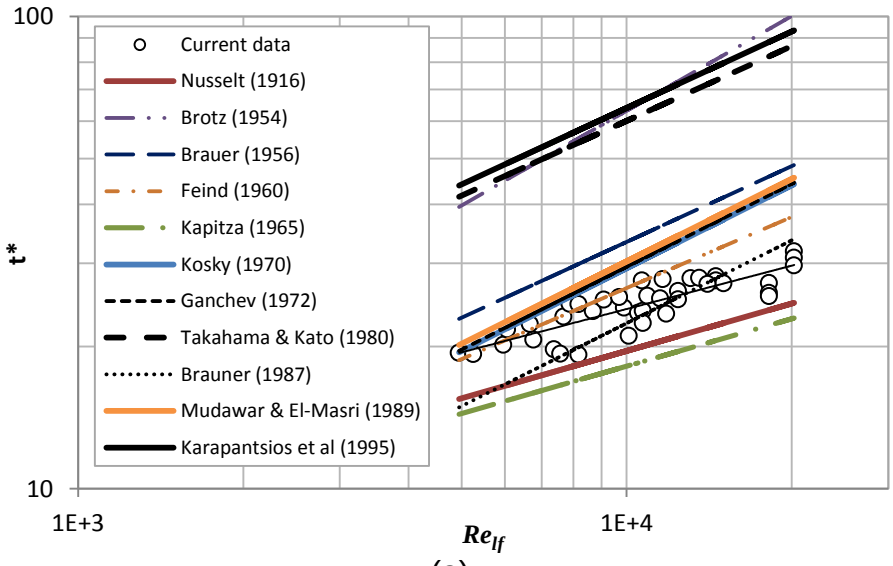

(a)

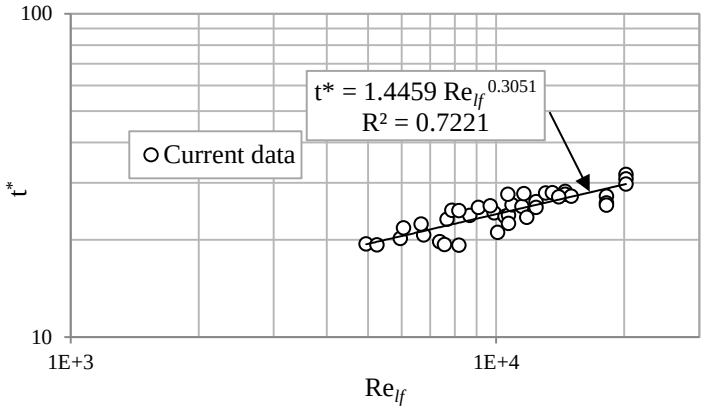

(b)

Figure 4-1: (a) Mean film thickness in falling film flow: comparing current experiments to existing models. Where $t^* = t\left(g/\nu_l^2\right)^{1/3}$ is the dimensionless film thickness and $Re_{lf} = 4\dot{m}_l/\mu_l$ the liquid film Reynolds number (b) Correlation of large pipe dimensionless film thickness

The value of *A* for the large pipe may seem quite large in relation to the others presented in Table 4-1 but is in fact only slightly out of the range of 0–1.22 consistent for smooth falling films as observed by Brauer who categorised the various flow regimes in falling film flow (Table 4-2). Summarily, agreement of experiments with data is generally good at high interfacial shear where the films are thin.

Table 4-2: Falling film flow regimes (Brauer, 1956)

A	Flow regime	Sublayer state
0–1.22	smooth stratified	laminar
1.22–2.88	ripple (sine) wave	laminar
2.88–140; Fr→1.0	roll (gravity) wave	laminar
140–1600; We→1.0	capillary (surge) wave	laminar
1600–2400	capillary (surge) wave	turbulent
> 2400	overriding (ring) swell wave	turbulent

Conversely, at lower gas flow rates where the interfacial shear stress is lower and huge waves occur, i.e. towards the transition region from intermittent to

annular two-phase flow, there is still room for improvement in terms of model development.

4.1.3 Conclusion

The mean film thickness data from this study was compared to existing correlations and theoretical models. It was observed that the current data presented a distinctly different slope to those of the correlations suggesting a change in the film tendency for large diameter pipes.

4.2 Downward gas–liquid two-phase flow pressure behaviour between top and bottom halves of vertical large diameter pipe

The purpose of this section is to discuss the findings of experimental pressure behaviour in vertical downwards annular two-phase flows in the large diameter 101.6 mm ID Serpent Rig.

4.2.1 Theoretical considerations

The total pressure gradient for a single phase fluid flowing in a vertical pipe at steady state is given by the momentum equation:

$$-\frac{\Delta P}{L} = \rho g + \frac{4\tau}{D} \quad \textbf{(4-5)}$$

Which for gas – liquid two phase flow is as follows:

$$-\frac{\Delta P}{L} = \left[\rho_g \varepsilon + \rho_l (1-\varepsilon)\right] g + \frac{4\tau}{D} \quad \textbf{(4-6)}$$

Where the first term on the right hand side of Equation (4-6) refers to the gravitational or static component of the pressure gradient, the second is the frictional pressure gradient with τ the shear stress given by $\tau = \frac{1}{2} f \rho u^2$; ρ_g and ρ_l are the gas and liquid densities respectively; ε is void fraction, the time-averaged cross-section occupied by the gas. Where $L, \rho, g, f, D, \text{and } U$ are: the pipe length, fluid density, acceleration due to gravity, fanning friction factor, pipe diameter, and fluid velocity respectively. Equations (4-5) and (4-6) are independent of pipe length. This means that ideally the pressure gradient of any pipe sections $dP_i/dL_i = constant$. Therefore, the ratio of pressure gradients in any pipe sections for all fluid velocities will be given as:

$$\left(-\frac{\Delta P_j}{L_j}\right)\Big/\left(-\frac{\Delta P_k}{L_k}\right)=\left(-\frac{\Delta P_j}{L_j}\right)\Big/\left(-\frac{\Delta P_n}{L_n}\right)=1 \quad \textbf{(4-7)}$$

Where j, k, n are arbitrary integers 1, 2, …, n. Knowledge of the extent both pressure gradients in Equation (4-7) differ from each other could provide better insight on flow development along the pipe length.

4.2.1.1 Static water pressure tests

Static water pressure tests were carried out by pumping water into the test rig then locked in by quickly and simultaneously shutting valve VW3 and the water pump. A vertical water column is maintained in the upright U section. Vent valve VV1 is opened in order to free the water column of additional pressure from trapped air. Pressure readings are captured for 2 minutes at a recording rate of 100 Hz via the LabView data acquisition software connected to the pressure transducers. These were later averaged to obtain mean pressures P_1, P_3 and P_4. The lengths of the pipe section L_1 and L_2 were measured with a tape rule to be 2.3 and 1.8 m which very closely match the differential pressure differences of $\Delta P_1 = P_3 - P_4 = 0.2325$ and $\Delta P_2 = P_1 - P_3 = 0.1795$ bar respectively. These serve to confirm the transducers give accurate readings prior to tests.

4.2.2 Results and discussion

4.2.2.1 Single phase water flow

Pressure gradient was calculated from the measured pressure drops ΔP_1 and ΔP_2 by dividing by the respective lengths of pipe segments to obtain $\Delta P_1/L_2$ and $\Delta P_2/L_2$ respectively (See Figure 4-2).

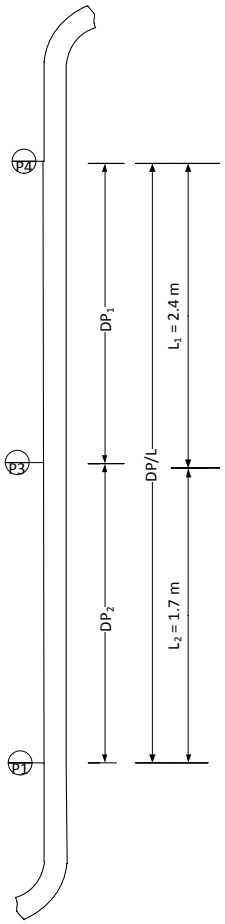

Figure 4-2: Details of downward section of flow rig with nomenclature

The ratio of these pressure gradients for all liquid velocities $u_{sl} \equiv u_l$ is roughly unity as can be seen in Figure 4-3.

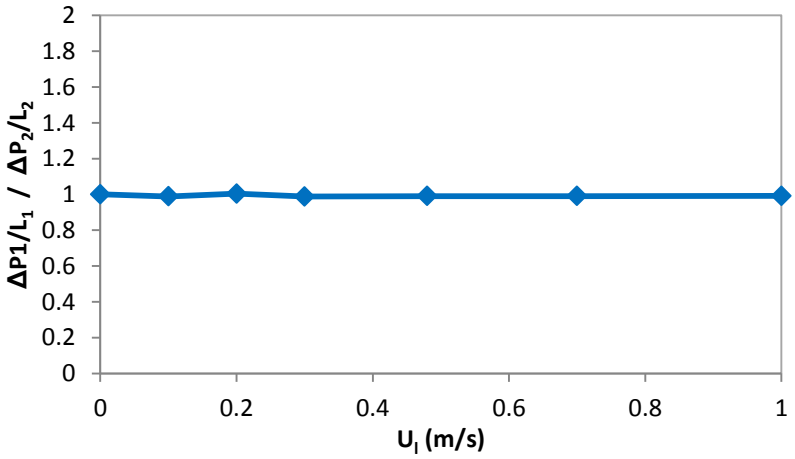

Figure 4-3: Ratio of single phase top to bottom pressure gradients in downwards flow

4.2.2.2 Air–water two-phase flow tests

Two-phase flow tests were carried out for $u_{sl} = 0.1 - 1.0\, m/s$ and $u_{sg} = 1.5 - 29.8\, m/s$. The obtained total pressure gradients are shown in Figure 4-4. Initially, positive pressure gradients are obtained which progressively decrease with increasing gas superficial velocity. This is expected because at low gas flow rates, the gravitational component of the pressure gradient dominates and this reduces due to the reducing liquid phase fraction as the gas flow increases. Close observation of Figure 4-4 (a) and (b) reveals larger pressure gradient at the bottom part of the pipe. This could be attributed to more rapid expansion occasioned by increasing energy losses by means of the mixture kinetic energy increases further downstream as the flow develops. Further increase in the gas superficial velocity results in rising influence of the frictional component of the pressure gradient. A point is reached when both gravitational and frictional components are equal which then results in zero pressure gradients. As can be seen in Figure 4-4 a and b, this occurs at approximately 7 and 9 m/s superficial gas velocity respectively for the top and bottom halves of the downward flowing leg of the Serpent Rig. Beyond 10 m/s, only negative pressure gradients are obtained and these progressively decrease with the rising dominance of the frictional component of the total pressure gradient.

The ratio of the pressure gradients in Figure 4-4 (i.e. $\Delta P_1/L_1/\Delta P_2/L_2$) results in the profile shown in Figure 4-5. As can be seen, except at very high gas flow rates from approximately 20 m/s, corresponding to regions in the annular flow regime, Equation (4-7) does not equal unity for all conditions of the gas and liquid velocities.

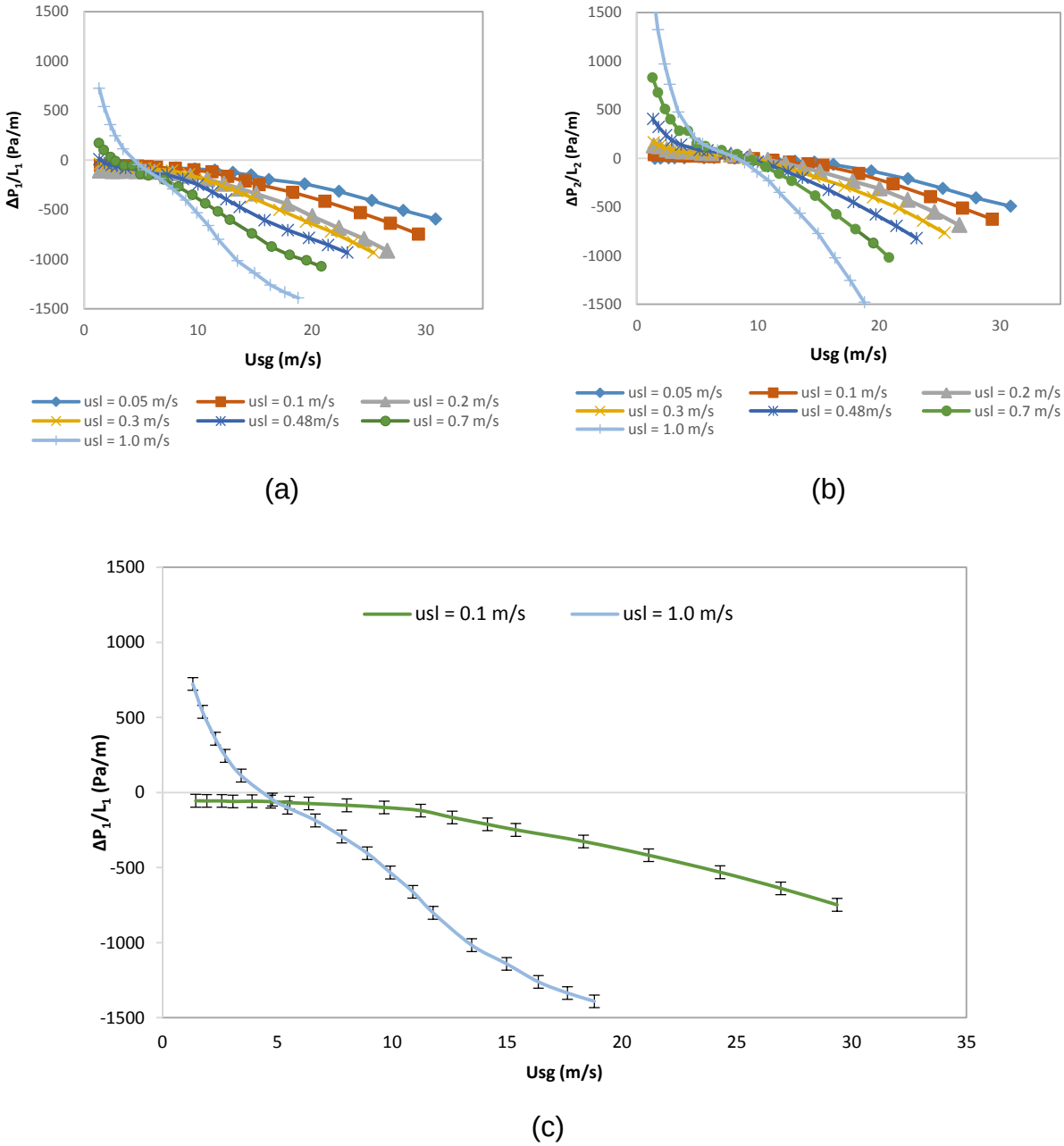

Figure 4-4: (a) Top and (b) bottom half pressure gradients in two-phase flow tests (c) Error bars for an uncertainty of 42.2 Pa/m in $\Delta P/L$ measurements for 0.1 and 1.0 m/s

Instead, a general trend in the profile for all liquid superficial velocities shows that there is a drop in the pressure gradient ratios (mostly negative) from u_{sg} = 1.3 m/s up until 7–10 m/s. Then a dramatic switch to positive ratios occurs of up to 25 meaning large pressure gradients in the top half of the pipe.

Thereafter there is a generally very steep drop from 10 m/s, finally stabilising at around a pressure gradient ratio of 1 beyond $u_{sg} = 20\, m/s$ for all superficial liquid velocities.

The value of the pressure gradient ratios at the reversal conditions may have been magnified by the values of experimental uncertainty in pressure drop measurement. Uncertainty in measured pressure gradient is estimated around ±42.2 Pa/m (full scale). This is depicted by the error bars for $\Delta P_1/L_1$ in Figure 4-4 (c) for $u_{sl} = 0.1 \text{ and } 10\, m/s$. For gradients nearer zero, large errors are propagated in the pressure gradient ratios as can be seen by the error bars for $u_{sl} = 0.1 \text{ and } 10\, m/s$ as shown in Figure 4-6. Nevertheless, a change in sign occurs in the pressure gradient ratios from negative to positive at the specified conditions.

In order to gain more insight on this “reversal”, an examination of the probability distribution functions (PDF) of the void fractions (measured using the Wire Mesh Sensor) at reversal conditions as well as other conditions was done. These PDFs were for void fractions taken at the middle and bottom positions of the test section. The PDFs at $u_{sl} = 0.48\, m/s$ are also shown in Figure 4-5. While the shapes of the PDFs at $u_{sg} = 2.86\, m/s$ and $23.12\, m/s$ are typical of what is obtained in annular flow conditions with a single peak at high void fractions, that at $u_{sg} = 8.67\, m/s$ which is in the reversal region shows characteristics obtainable at transition flow regime conditions with more than a single peak.

There also seems to be a connection between the pressure gradient reversal and liquid film thickness profile. Normally, liquid film thickness declines with increasing gas flow.

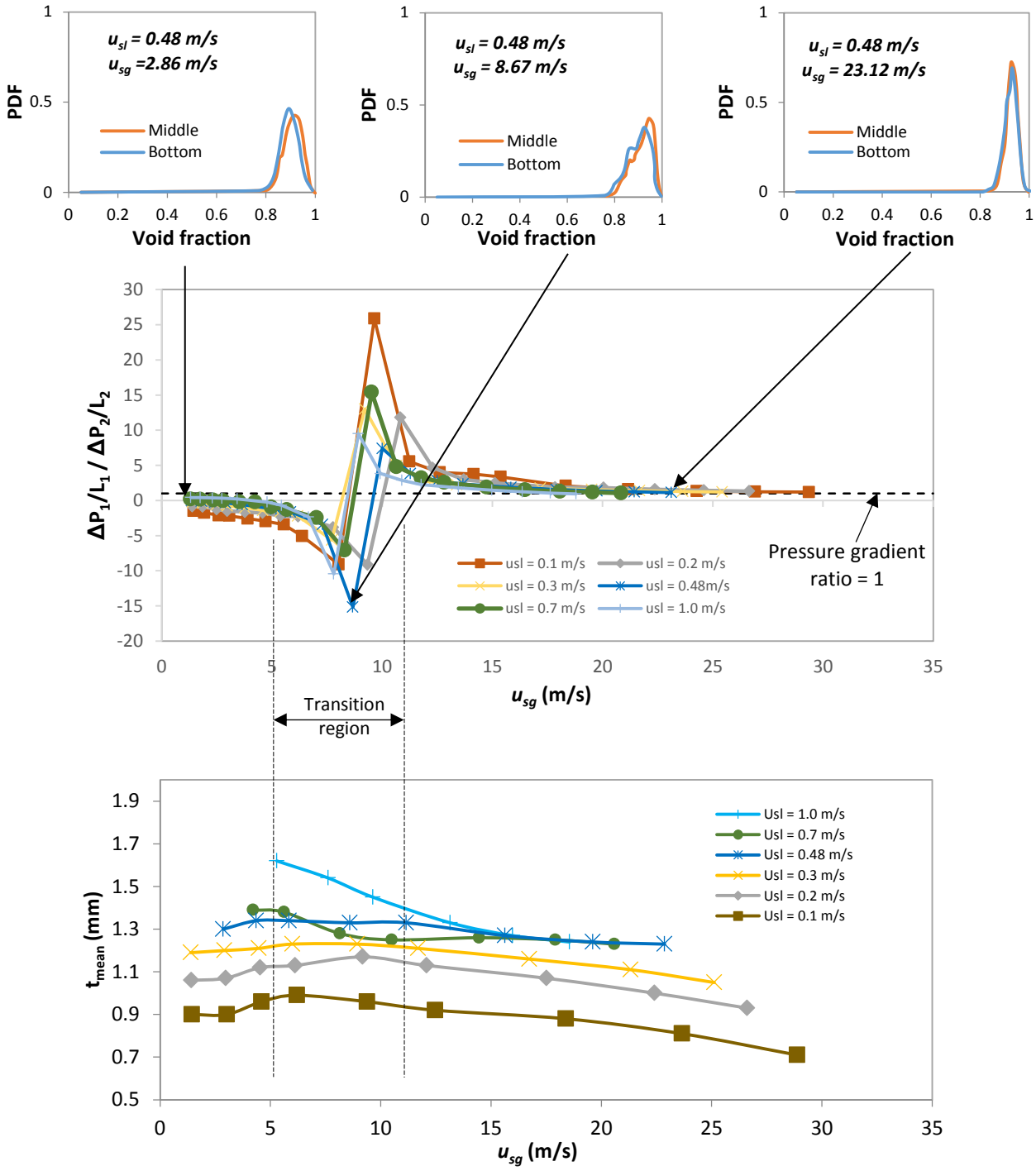

Figure 4-5: Ratio of bottom to top halves pressure gradients for two-phase flow tests with PDF of void fractions at selected conditions and liquid film variation with gas superficial velocity

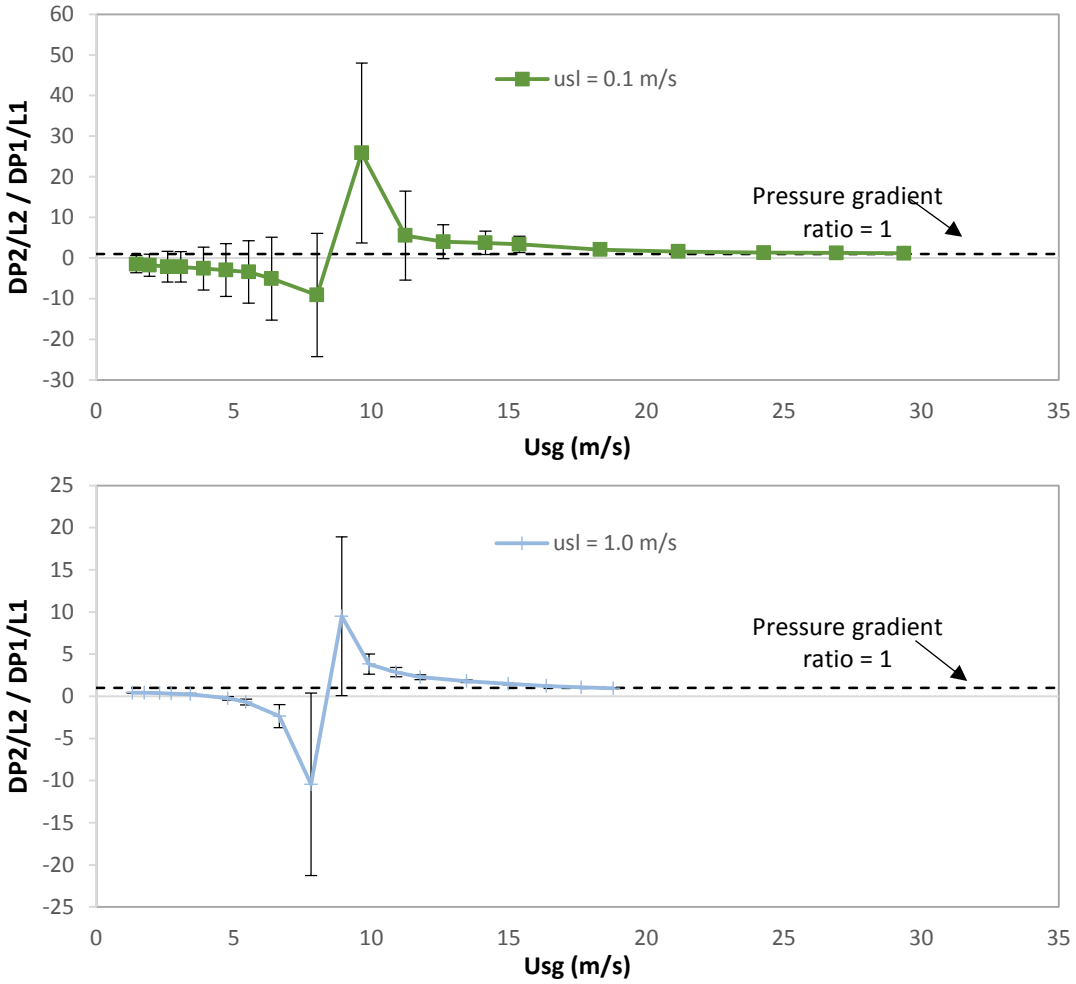

Figure 4-6: Bottom to top half pressure ratios showing error bars for (a) usl = 0.1 m/s and (b) usl = 1.0 m/s

However, that is not the case here as the measured liquid film thickness initially rises, reaching a peak at between u_{sg} = 5–10 m/s depending on the u_{sl}, then falling subsequently as expected with increasing gas flow. An understanding of this behaviour might be reached by considering the velocity slip at the gas–liquid interface. At low gas superficial velocity, falling film velocity could be significantly higher than the local gas velocity (for liquid velocity measurements see Table 4-3 in Section 4.3.2).

At such conditions the falling liquid film slides past the slower gas entraining liquid droplets into the gas core, thus reducing the thickness of the falling film. This entrainment should reach a minimum at zero gas–liquid phase slip corresponding to a maximum of the liquid film thickness. Conversely, when the gas superficial velocity is increased leading to gas moving faster than the local velocity at the interface, there will again be increased entrainment. After the maxima in the mean film thickness, progressive decrease occurs with increasing gas superficial velocity.

Since annular flow dominates two-phase flow in a downcomer, the instability occurring at between 5–10 m/s may well be as a result of reversal in shear caused by either phase being the driving phase due to its larger velocity.

4.2.3 Conclusion

Experiments have been conducted in downwards two-phase flow where annular flow is the dominant flow regime even in conditions that will otherwise produce bubbly or churn flow in upflow. Pressure measurements were made from which pressure drop hence pressure gradients were determined respectively for the top and bottom halves of the down-coming two-phase flow. It was observed that the ratio of the top and bottom pressure gradients produces a unique and consistent pattern when plotted against the superficial gas velocity. Large fluctuations from negative to positive pressure gradients (a so-called “pressure drop reversal”) observed between 5 and 10 m/s gas flow for all liquid velocities are consistent with a change in direction of phase slip when the liquid initially has a larger velocity and later on the gas travels faster as its flow rate increases.

4.3 Interfacial shear in downwards co-current annular two-phase flow in large diameter pipes

4.3.1 Film thickness and flow development

The film thickness was measured at three different axial positions downstream of inverted U-bend. It is a mean value of four circumferential measurements made on the probe spool. Three such spool assemblies installed on the downward flowing section of the test rig were used to obtain the mean film thickness which enables the study of its axial variation. Axial positions at the top, middle, and bottom of the downward flowing part of the rig are respectively at 10, 30 and 46 pipe diameters from the inverted U-bend. Figure 4-7 shows normalised mean film thicknesses obtained from the conductance probes at the stated axial positions. These normalised film thicknesses are defined as the ratios of film thicknesses at other L/D positions to that at L/D = 46 (i.e. $t_{norm} = t/t_{L/D=46}$). This means that t_{norm} at 46 pipe diameters is unity. It can be seen that there is minimal change in the normalised mean film thickness between the middle and bottom positions. This signifies a reasonably developed flow which is expected and is due to the prevailing influence of gravity on downwards flow. Therefore, the film thicknesses used for the analyses in this paper are those at L/D = 46, representing a film thickness in fully developed downwards annular flow.

For vertical upflows, liquid film thickness decreases with increasing superficial gas velocity. In the case of vertical downwards flows, as can be seen from Figure 4-7, for low liquid flow rates (u_{sl} < 0.48 m/s) there is an initial increase

before the expected progressive decrease in the mean film thickness as the gas flow rate is increased.

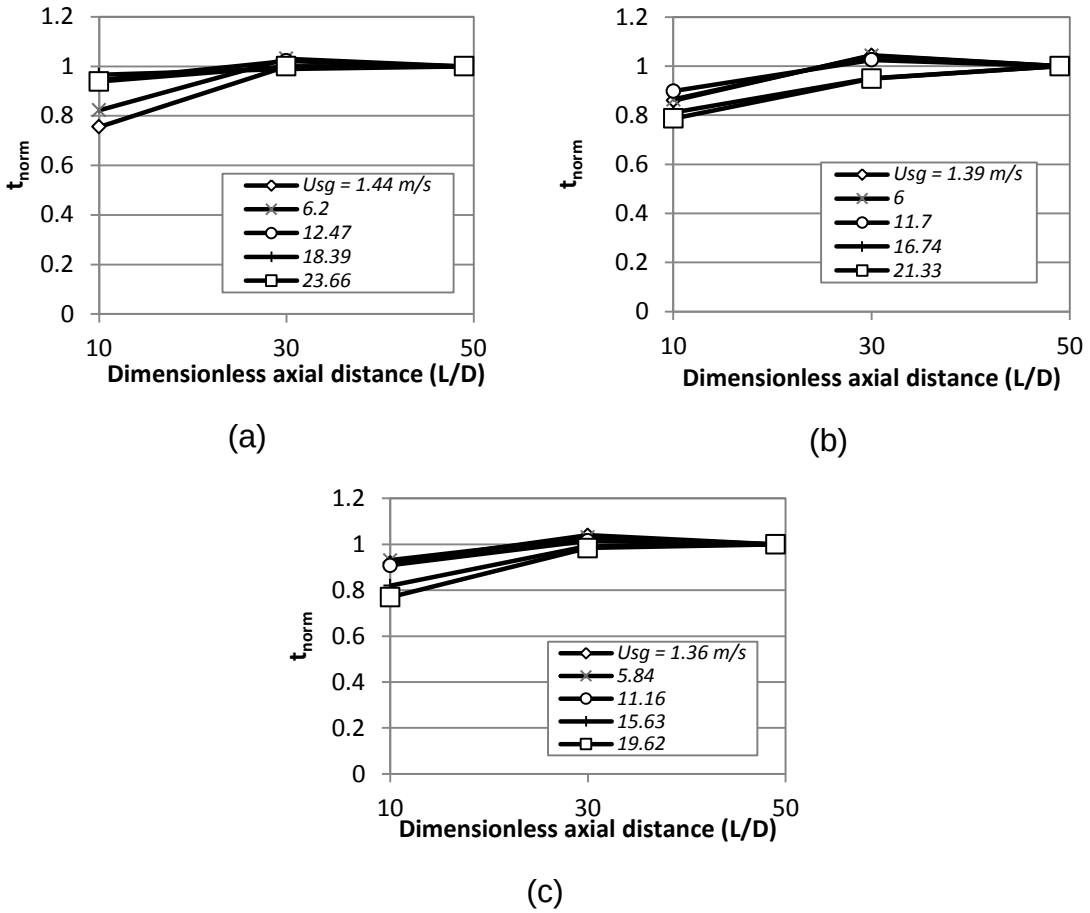

Figure 4-7: liquid film thickness variation along the axial distance of L/D = 10, 30, and 49 (top middle and bottom respectively) from inverted U-bend for a. u_{sl} = 0.1 m/s b. u_{sl} = 0.3 m/s and c. u_{sl} = 1.0 m/s (From Almabrok 2014)

This behaviour might be explained by considering the velocity slip at the liquid film/gas core interface. In low gas flow rates, falling film velocity could be significantly higher than the local gas velocity. At such conditions the falling liquid film glides past the slower gas thereby sweeping liquid droplets into the gas core and hence reducing the thickness of the falling film. This entrainment should reach a minimum when no velocity slip at the liquid film/gas core interface corresponding to a maximum of the liquid film thickness. Conversely,

when the gas velocity is increased leading to the gas moving faster than the liquid film in the interface, there will be increased interfacial shear, again resulting in increased entrainment. After the maxima in the mean film thickness, it then asymptotically reduces with increasing u_{sg}. For those high liquid flow rates (u_{sl} > 0.7m/s), annular flow can only be established in the downcomer with a U bend following it if the gas velocity is significantly high, as reported by Almabrok (2014). Thus in those annular flows the film thickness progressively decreases against the gas velocity due to increased film velocity and liquid entrainment.

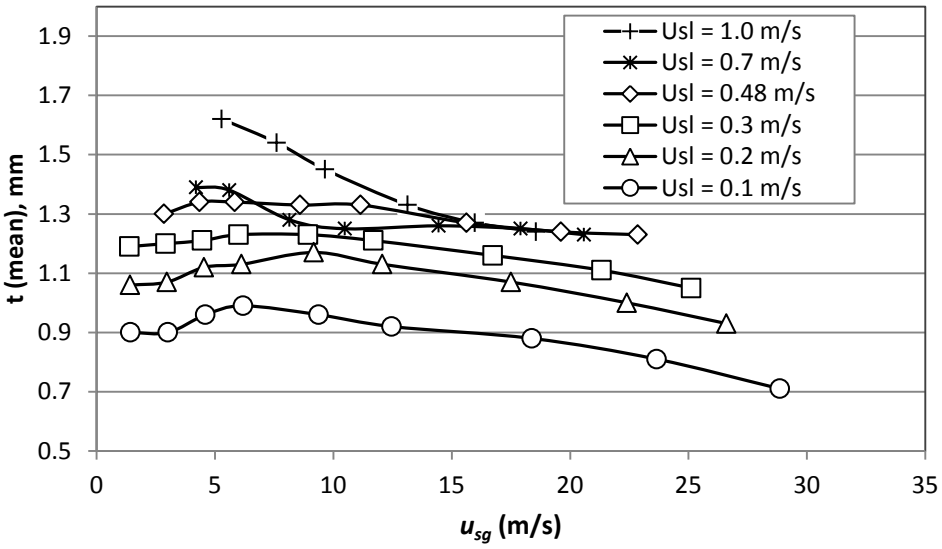

Figure 4-8: Variation of liquid film thickness with superficial gas velocity at different liquid superficial velocities taken at L/D = 46 from inverted U-bend entrance region (See Almabrok 2014).

4.3.2 Film velocity measurements and entrained droplet fraction

Film velocity measurements were obtained by way of the electrolyte injection method. This method is based on injecting sodium chloride electrolyte into the liquid film in order to increase its conductivity. The transit time between the two sensors in the integrated probe can be determined by the cross correlation

method, and then the film velocity calculated by dividing the distance between two sensors by the transit time or delay between its two electrodes. These are shown in Table 4-3. It is important to note the large differences in gas velocity and liquid film velocity (u_{lf}) as the superficial gas velocity is increased. An increase in slip velocity occurs. This in turn brings about rising shear at the gas–liquid interface. Several mechanisms have been put forward as to how this shearing contributes to liquid breakup hence entrainment; these include a “roll wave” mechanism as observed by early researchers such as Green (1950) using high speed photography and Lane's (1951) wave “undercutting” mechanism.

Table 4-3: Measured liquid velocities

u_{sl} m/s	u_{sg} m/s	u_{lf} m/s	u_{sl} m/s	u_{sg} m/s	u_{lf} m/s	u_{sl} m/s	u_{sg} m/s	u_{lf} m/s
	1.44	1.38		1.39	1.63		4.21	2.43
	3.02	1.46		2.92	1.74		5.61	2.65
	4.6	1.56		4.47	1.87		8.15	2.91
	6.2	1.72		6	1.99		10.5	3.09
0.1	9.38	1.93	0.3	8.94	2.22	0.7	14.45	3.14
	12.47	2.06		11.7	2.43		17.91	3.22
	18.39	2.34		16.74	2.7		20.59	3.24
	23.66	2.45		21.33	2.81			
	28.87	2.51		25.12	2.84			
	1.42	1.45		2.86	2.02		5.29	2.87
	2.97	1.57		4.36	2.23		7.62	3.07
	4.54	1.71		5.84	2.44		9.65	3.26
	6.12	1.91		8.6	2.54		13.15	3.26
0.2	9.18	2.14	0.48	11.16	2.72	1.0	15.98	3.38
	12.08	2.32		15.63	2.87		18.56	3.38
	17.51	2.52		19.62	3.02			
	22.41	2.68		22.87	2.92			
	26.61	2.71						

These measured velocities were used to calculate the entrainment rate of water droplets into the gas core. The entrained droplet fraction which is given by

$$e = \frac{W_E}{W_t} = \frac{W_t - W_{lf}}{W_t} \qquad \textbf{(4-8)}$$

where W_E is the droplet entrainment rate, W_t is the total liquid mass flow rate and W_{lf} is the liquid film mass flow rate. The liquid film flow rate W_{lf} (in kg/s) is calculated as follows

$$W_{lf} = \rho_l u_{lf} A_{lf} \quad \textbf{(4-9)}$$

where u_{lf} is the measured liquid film velocity and A_{lf} is the liquid film wetted cross-sectional area determined by

$$A_{lf} = \pi(Dt - t^2) \quad \textbf{(4-10)}$$

4.3.3 Calculation of interfacial properties from experimental measurements

Eighty data points were obtained for this study in the range of Re_g = 8400–187000 and Re_{lf} = 646–9700. The liquid film Reynolds number is calculated using the relation

$$Re_{lf} = 4W_{lf}/\pi D\mu_l \quad \textbf{(4-11)}$$

The interfacial friction factor is estimated from the measured pressure gradient by taking a momentum balance at the gas–liquid interface with the assumption that the flow is fully developed

$$f_i = \frac{2\tau_i}{\rho_g u_{sg}^2} \quad \textbf{(4-12)}$$

where τ_i is the interfacial friction factor given by

$$\tau_i = \left(-\frac{dP}{dz} + \rho_c g\right)\frac{D - 2t}{4} \quad \textbf{(4-13)}$$

This equation assumes a uniform film thickness around the pipe cross-section.

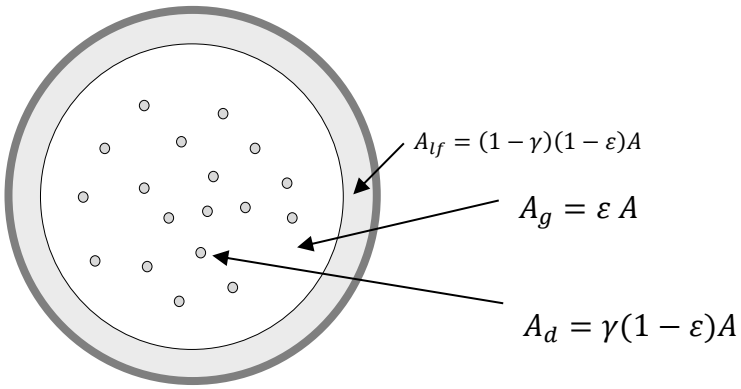

Figure 4-9: Representation and notation of the various phase splits (film, gas and droplets) occupying the total pipe area (Adapted from Cioncolini et al. 2012)

Here it should be noted that since there is significant droplet entrainment in the gas core, as is depicted in Figure 4-9, pure gas properties are replaced by linearly phase-averaged density of droplet laden gas core.

$$\rho_c = (1-\varepsilon_c)\rho_l + \varepsilon_c \rho_g \qquad \textbf{(4-14)}$$

Historically, obtaining a satisfactory mixture rule for viscosity has not been straight forward, with different authors preferring to define different two-phase viscosities. Two typical definitions for the viscosity of two-phase mixture are that of the reciprocal mean by Isbin et al. (1957) and that by Dukler et al. (1962) using the gas quality. For the present study however, a linear phase-averaged mixture rule was used as defined by Cicchitti et al. (1960) and Hewitt & Hall-Taylor (1970); it was recently used by Cioncolini et al. (2009a, 2009b); and Cioncolini & Thome (2010) as

$$\mu_c = (1-\varepsilon_c)\mu_l + \varepsilon_c \mu_g \qquad \textbf{(4-15)}$$

where ε_c is the gas core void fraction estimated as

$$\varepsilon_c = \frac{\varepsilon}{\varepsilon + \gamma(1-\varepsilon)} \quad \textbf{(4-16)}$$

with ε being the cross-sectionally averaged void fraction and γ the droplet holdup, estimated by ignoring the slip between the entrained droplets and the gas as follows

$$\gamma = e\frac{\varepsilon}{(1-\varepsilon)}\frac{1-x}{x}\frac{\rho_g}{\rho_l} \quad \textbf{(4-17)}$$

where *e* is the entrained droplet fraction defined in Equation **(4-8**) and *x* is the gas quality, ratio of the gas mass flux to the total mas flux. It has been pointed out that as the homogenous model neglects the phase slip between the gas and liquid, it is theoretically more suited to two phase flows characterised by proper mixing between the phases e.g. dispersed bubbly flow and less accurate in the case of separated flow where slip is more prevalent such as annular flow. Even so, Hewitt & Hall-Taylor (1970) have shown that it can equally handle annular flow insofar as the mixture viscosities and densities are appropriately defined.

4.3.4 Comparison of experimental interfacial friction factor with published correlations

Henstock & Hanratty (1976) described a method to predict the height of the liquid film and interfacial friction factor in both upward and downward annular flow in circular pipes. For downward flow, they used pipe flow data from Chien & Ibele (1964), Charvonia (1959), and Wright & Laufenbrenner (1975) obtained from 50.8, 63.5 and 25.4 mm diameter pipes respectively. Henstock & Hanratty argued that the wave surface of relatively thick films is well represented by two

characteristic lengths t/D and t^+ which describe Bergelin et al's (1959) roughened sand surface analogy of the gas–liquid interface.

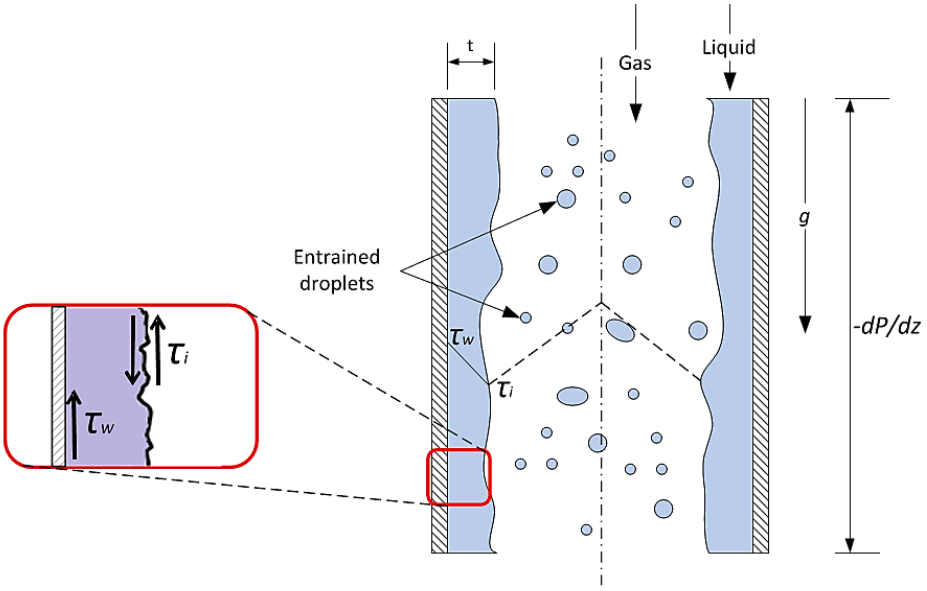

Figure 4-10: Flow configuration for vertical downwards annular two-phase flow

However, for very thin films the waves are small enough for f_i to be approximated by f_s, the friction factor of a smooth pipe. They then reasoned that at this point, the true shear stress has a magnitude between the wall shear and the interfacial shear stress. They therefore offered to correct this interfacial shear with a characteristic shear stress τ_c as a weighted sum dominated by the wall shear stress as

$$\tau_c = \frac{2}{3}\tau_w + \frac{1}{3}\tau_i \qquad \textbf{(4-18)}$$

where the wall shear stress which acts in opposition to the direction of flow (Figure 4-10), is given as

$$\tau_w = -\frac{dP}{dz}\frac{D}{4} + \rho_l g \frac{D}{4}\left[1 - \left(\frac{D-2t}{D}\right)^2\right] + \rho_c g \frac{D}{4}\left(\frac{D-2t}{D}\right)^2 \qquad \textbf{(4-19)}$$

The first term on the right hand side represents the total measured pressure gradient and the other two are the gravitational pressure gradients as contributed by the liquid film and the droplet-laden gas core respectively. Here, it is assumed that the system is at equilibrium and adiabatic, therefore the accelerational pressure gradient is negligible. The factor $[(D-2t)/D]^2$ is a measure of the void fraction given the film thickness measurement and assuming it is uniform on the pipe periphery. The dimensionless film thickness $t_g^+ = tv_c^*/\nu_L$ akin to y^+ the friction distance parameter is hence re-defined in terms of the liquid film thickness as follows

$$t^+ = \frac{t}{\nu_l}\sqrt{\frac{\tau_c}{\rho_l}} \tag{4-20}$$

with a rather lengthy theoretical argument, Henstock & Hanratty were able to eliminate the dependence of the frictional forces acting on the liquid film on t^+ and derived a modified Martinelli flow parameter *F* defined as

$$F = \frac{M}{Re_g^{0.9}}\frac{\nu_L}{\nu_g}\sqrt{\frac{\rho_l}{\rho_g}} \tag{4-21}$$

where

$$M = [\left(0.707{Re_{lf}}^{0.5}\right)^{2.5} + \left(0.0379{Re_{lf}}^{0.9}\right)^{2.5}]^{0.4} \tag{4-22}$$

It should be noted that this flow parameter only holds for fully turbulent flow (with entrainment) where $Re_{lf} \to \infty$ and is negligible for laminar flow as $Re_{lf} \to 0$ where interfacial drag is trivial. They used this approach to study experimental results where the pressure gradient, film thickness and film flow rate were

measured and then derived a relation for the interfacial friction factor f_i in terms of *F* by fitting the data finding reasonable agreement as follows

$$\frac{f_i}{f_s} = 1 + 1400F \tag{4-23}$$

where f_s is the single phase friction factor given by

$$f_s = 0.046Re_g^{-0.2} \tag{4-24}$$

This was tested against the present experimental data as is shown in Figure 4-11. The correlation exhibits huge deviations resulting in both over- and under-predictions of the large pipe data by a factor of up to 1500 thereby being consistent with Asali et al.'s (1985) assertion that the correlation is unsuitable for capturing the effect of pipe diameter such as the 101.6 mm ID used for this study.

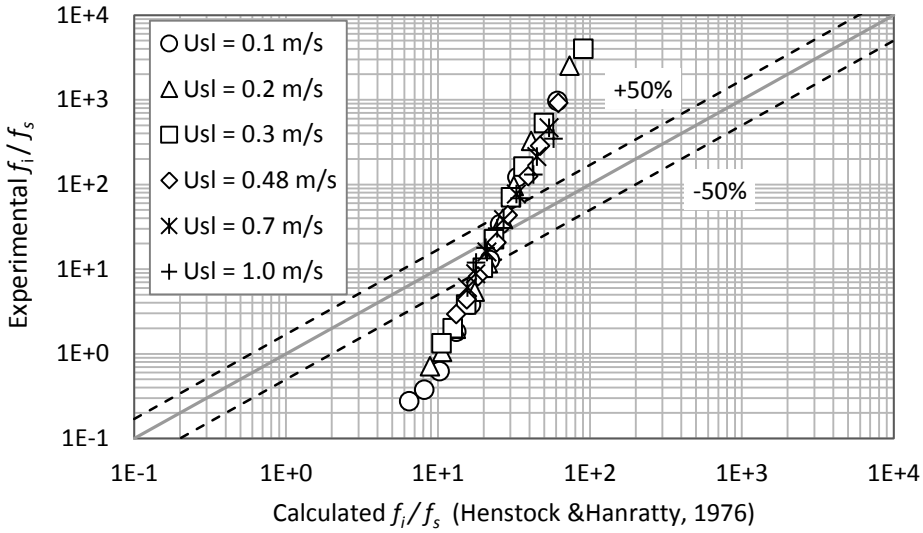

Figure 4-11: Prediction of interfacial friction factor by Henstock & Hanratty (1976) vs experimental friction factor

In their attempt to account for pipe diameter, Asali et al. (1985) showed that $(f_i/f_s - 1) \propto t_g^+$ is a better representation of the effect of film thickness than

$(f_i/f_s - 1) \propto \frac{t}{D}$ for gas velocities greater than 25 m/s. Where t_g^+ the dimensionless film thickness based on the gas properties is defined as

$$t_g^+ = \frac{t}{\nu_g}\sqrt{\frac{\tau_i}{\rho_g}} \quad \textbf{(4-25)}$$

For the roll wave regime, (at $Re_{lf} > Re_{lfc}$, the critical Reynolds number at the start of entrainment) they found that t_g^+ correlated well with Re_{lf} for downflows as follows

$$t_g^+ = 0.19 Re_{lf}^{0.7} \frac{\nu_L}{\nu_g}\sqrt{\frac{\rho_L \tau_i}{\rho_G \tau_c}} \quad \textbf{(4-26)}$$

This was then correlated with the interfacial friction factor

$$(f_i/f_s - 1) = 0.45 Re_g^{-0.2}(t_g^+ - 5.9) \quad \textbf{(4-27)}$$

Our data is however not well described by this correlation as shown in Figure 4-12. At high liquid velocities (corresponding to the thick films), f_i/f_s are far more over-predicted than at lower liquid velocities.

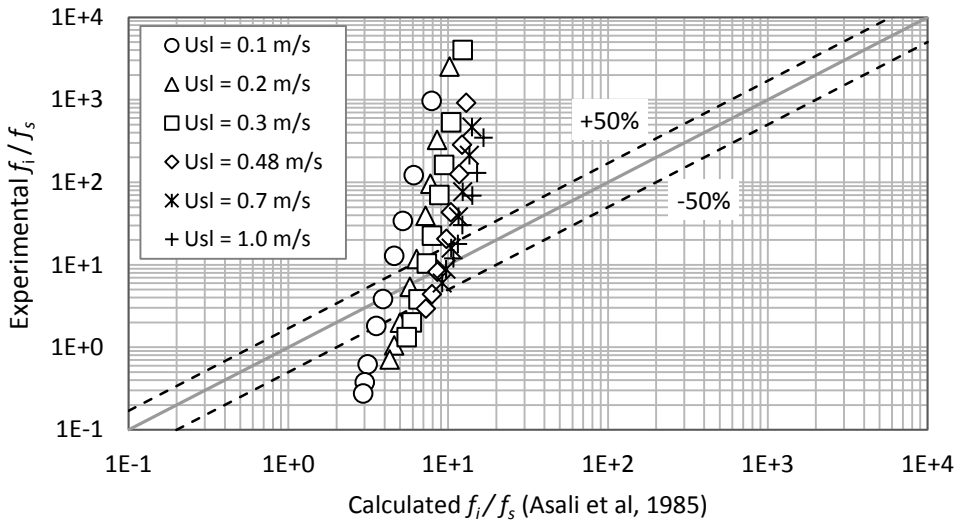

Figure 4-12: Prediction of interfacial friction factor by Asali et al. (1985) vs experimental friction factor

This is not surprising given that Asali et al (1985) correlated their data at high gas velocities above 25 m/s whereas for the present study, the gas velocities are within the range 1.41 – 28.87 m/s with only a few measurements taken above 25 m/s. Despite the failure of Asali et al.'s (1985) correlation to adequately describe the present data, it is noted that their scheme of using the group $t_g^+ Re_g^{-0.2}$ (adapted from Asali, 1983) very well correlates friction factor data with entrainment better than t_g^+.

Fukano et al. (1991) investigated interfacial shear using an air–water system in three tube diameters of 10, 16, and 26 mm within the range of 20–60 m/s and 0.006–0.1 m/s superficial gas and liquid velocities corresponding to Re_g and Re_L values of 12720–99218 and 67–2900 respectively. The very low liquid velocities and relatively high gas velocities (Table 4-3) give large slip ratios hence high shear potentially leading to large droplet entrainments. Interestingly, Fukano et al. in their analyses assumed a smooth film with no entrainments. Measurements were carried out in horizontal annular flow and in both upwards and downwards vertical flow. They correlated their interfacial friction factor as a function of the superficial liquid and gas Reynolds numbers and notably, the Lockhart–Martinelli parameter. They obtained the following empirical model which they claimed holds irrespective of tube size and pipe orientation

$$(f_i/f_s - 1) = 8.53 \times 10^{-4} X^{2.82} Re_g^2 Re_l^{-1} \quad \textbf{(4-28)}$$

where *X* is the Lockhart–Martinelli flow parameter defined as follows

$$X = \sqrt{\frac{\Delta P_{lo}}{\Delta L} \Big/ \frac{\Delta P_{go}}{\Delta L}} \quad \textbf{(4-29)}$$

The quantities $\Delta P_{lo}/\Delta L$ and $\Delta P_{go}/\Delta L$ are the single phase pressure gradients as if the phases are flowing alone in the pipe. They are respectively calculated by the Darcy–Weisbach formulae for single phase pressure loss

$$\Delta P_{LO}/\Delta L = \tfrac{1}{2}(f_L/D)\rho_L u_{sl}^2 \quad \textbf{(4-30)}$$

$$\Delta P_{gO}/\Delta L = \tfrac{1}{2}(f_g/D)\rho_g u_{sg}^2 \quad \textbf{(4-31)}$$

Where f_L and f_G are the single phase friction factors for smooth pipes

$$f_l = 0.046 Re_l^{-0.2} \quad \textbf{(4-32)}$$

$f_g = f_s$ as defined in Equation **(4-24)**. Figure 4-13 shows the present data compared to this model. There is no systematic agreement with respect to superficial liquid velocities; instead, agreement exists at middle points across most liquid velocities. However, large errors still remain at many data points with over- and under-predictions of up to 1000 times the experimental values.

Hajiloo et al. (2001) used the same correlating method as Asali et al. (1985) for interfacial friction data obtained using four pipe diameters ranging from 15.6–41.2 mm. They used the group $t_g^+ Re_g^{-0.7}$ and obtained the correlation for interfacial friction factor

$$f_i/f_s = 125.2\, t_g^{+1.51} Re_g^{-1.05} \quad \textbf{(4-33)}$$

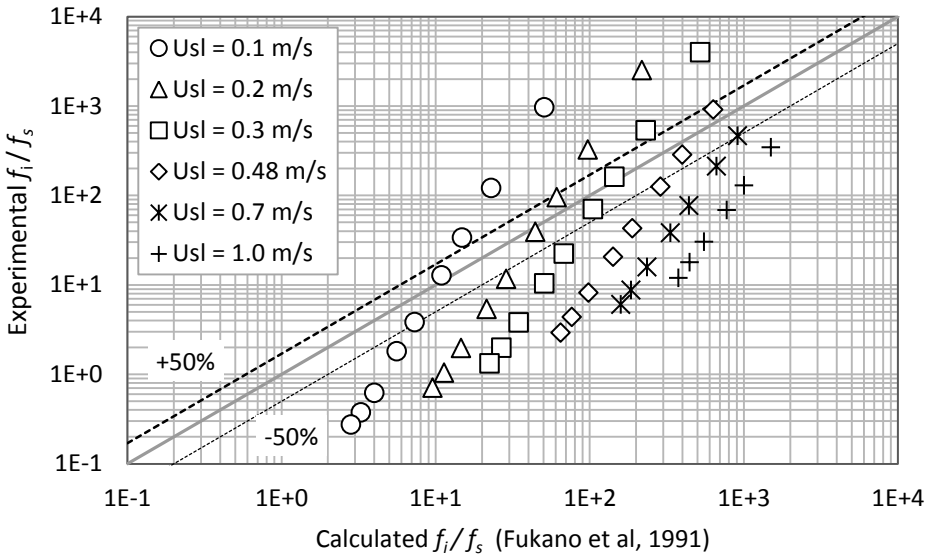

Figure 4-13: Prediction of interfacial friction factor by Fukano et al. (1991) vs the current experimental friction factor

The effect of pipe diameter on interfacial friction factor was apparent in their correlation when plotted against the experimental data obtained from the four different pipes in the study. They used superficial instead of the liquid film Reynolds number to calculate t_g^+ using Equation **(4-26)** while noting that their data was without entrainment. They clearly pointed out that entrainment was undesirable for the design application (falling films in scrubbers) which motivated their study and have made no attempt to measure or account for droplet entrainment. Here, it is stressed that entrainment is important in dispersed annular flow and is frequently encountered in gas condensate pipe systems and other industrial applications involving turbulent liquid films flowing with a gas core as it alters the film hydrodynamics.

Nonetheless, as can be seen in Figure 4-14, their empirical model provides better predictions with respect to the present data over a wider range of conditions than Henstock & Hanratty (1976) and Asali et al. (1985).

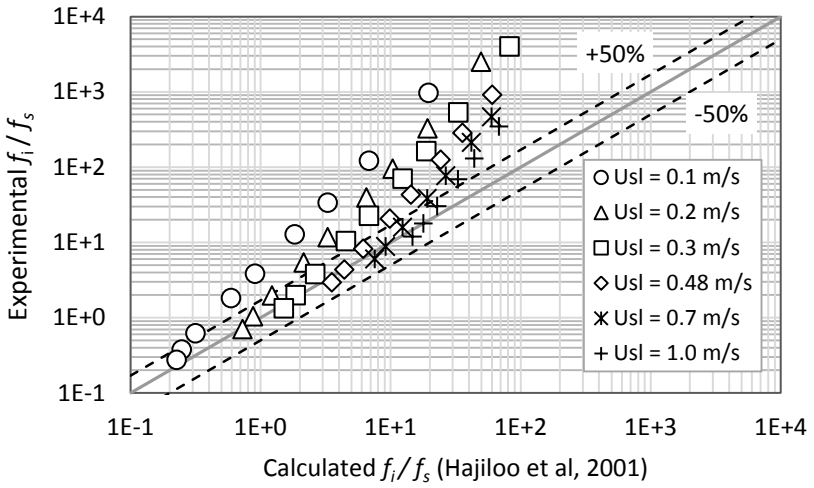

Figure 4-14: Prediction of interfacial friction factor by Hajiloo et al. (2001) vs the current experimental friction factor

Particularly good are the predictions for the thicker films at higher liquid Reynolds numbers where the velocities of both phases are closer (less phase slip) and there is less interfacial shear. As a result, the entrainment is minimal. These conditions very much resemble those in which Hajiloo and co-workers obtained their data. More importantly, this relative agreement suggests that the model was able to capture the effect of pipe diameter within this short range of conditions.

Other investigators have used various approaches in modelling two-phase frictional pressure drop in downward annular flow by treating both phases as a homogeneous mixture. In this case the friction factor is termed a two-phase friction factor and in reality, such methods are flow regime independent notably in the style of Lockhart–Martinelli (1949). The works of Klausner et al. (1991), Dalkilic et al. (2009) and Bhagwat et al. (2012) are cases in point. Hewitt & Hall-Taylor (1970) have shown using the data of Gill et al. (1964) that the

homogeneous model method is less accurate than flow regime specific methods.

4.3.5 New empirical correlation

In light of the various shortcomings of the published correlations, it is imperative to attempt to correlate the large pipe data separately which are characterised by large entrainment caused by large shear resulting from the significant velocity differences between the phases. These resemble the premises used by Asali (1983) and Asali et al. (1985) to correlate their data which were improvements to the rough sand analogue used by Henstock & Hanratty (1976). As turbulent two-phase flow consists of complex interaction of forces and phenomena, Hajiloo et al. (2001) noted that the rough sand analogue is simplistic. However, none of the correlations developed by these researchers described the present data satisfactorily.

Attempts have been made to use Asali et al.'s (1985) method, but failed to collapse the data (Figure 4-15) as well as their modified method as utilised by Hajiloo et al. (2001) (Figure 4-16). The latter method involves plotting f_i/f_s against the dimensionless group $t_g^+ Re_g^{-0.7}$ and fitting a power law curve through the data points. As earlier mentioned, this is in fact a modification of the correlation scheme of Asali et al. (1985) where $t_g^+ Re_g^{-0.2}$ was originally used. The former scheme produced a correlation coefficient R^2 value of 0.8078 immensely inferior to the 0.9671 value obtained for the latter method.

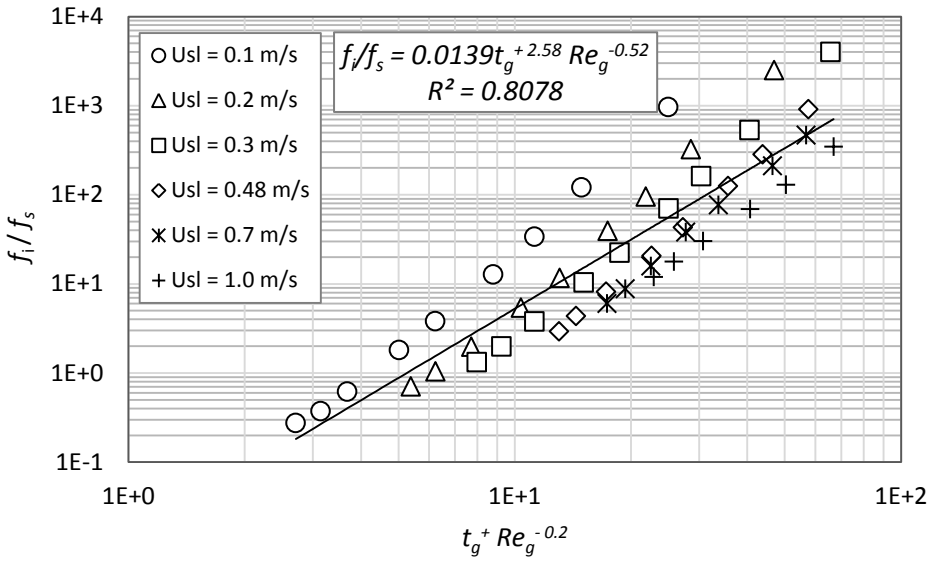

Figure 4-15: Attempted correlation of downward flow air–water two-phase interfacial friction factor using the method of Asali et al. (1995)

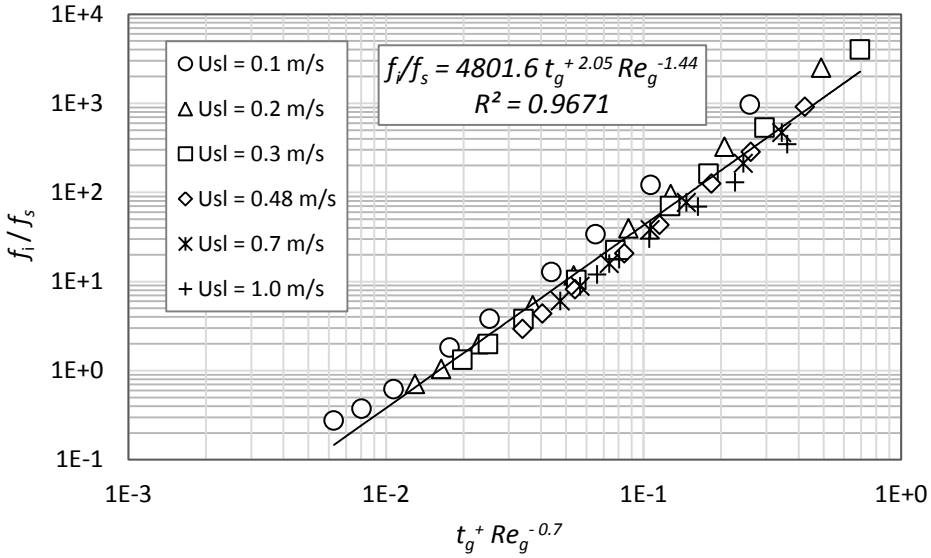

Figure 4-16: Correlation of interfacial friction factor for downward annular air–water two-phase flow

Therefore, the following empirical correlation is proposed for estimating the interfacial friction factor in downwards air–water two-phase annular flow in circular tubes for large diameter pipes, those with diameters up to 101.6 mm

$$f_i/f_s = 4801.6 t_g^{+\,2.05} Re_g^{-1.44} \quad \textbf{(4-34)}$$

Where t_g^+ is calculated using

$$t_g^+ = \frac{t}{\nu_g}\sqrt{\frac{\tau_i}{\rho_g}} \qquad \textbf{(4-35)}$$

In cases where liquid film thickness measurements *t* are not available, this can be estimated with a suitable correlation. Knowledge of the entrained droplet fraction is needed to calculate the droplet-laden core properties which are in turn needed to calculate τ_i given in Equation **(4-13)**. The correlation developed for entrainment droplet fraction in Section 5.2.7 can be used to estimate this in the absence of measured droplet fraction data.

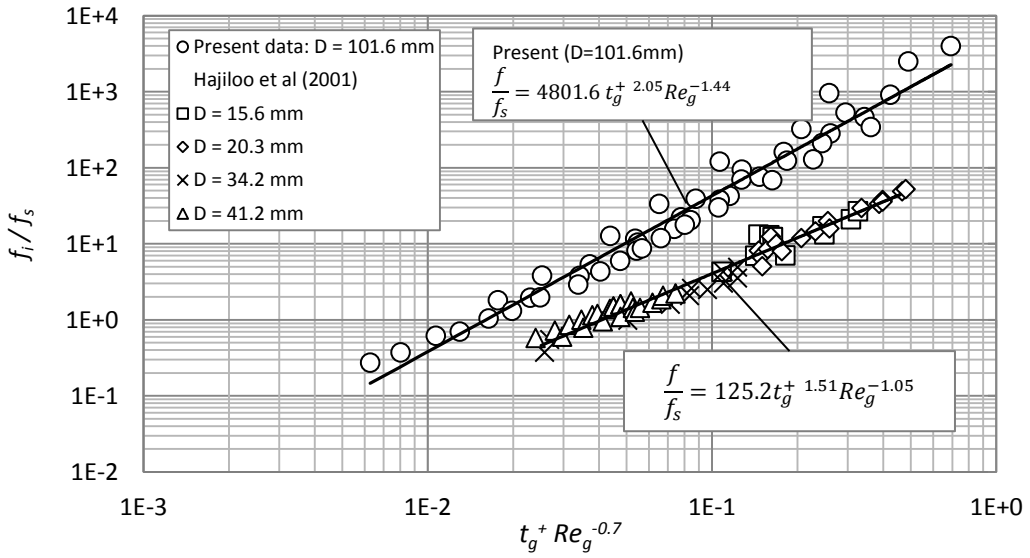

Figure 4-17: Effect of pipe diameter on annular downflow interfacial friction factor

To give some perspective on the effect of pipe diameter, Hajiloo et al.'s (2001) correlation was plotted side by side Equation **(4-34)** in Figure 4-17. A large difference is seen between the two models which can give quite erroneous

results if one is used in place of the other for interfacial friction factor estimations. The use of Equation **(4-34)** is therefore tentatively suggested.

Also, attempts have been made to find a new correlation for both large and small pipes using the data of Hajiloo et al (2001) from four different pipe diameters ranging between 15.6–41.2 mm and the large pipe data of 101.6 mm. That is one that effectively merges the two curves in Figure 4-17 meaning a model for interfacial friction factor that holds irrespective of pipe diameter. The correlation procedure involves the introduction of a factor $(\frac{t}{D} Fr_g)^{-1.1}$ which is a dimensionless group comprising the gas phase Froude number characterising the gravitational wave velocity of the gas–liquid interface and the film thickness non-dimensionlised by pipe diameter t/D. The index (-1.1) is obtained by regression analysis to produce the best fit. Both t/D and Fr_g are functions of the pipe diameter, thereby making the dimensionless group $(\frac{t}{D} Fr_g)^{-1.1}$ an even stronger function of pipe diameter. This new group remarkably collapsed all the data producing a reasonably good fit (see Figure 4-18). The data of Chung & Mills (1974) was also added thus showing that these are fairly consistent with the current results. The slight under-prediction of Chung & Mills (1974) data can be attributed to the fact that for their work, the film thickness was not measured directly but was calculated by a relation developed by Brotz (1954), however, the consistency with the current data is noted.

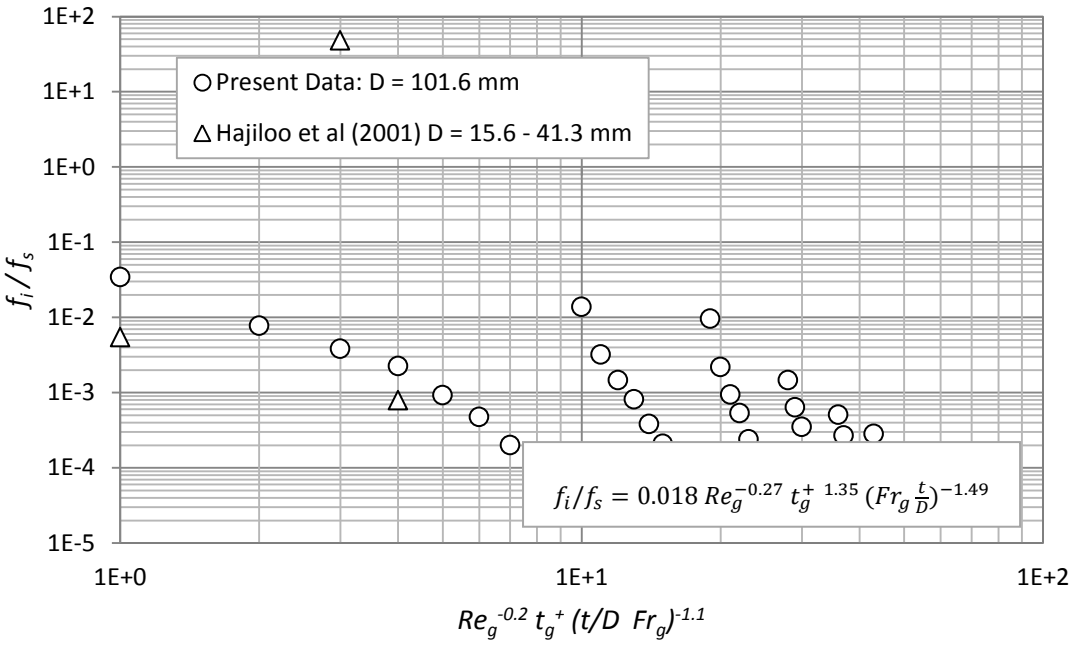

(a)

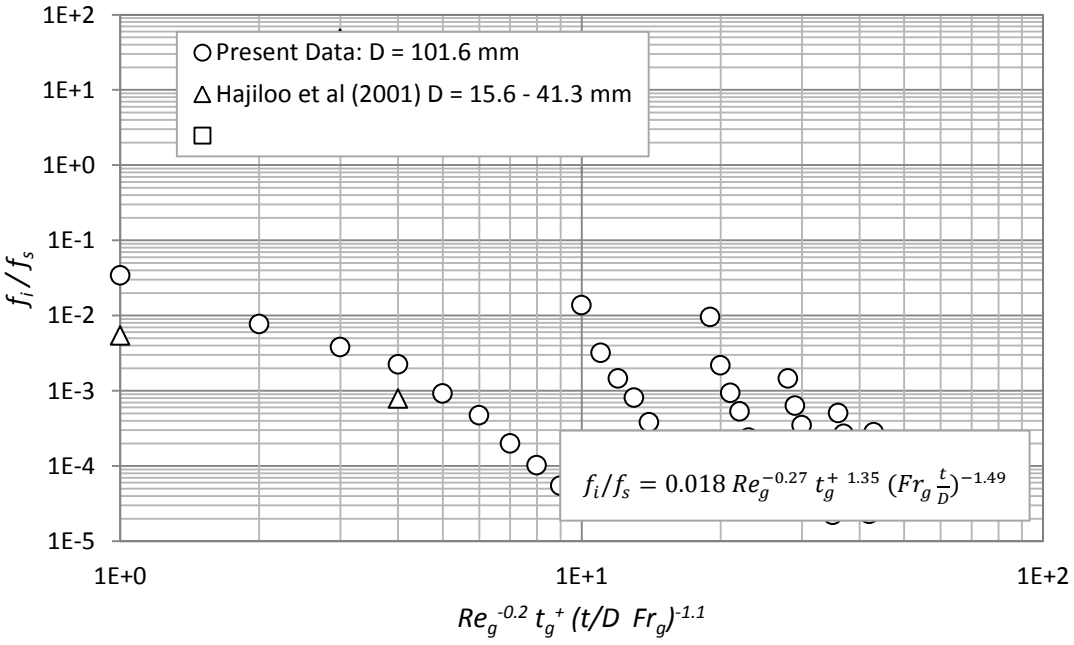

(b)

Figure 4-18: (a) Empirical correlation for downward interfacial friction factor covering both large and small diameter pipes. (b) Test of correlation using the data of Chung & Mills (1974)

The resulting correlation is as follows

$$\frac{f_i}{f_s} = 0.018\, Re_g^{-0.27}\, t_g^{+\ 1.35}\, (Fr_g \frac{t}{D})^{-1.49} \quad \textbf{(4-36)}$$

Where Fr_g the superficial gas Froude number calculated as

$$Fr_g = \frac{u_{sg}}{\sqrt{gD}} \quad \textbf{(4-37)}$$

In the application of Equation **(4-36**) situations may arise where t/D is not readily available from measured data and may have to be estimated by correlation. The film thickness correlation of Almabrok et al. (n.d.) developed for large pipes (given in Equation **(4-4)**) can be used

$$t^* = t(g/\nu_l^2)^{1/3} = 1.4459\, Re_{lf}^{0.3051} \quad \textbf{(4-38)}$$

Figure 4-19(b) shows that using Almabrok et al's film thickness correlation produces more scatter than if experimental film thicknesses are used (Figure 4-19(a)); it nevertheless predicts f_i/f_s with 56.3% of all data points within ±50% of the experimental f_i/f_s .

All data for 101.6 mm ID pipes obtained for this work fell within ±90.6% of Equation **(4-36)**, the developed correlation. In fact, 85.42% of all data points (large and small) fell within ±50% of this equation, thereby outperforming the other models surveyed (Table 4-4). Hajiloo et al.'s (2001) model was the best performer among the previously published correlations in terms of predicting the large diameter data with 39.58% of its predictions within 50% of the data and all of its predictions within 100% together with having the lowest percentage mean absolute error.

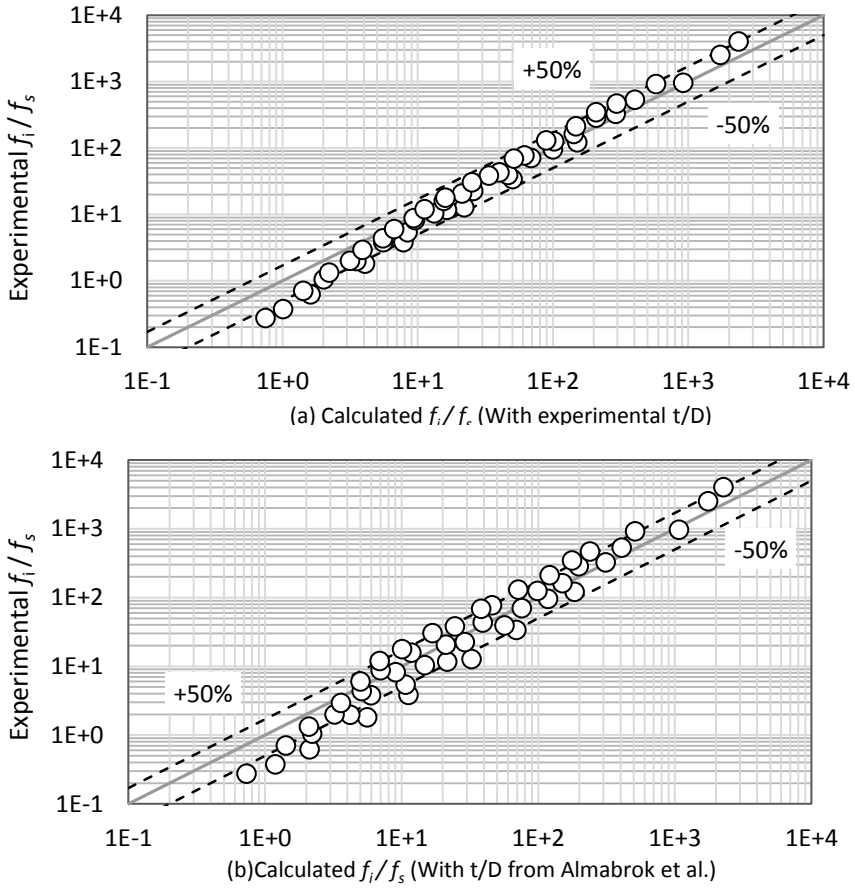

Figure 4-19: Interfacial friction factor calculations: using measured experimental film thickness data from (top) 101.6 mm ID pipe and (bottom) that predicted with Equation (4-36**)**

The other models all produced predictions above 100% mean absolute error with Fukano et al. recording over 700% as is seen in Figure 4-13 with predictions exhibiting large scatter. In the case of the new model correlated for both large and small pipes Equation **(4-36)**, the mean absolute error is slightly higher than that for large pipes (Equation **(4-34)**). This could be as a result of uncertainty introduced by Hajiloo et al's film thicknesses which were predicted rather than measured. In any case, Equation **(4-36)** outperforms all the previously published correlations and can be used more conveniently irrespective of pipe diameter, but produces slightly less accuracy when

compared to the correlations of Hajiloo et al for small pipes and Equation **(4-34)** for larger pipes respectively.

Table 4-4: Statistical comparison between large diameter experimental data and correlations

Performance parameter	Henstock & Hanratty (1976)	Asali et al.(1985)	Fukano et al. (1991)	Hajiloo et al. (2001)	Present work		
					Equation (4-34)	Equation (4-36)	Equation (4-36)†
% Mean Absolute Error*	295.91	135.19	700.45	56.5	31.69	42.49	63.93
% within ±50% of data	20.83	18.75	14.58	39.58	85.42	75	56.25
% within ±100% of data	64.58	81.25	33.33	100	100	87.5	83.33

† Using t/D calculated from correlation

* $Percentage\ mean\ absolute\ error = \frac{100}{n}\sum_1^n \frac{\left|(f_i/fs)_{exp} - (f_i/fs)_{model}\right|}{(f_i/fs)_{exp}}$

Despite the improved predictions of the developed correlation, it is worth mentioning that it must be applied with great caution outside Re_l and Re_g ranges of 11300–113000 and 3756–187000 respectively from which the correlation were developed. Figure 4-20 is a flowchart that summarises the model development procedure.

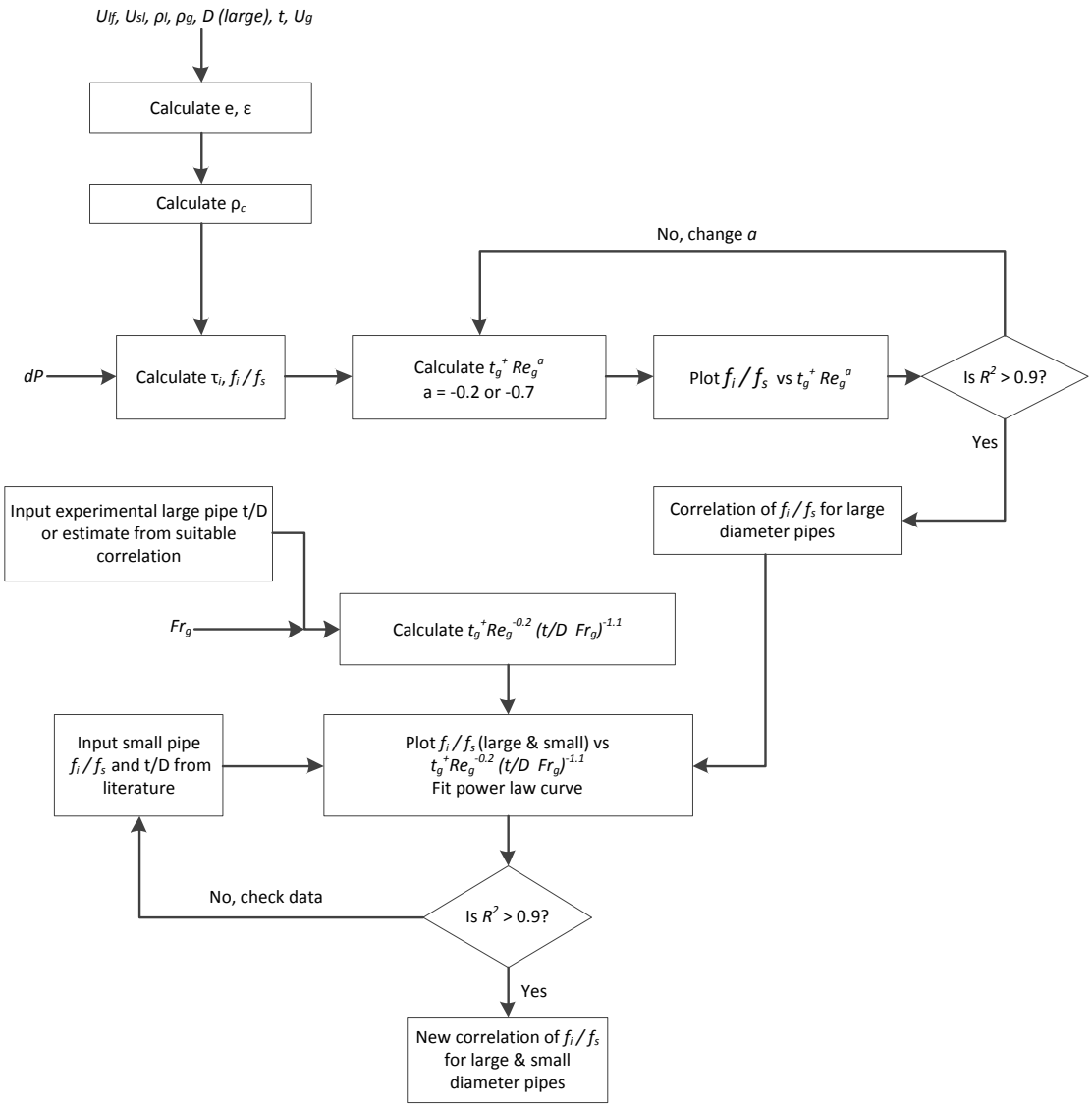

Figure 4-20: Flowchart for model development process

4.3.6 Conclusions

Several investigators have published studies showing that in turbulent multiphase flow systems, using correlations obtained from small diameter pipe systems to predict the behaviour of larger pipelines leaves much to be desired. An important class of such correlations are those predicting friction losses for the determination of pressure drops. Unfortunately, large diameter friction flow data is scarce in the open literature for developing new correlations, particularly

for downward two-phase flow. This chapter reports new experimental data obtained in an air–water downward co-current large diameter flow loop in Cranfield University's Oil and Gas Engineering Laboratory. The range of experimental superficial air and water superficial velocities covered are 1.42–28.87 and 0.1–1.0 m/s corresponding to Reynolds numbers of 8400–187000 and 11300–113000 respectively. Measurements were made for liquid film thickness, film velocity, pressure gradient and void fraction in the annular flow regime. All these were used to calculate the interfacial friction factor in a system characterised by large entrainment. Published correlations did not sufficiently fit these interfacial friction experimental data. Consequently, a new correlation was developed that fits the present large pipe data and which has been proposed for better interfacial friction factor estimations. It was extended for use in pipes for air–water systems covering 15.6–101.6 mm diameters as results show that literature data are consistent with the developed correlation.

4.3.7 Chapter summary

Interfacial friction and liquid film thickness are key variables for predicting annular two-phase flow behaviours in vertical pipes. In order to develop improved correlations for both in downward co-current annular flow, the pressure gradient, film thickness, and film velocity data were obtained from experiments carried out on Cranfield University's Serpent Rig, an air/water two-phase vertical flow loop of 101.6 mm internal diameter. The air and water superficial velocity ranges used are 1.42–28.87 and 0.1–1.0 m/s respectively. These correspond to Reynolds number values of 8400–187000 and 11000–113000 respectively. The findings can be summarised as follows:

- Pressure gradient behaves differently in the two halves of a downcomer. In the ranges of 5–10 m/s gas superficial velocity,
- The mean film thickness data from this study was compared to existing correlations and theoretical models. It was observed that the liquid film thickness from large diameter pipes present a distinctly different slope to those of the existing small diameter correlations/theoretical models, suggesting a change in the film character for large diameter pipes. Therefore, new fitting parameters have been obtained for the Nusselt equation as it applies to larger pipes using the current data from the downward section of the 101.6 mm pipe.
- The proposed interfacial friction factor correlation, takes into account the effect of pipe diameter by using the interfacial shear data and dimensionless liquid film thicknesses related to different pipe sizes ranging from 10 to 101.6 mm, including those from published sources by numerous investigators. It is shown that the predictions of this new correlation outperform those from previously reported studies for tubes greater than 100 mm internal diameter in size.

Chapter Five

UPWARDS ANNULAR FLOW

5.1 Interfacial friction factor in upwards adiabatic co-current gas–liquid annular two-phase flow in large diameter pipes

5.1.1 Summary of upwards large pipe two-phase flow data obtained from the open literature

Large diameter pipe annular two-phase flow literature data with respect to pressure gradient, film thickness and void fraction is scarce. However two were found in the open literature: the works of Zangana (2011) and Skopich et al. (2015) who worked on air/water upflow annular flow in vertical pipes of 127 and 101.6 mm internal diameters respectively. As shown in Figure 5-1, their experiments fall in the annular flow regime. Zangana made simultaneous measurements of wall shear stress (using uni- and multi-directional hot wire probes), liquid film thickness (using pin probes), and pressure gradient. He observed that the onset of annular flow occurred at the same dimensionless gas velocity as it would in smaller pipes and that the total pressure gradient for given liquid and gas superficial velocities fall as the pipe diameter increases.

Similarly, in the work of Skopich et al. (2015) measurements were made of time averaged pressure gradient, liquid holdup, and cross-sectionally averaged liquid film thickness; in order to study liquid loading phenomenon in gas transport pipes. Liquid holdup measurements were made using quick closing valves in the middle of the 15.4 m long test section.

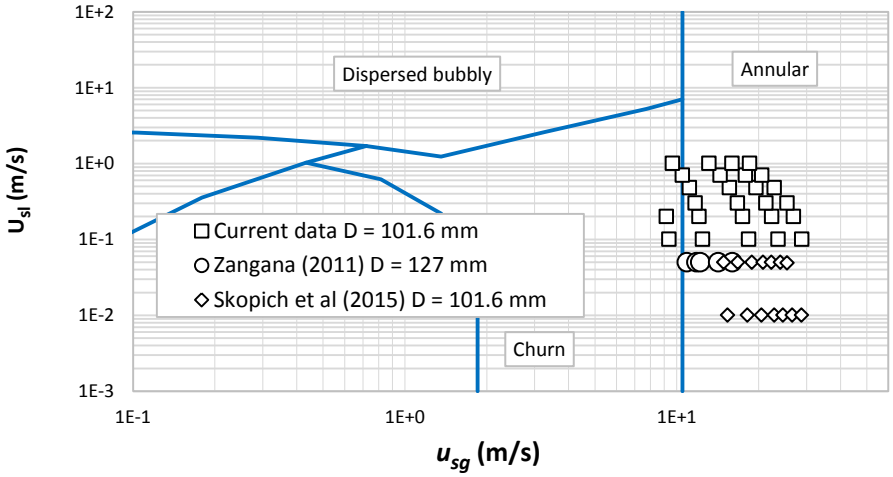

(a)

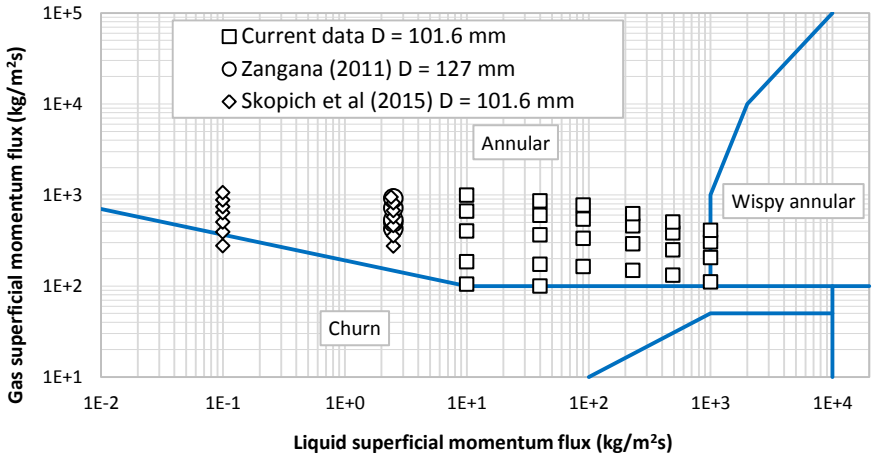

(b)

Figure 5-1: Flow regime maps (a) Taitel and Dukler (1976) (b) Hewitt and Roberts (1969) showing experimental conditions for data points obtained for this study and those from the literature.

They noted that discrepancies observed between experimental pressure gradient, liquid holdup and mechanistic model predictions are due to inaccurate flow regime prediction resulting from the different regime transitions occurring at different pipe scales.

5.1.2 Calculation of interfacial properties from experimental measurements

A total of 45 data points were obtained for this study in the range of Re_g = 59000–400000 and Re_l = 1100–113000. The interfacial friction factor is

estimated from measured pressure gradient by taking a momentum balance at the gas–liquid interface with the assumption that the flow is fully developed:

$$f_i = \frac{2\tau_i}{\rho_G u_{sg}^2} \quad \textbf{(5-1)}$$

where τ_i the interfacial friction factor is estimated from the measured pressure gradient by

$$\tau_i = \left(-\frac{dP}{dz} - \rho_c g\right)\frac{D-2t}{4} \quad \textbf{(5-2)}$$

This equation assumes a uniform film thickness around the pipe cross-section. Here it should be noted that since there is significant droplet entrainment in the gas core, pure gas properties are replaced by linearly phase-averaged density of droplet laden gas core:

$$\rho_c = (1-\varepsilon_c)\rho_L + \varepsilon_c \rho_g \quad \textbf{(5-3)}$$

Core flow viscosity was also calculated using a linear phase-averaged mixture rule as defined by Cicchitti et al. (1960); Hewitt & Hall-Taylor (1970); recently used by Cioncolini et al. (2009) and Cioncolini & Thome (2010); where ε_c is the gas core void fraction estimated as:

$$\varepsilon_c = \frac{\varepsilon}{\varepsilon+\gamma(1-\varepsilon)} \text{ where } \gamma = e\frac{\varepsilon}{(1-\varepsilon)}\frac{1-x}{x}\frac{\rho_g}{\rho_l} \quad \textbf{(5-4)}$$

And ε being the cross-sectionally averaged void fraction; γ is the droplet holdup, estimated by ignoring the slip between the entrained droplets and the gas; *e* is the entrained droplet fraction; and *x* is the gas quality.

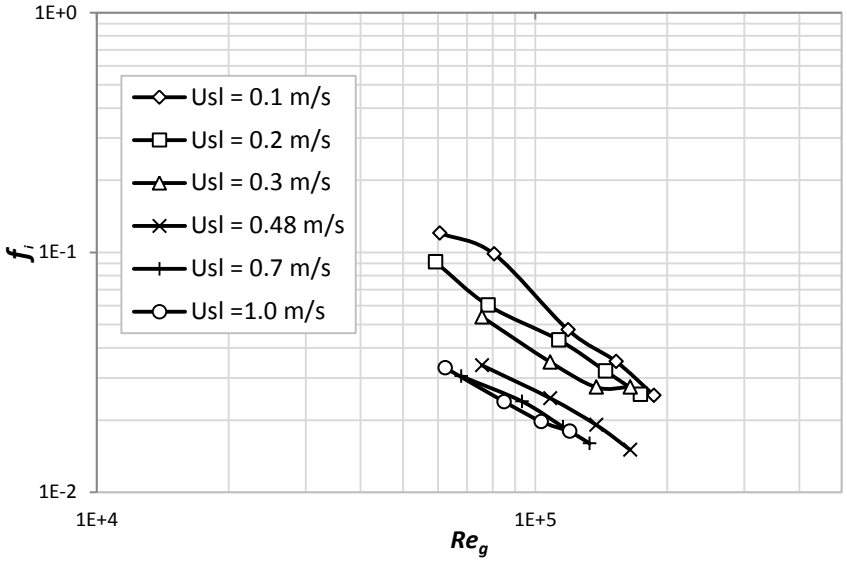

Figure 5-2: Variation of interfacial friction factor with superficial gas Reynolds number

The experimentally obtained interfacial friction factor was plotted as a function of the gas Reynolds number as shown in Figure 5-2. It is clear from the figure that f_i monotonically decreases with increasing Re_g irrespective of liquid superficial velocity. However, there is a direct relationship with the superficial liquid velocity. The inverse relationship with the gas Reynolds number is not dissimilar with that given in the turbulent flow region of the Moody diagram for single phase water flow. Here the liquid film acts in a similar fashion to the pipe wall for the flowing gas core.

5.1.3 Comparison of experimental interfacial friction factor with published correlations and new empirical correlation

Wallis's (1969) developed a correlation for interfacial friction factor in vertically upwards annular two-phase flow which solely depends on the relative liquid film thickness as follows:

$$f_i = 0.005(1 + 300t/D) \quad \textbf{(5-5)}$$

Since then, a number of Wallis-type empirical relations have been developed such as that by (Moeck 1970) for the disturbance wave regime. Noting that existing correlations do not adequately cater for thick films at low gas Reynolds numbers, Fore et al. (2000) combined new data obtained at high pressures in a 5.08 × 101.6 mm rectangular duct with those of Asali (1983) and Fore & Dukler (1995) to obtain a new correlation for f_i as follows:

$$f_i = 0.005[1 + 300(t/D - 0.0015)] \quad \textbf{(5-6)}$$

In order to account for a change in liquid viscosity, Fukano and Furukawa (1998) carried out experiments in a 26 mm diameter pipe with air/water and air/glycerol mixtures; they proposed a correlation which was within ±15% of the experimental data as:

$$f_i = 0.425(12 + \nu_l/\nu_w)(1 + 12t/D)^8 \quad \textbf{(5-7)}$$

Where ν_l and ν_w are liquid kinematic viscosity of liquid and water at 20˚C. It is however illustrated that these equations do not amply represent the present large pipe friction factor as well as those of Zangana (2011) and Skopich et al. (2015) as shown in Figure 5-3. While there is reasonable agreement at high interfacial shear stress regions where the film is smooth, a sharp change in slope of the experimental data lead to large deviations at lower interfacial shear stresses due to the rougher gas–liquid interface of thicker films. The reason for the deviations (apart from the difference in hydrodynamics occurring in different pipe scales) could be that the increasing influence of the gas velocity has been ignored.

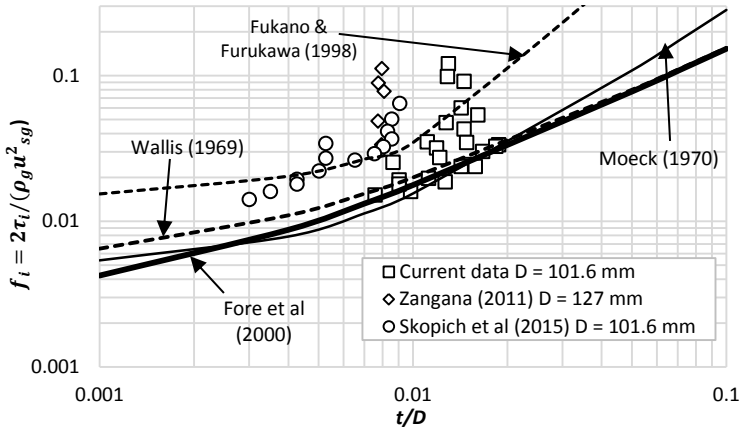

Figure 5-3: comparison of measured friction factors with Wallis, Moeck, Fukano & Furukawa, and Fore et al. correlations.

Therefore another group of relations were proposed that comprise the gas Reynolds number. These include those of Hori et al. (1978), Asali et al. (1985), Fukano et al. (1991) and Wongwises & Kongkiatwanitch (2001). Fukano & Furukawa (1998) noted that the correlation of Hori et al given in Equation **(5-8)** over-predicts their data at small t/D values.

$$f_i = 1.13\, Re_g^{-0.89} Re_l^{0.68} Fr_g^{0.25} Fr_l^{-0.45} (\mu_l/\mu_w)^{0.7} \qquad \textbf{(5-8)}$$

Where μ_w is the viscosity of water at 20˚C. Here over-prediction in all t/D regions is reported for the current, Skopich et al.'s and most of Zangana's data using Hori et al.'s model (Figure 5-4b).

Asali et al. (1986) derived the following semi-empirical correlation for upwards flow f_i in the roll wave regime:

$$f_i = f_g \left[1 + Re_g^{-0.2} \left(Re_g \sqrt{\frac{f_i}{2}} \frac{t}{D} - 4 \right) \right] \qquad \textbf{(5-9)}$$

Where f_g is the single phase gas friction factor. They used their upflow experimental data in 22.9 and 42 mm pipes together with that of (Andreussi &

Zanelli 1979) (24 mm downflow), Webb & Hewitt (1975) (31.8 mm upflow), Cousins et al. (1965) (95 mm vertical upflow) and Shearer & Nedderman (1965) (15.9 mm, 31.8 mm upflow).

Fukano et al. (1991) regressed experimental parameters obtained from pipes of 10, 16, and 26 mm diameter at 1–1.3 bara pressure. The flow inclinations used were -90˚, 90˚, and 90˚ indicating upwards, downwards, and inclined flow. A correlation for the interfacial friction factor was obtained which they claimed applies irrespective of flow direction or pipe size:

$$f_i = f_g\left[1 + 8.53 \times 10^{-4}\, X^{2.82} Re_g^2 / Re_l\right] \quad \textbf{(5-10)}$$

Where X is the Martinelli parameter. For the work of Wongwises & Kongiatwanich (2001), a 3 m-long 29 mm internal diameter pipe was used to measure liquid film thickness using ring electrodes. They found out that the interfacial friction factor well correlates with the measured film thickness and the gas Reynolds number as follows:

$$f_i = 17.172\, Re_g^{-0.768} (t/D)^{-0.253} \quad \textbf{(5-11)}$$

They showed that the correlation predicted to within a ±25%.

These correlations do not describe the collected large pipe data satisfactorily either; with a large part of the predictions of Hori et al. (Figure 5-4a) and Fukano et al. falling outside the ±50% error band. Consistent under-predictions were obtained using the models of Wongwises & Kongkiatwanitch (Figure 5-4b) and that of Asali et al. even though the latter gave better predictions at low shear region.

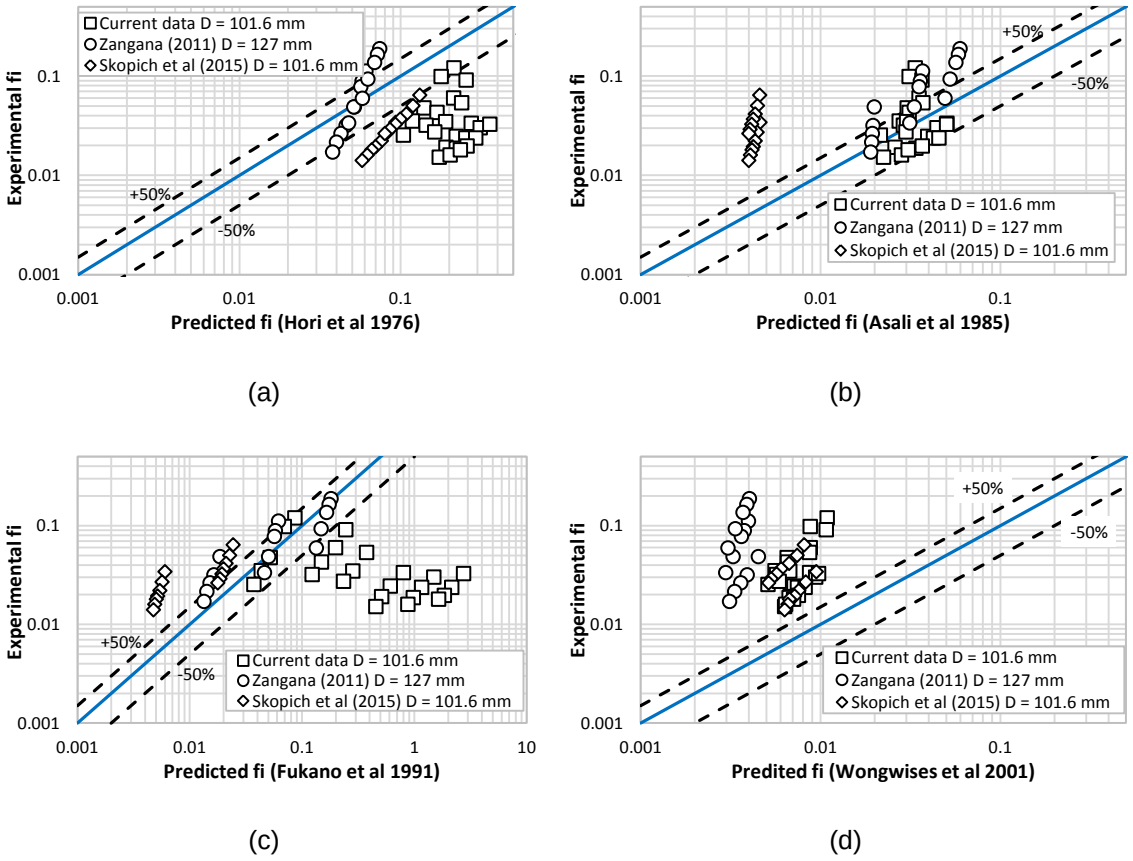

Figure 5-4: Experimental vs friction factors predicted with Hori et al., Asali et al., Fukano et al., and Wongwises & Kongkiatwanitch correlations

These form the basis for a separate correlation of the large pipe friction data. It was important to capture the effect of the flowing gas with the insertion of the gas Reynolds number (based on superficial velocity) in any new correlation going by the deficiencies of Equations **(5-5) – (5-7)** (Figure 5-3). Also, the effect of pipe diameter is represented by inclusion of a gas Froude number. Including t/D is based on both the Wallis type correlations (which are sole functions of the dimensionless film thickness) and that used by later researchers such as Hori et al., Wongwises & Kongiatwanich, Asali et al., and Fukano et al. who also used dimensionless quantities such as liquid and gas Reynolds numbers. The inclusion here of the gas Froude number – a ratio of gravitational and wave velocity forces – is for capturing different pipe scales; its inclusion also seems

logical since it is a non-linear and hence strong function of pipe diameter. Additionally, as Azzopardi et al. (1982) have observed from their experiments, the liquid wave structure in large pipes is different from that present in smaller pipes, in that the waves are circumferentially localised and not perpendicular to the flow and are said to be “incoherent”. As a result, the interface wave velocity behaviour (affected by the gas flow at the interface) will differ from those experienced in smaller pipes. Thus, for larger channels, the friction factor is assumed to follow the power law function:

$$f_i = \alpha\, Re_g^{\beta} Re_l^{\gamma} Fr_g^{\delta} Fr_l^{\varepsilon} (t/D)^{\theta} \qquad \textbf{(5-12)}$$

Initial trials of multiple non-linear regression showed that correlating with the liquid Froude number had negligible effect on f_i prediction. It was therefore eliminated from the list of dimensionless groups such that the final form of the power law is as follows:

$$f_i = \alpha\, Re_g^{\beta} Re_l^{\gamma} Fr_g^{\delta} (t/D)^{\varepsilon} \qquad \textbf{(5-13)}$$

Application of the regression procedure to determine the factor α and indices $\beta - \varepsilon$ resulted in the following correlation being obtained for interfacial friction factor:

$$f_i = 6059\, Re_g^{-0.05} Re_l^{-0.38} Fr_g^{-1.6} (t/D)^{0.7} \qquad \textbf{(5-14)}$$

Equation **(5-14)** produces a better fit to the experimental data as can be seen in Figure 5-5 with 86% of all predicted points within 50% of the experimental values when compared to the existing correlations. This fact is shown in Table 5-1. Also the new correlation had the least percentage mean absolute error (PMAE) of 33.9%. The PMAE is defined as $PMAE = \frac{1}{n}\sum_i^n |\epsilon_i|$, where $|\epsilon_i| =$

$\left|\frac{E_{exp}-E_{pred}}{E_{exp}}\right| \times 100\%$. Only the correlation of Asali et al. and Fore et al. come close producing 58.3 and 58.8% respectively, while that of Fukano et al (1991) had PMAE of 1675.6%. In the case of the latter correlation, use was made of the Lockhart-Martinelli parameter *X* for correlation which treats both phases as a homogeneous liquid. Homogeneous models are known to work for flows where there is good mixing of the phases and are assumed to travel at the same velocity. But in the case of annular flow where phase slip is high, homogeneous models' predictive quality degenerates with increasing velocity difference at the interface.

Table 5-1: Comparison of new correlation with existing ones

	New	1	2	3	4	5	6	7	8
PMAE	33.9	122.0	95.1	119.6	1675.6	58.3	91.8	58.8	541.1
% within ±50% of data	86.9	33.3	28.6	50.0	19.0	64.3	9.5	45.2	0.0
% within ±100% of data	100.0	64.3	57.1	54.8	28.6	88.1	83.3	92.9	0.0

Where 1. Wallis et al. (1969), 2. Moeck (1971), 3. Hori et al (1976), 4. Fukano et al (1991), 5. Asali et al (1985), 6. Fukano & Furukawa (1998), 7. Fore et al (2000), 8. Wongwises & Kongiatwanich (2001)

As can be seen, 100% of all predictions of the new correlation are within 100% of the experimental values with those of Asali et al., Fukano & Furukawa and Fore et al. coming close at 88–93% of predictions being within a 100% error band.

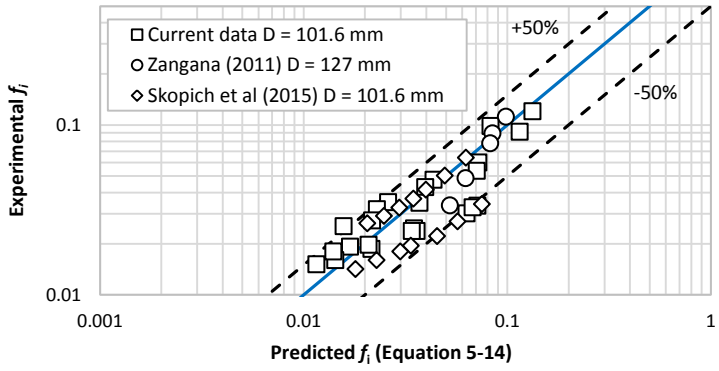

Figure 5-5: Comparison of new correlation with experimental data

5.1.4 Conclusion and future work

Experiments were performed to obtain pressure gradient and film thickness data for annular two-phase flow in large diameter vertical pipes. Published correlations did not sufficiently describe the interfacial friction factors calculated from the data and those from other sources. For example, most of the Wallis–type correlations underpredicted large pipe interfacial friction factors, signifying that interfacial friction factor in large pipes does not vary with dimensionless film thickness alone. Therefore, a new correlation has been proposed exclusively for large pipes from the measurements of this study and those from two other authors, using the dimensionless film thickness, gas/liquid Reynolds numbers and the gas Froude number. The new correlation enhanced the prediction of the friction factors. It therefore provides better frictional pressure gradient estimation for example in industrial scale gas condensate pipes and boilers. It is simple and can be easily incorporated into existing flow simulator codes for improved prediction in the annular flow regime. Incorporation of smaller pipe data will additionally increase the robustness of the empirical correlation for application over a wider range of flow conditions and pipe sizes.

5.2 Correlation of entrained droplets in co-current annular flow in large diameter pipes

5.2.1 Introduction

Annular flow has been identified as one of the most commonly observed flow regimes in a wide variety of gas–liquid two-phase flows in industrial applications such as air conditioning, heat exchangers and wet gas pipelines. This type of flow pattern is characterised by a continuous flow of liquid film along the pipe inner periphery with a centralised gas core containing liquid droplets entrained from the flowing liquid film. Accurate modelling of the amount of liquid entrained into the gas core (the entrained droplet fraction) is important in correctly determining pressure drop/pumping requirements in pipes, appropriate design of facilities downstream of vertical gas well tubing, estimating the inception of dryout in boiling heat transfer and the efficiency of nuclear reactor core cooling as well as prevention of Loss of Coolant Accidents (LOCA). These models (mostly in the form of empirical correlations) are embedded in thermal-hydraulic codes as constitutive relations (closure relationships) for either the determination of entrainment rate or entrained droplet fraction.

Correlation of entrained droplet fraction data has been carried out over the years by many investigators (Paleev & Filippovich 1966; Wallis 1968; Oliemans et al. 1985; Ishii & Mishima 1989; Hewitt & Govan 1990; Pan & Hanratty 2002; Barbosa et al. 2002; Sawant et al. 2008; Sawant et al. 2009; Cioncolini & Thome 2010; Cioncolini & Thome 2012) with a majority using air and water as the working fluids in their experimental campaigns. However, these studies were done with pipes of internal diameters (ID) between 5–57 mm smaller than

typical wet gas risers for example, where the tubes have diameters in excess of 200 mm. Several authors (Oliemans et al. 1986; Pickering et al. 2001; Schlegel et al. 2012; Lao et al. 2012) have warned of the danger of extrapolating multiphase flow parameters (such as liquid film thickness, two-phase/interfacial friction factor, or droplet fraction) from small to large diameters as is done for single phase flows. Based on a thorough literature search, such correlations developed using data exclusively from large pipes are not in existence.

The purpose of this section is to do a comparative study of several published correlations used for the prediction of entrained droplet fraction in vertical annular two-phase flow; determine their suitability for use in estimating large pipe (ID>100 mm) data and hence produce a new correlation of droplet entrainment for use in large diameter pipes as result of the inadequacies of using reported correlations.

Use will be made of liquid film thickness, velocity and droplet entrained fraction data from the 101.6 mm Serpent Rig together with that from a 125 mm ID vertical pipe by (Azzopardi et al. 1982) and from the work of (Van der Meulen 2012) who studied droplet entrainment in annular flow in a 127 mm ID riser.

5.2.2 Visualisation of entrained droplets via reconstructed WMS images

Wire mesh sensor reconstructed videos and images were used for flow visualisation. The reconstructed videos, obtained by stacked cross-sectional images obtained at a recording rate of 1000 Hz, provided corroboration of flow regimes previously identified by visual observation (See Almabrok 2014). Furthermore, the time averaged cross-sectional void fraction produced the

reconstructed images shown in Figure 5-6. The figure shows flow visualised at $u_{sl} = 0.48$ and 0.7 m/s respectively. As can be seen, the thickness of the liquid film on the pipe periphery diminishes with increasing gas velocity. Conversely, droplet entrainment increases as a result; with the entrained droplets in the gas core clearly visible as indicated by the arrows. The same can be said at similar gas velocities when liquid velocity increases. The droplet fraction is seen to be marginally higher at $u_{sg} = 17.55$ m/s, $u_{sl} = 0.7$ m/s when compared to that at $u_{sg} = 23.20$ m/s, $u_{sl} = 0.48$ m/s. Based on this evidence, the gas and liquid superficial velocities as well as liquid film thickness – when expressed in dimensionless form – are good candidates for correlating entrained droplet fraction data.

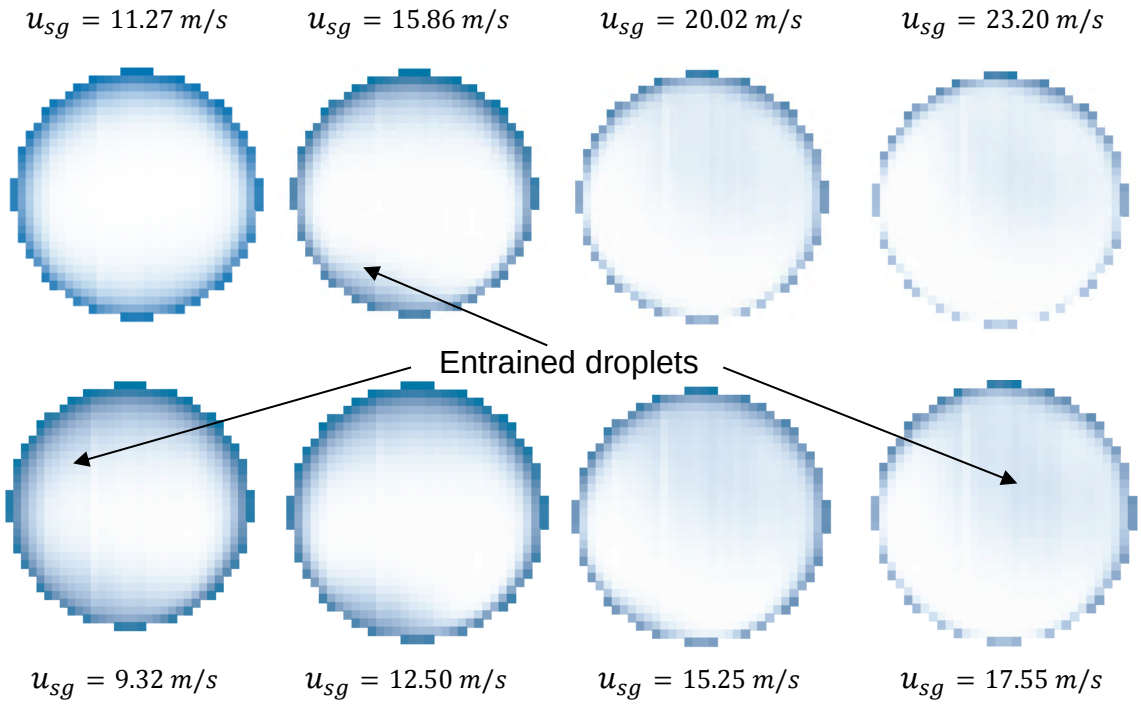

Figure 5-6: Examples of reconstructed vertical upflow time averaged WMS void fraction images at $u_{sl} = 0.48\ m/s$ (top row) and $u_{sl} = 0.7\ m/s$ (bottom row). Blue signifies water at low void fractions while white signifies air at high void fractions nearer 1.

5.2.3 Flow regime identification and regime maps

For downward flow, the range of the experimental conditions chosen corresponds to conditions in the falling film and annular flow regime characterised by liquid film on the pipe circumference and a gas core (i.e. without liquid droplets entrained) or gas/droplet mixture (i.e. with liquid droplets entrained) in the central area.

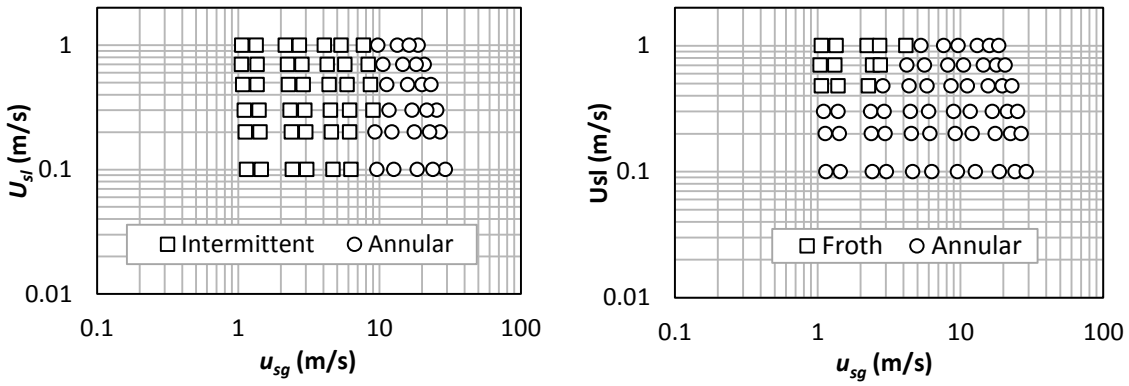

Figure 5-7: Flow regime maps based on visual observation (a) at top position of upward (b) at bottom position of downward flowing section of test rig

Figure 5-7(a) shows the flow regime map based on the tested superficial gas and liquid velocities in upwards flow. As can be seen, regions where annular flow occurs are between 9 and 30 m/s Usg for the chosen liquid superficial velocities of 0.1–1.0 m/s. Flow regimes marked as intermittent were characterised by highly oscillatory and rough gas–liquid interface. These observations are consistent with the earlier study of Almabrok (2014) who worked on the same experimental setup. The flow regime identification was done by way of visual observation of the flow configuration during tests, and by studying high speed videos and images of the flow. These observations were

made via transparent Perspex sections provided at the top, middle and bottom sections of the test rig.

Figure 5-7 (b) shows the flow regime map based on the tested superficial liquid and gas velocities for downward flow. Unlike for the upwards flow, the region where annular flow occurs is wider: 1.1–29 m/s u_{sg}. As can be seen, annular flow dominates, which is due to the over-riding effect of gravity on the flow more so by increasing the momentum of the denser liquid phase. The other regions of non-annular flow can best be described as “froth” flow regime, characterised by severe well-mixed gas–liquid flow thereby leading to a larger interaction of the phases. This was similarly observed by Usui (1989), Usui & Sato (1989) in 16 and 24 mm pipes; and Bhagwat et al. (2012), Bhagwat, et al. (2012) in a 12.5 mm internal diameter pipe. It is instructive to note that flow conditions producing frothy behaviour were not used in the analyses subsequently presented in this study.

5.2.4 Large diameter pipe literature data

Literature data for entrained liquid droplet in large pipes is scarce. However, data was obtained from the works of Azzopardi et al (1982) and Van der Meulen (2012) who carried out air/water experiments on vertical pipes of 125 and 127 mm internal diameter. As can be seen in both the flow regime maps of Hewitt & Roberts (1969) and Taitel & Dukler (1976) (Figure 5-8 (a) and (b)), the experimental conditions for Azzopardi et al’s entirely fall in the annular flow region. However, some overlaps occur in both flow regime maps for the case of Van der Meulen where the data straddles annular and churn flow. The extent of overlap is higher on the flow pattern map of Hewitt & Roberts where the fluid

superficial momentum fluxes (ρU^2) are plotted as against superficial velocities for Taitel & Dukler's. Nevertheless, Van der Meulen noted that the majority of his data fell in the annular flow region based on visual observation and the analysis of high speed photographs. In addition, since flow regime transitions actually occur over ranges rather than the sharp transitions represented by the lines (Whalley 1996; Kim 2000; Ghajar 2005), all the collected data are treated as annular flow given that a complete set of data was obtained comprising liquid film thickness, film velocity, entrained droplet fraction and pressure gradient. Similarly, annular flow was observed for the majority of flow conditions in downward flow as previously shown in Figure 5-7 (b). The identified annular flow conditions are plotted against the flow regime map of Bhagwat et al. (2012) (Figure 5-8 (c)). Although some of these points fall in the falling film and froth flow regions of the map, visual observation and analysis of void fraction PDFs show that the flow regimes are distinctly annular.

Azzopardi and co-workers carried out their measurements in a 125 mm diameter vertical tube at AERE Harwell with the fluids (air and water) flowing concurrently upwards. Entrained liquid droplet fraction was measured indirectly by extracting the liquid film through a porous wall feature thereby obtaining the liquid film flow rate. Their measured entrained liquid fractions are shown in Table 5-2. The ranges of liquid and gas mass fluxes covered in their experiments were 2.6–20.6 kg/m^{2}s and 35.9–61.6 kg/m^{2}s corresponding to liquid and gas Reynolds number ranges of 579–2341 and 196000–336200 respectively.

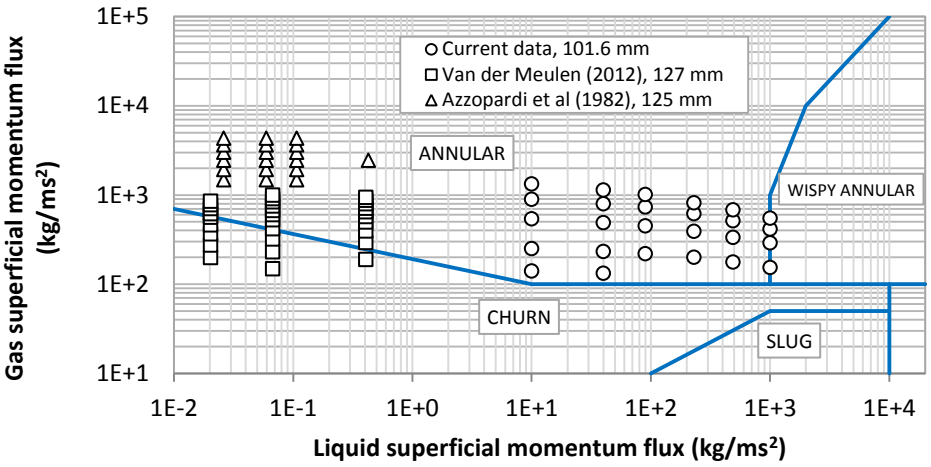

(a)

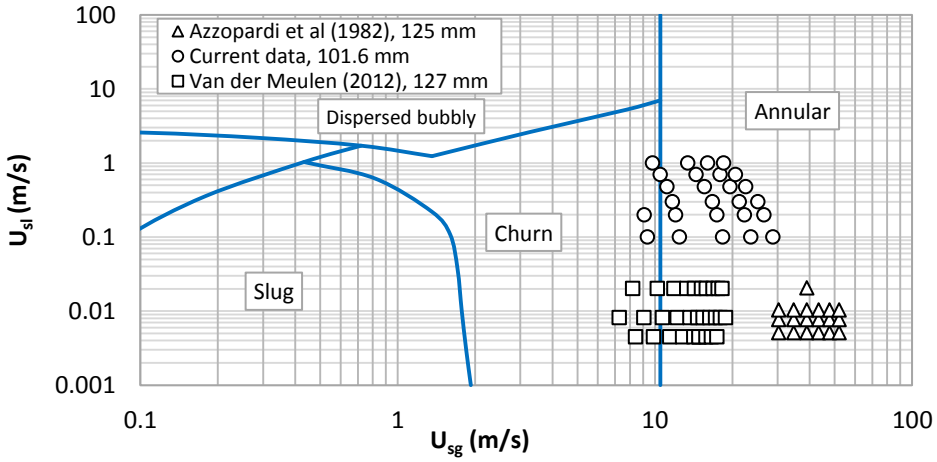

(b)

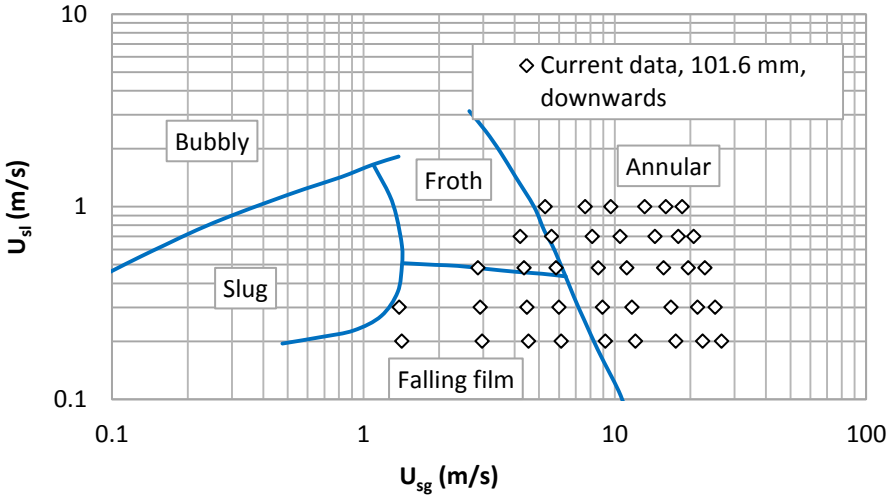

(c)

Figure 5-8: Comparison of present and literature annular flow data with the flow regime maps of (a) Hewitt & Roberts (1969) for vertical flow (b) Taitel & Dukler for vertical flow (c) Bhagwat et al. (2012) for downward annular flow

Table 5-2: Fraction of liquid entrained (Azzopardi et al 1982)

Liquid mass flux (kg/m^{2}s)	2.6	5.1	7.7	10.3	20.6
Gas mass flux (kg/m^{2}s)					
35.9	0.08	0.21	0.37	0.48	
41.1	0.08	0.25	0.38	0.49	
46.2	0.08	0.25	0.43	0.51	0.63
51.3	-	0.27	0.45	0.52	
56.5	0.1	0.34	0.49	0.57	
61.6	0.09	0.36	0.51	0.59	

Van der Meulen (2012) performed experiments at 2 bar pressure in the vertical 127 mm internal diameter pipe at the University of Nottingham. Measurements were made for the liquid film thickness using conductance ring probes. Measured liquid film velocities at different superficial liquid velocities were also obtained from which he used to calculate the entrained droplet fraction using Equation (5-15).

Table 5-3: Summary of large diameter entrained droplet fraction experimental data

Study	D (mm)	L/D to sensor(s)	Data type(s)	P (bara)	Re_g range	Re_l range	Flow direction	No. points
Azzopardi et al. (1982)	125	40	*E*	1.30	195000–336000	700–2880	↑	19
Van der Meulen (2012)	127	83	*E, t*	1.15	67000–147500	637–2861	↑	31
Current upwards	101.6	39	*E, t*	1.50	58000–187000	11300–113300	↑	26
Current downwards	101.6	39	*E, t*	1.50	9000–162000	22600–113000	↓	39

5.2.5 Film velocity results and determination of entrained fraction

Film velocity measurements were obtained by way of the electrolyte injection method. This method is based on injecting sodium chloride electrolyte into the liquid film in order to increase its conductivity. The transit time between two sensors was determined by using the signal time delay between its two

electrodes, the film velocities were determined. It is important to note the large differences in liquid film velocity (U_{lf}) and superficial gas velocity (U_{sg}) as the superficial gas velocity for each superficial liquid velocity (U_{sl}) are increased. There is then an increase in slip velocity (U_{sg}/U_{lf}) which in turn results in rising shear at the gas–liquid interface. Several mechanisms have been proposed as to how the shearing contributes to liquid breakup hence entrainment; these include a “roll wave” mechanism as observed by early researchers such as Green (1950) using high speed photography and Lane's (1951) wave “undercutting” mechanism. The measured velocities were used to calculate the droplet fraction using the relationship:

$$e = \frac{\dot{m}_E}{\dot{m}_l} = \frac{\dot{m}_l - \dot{m}_{lf}}{\dot{m}_l} = 1 - \frac{4u_{lf}t}{u_{sl}D} \quad \textbf{(5-15)}$$

Where $\dot{m}_E$, $\dot{m}_l$, and $\dot{m}_{lf}$ are the entrainment rate, total liquid flow rate and liquid film flow rate respectively, while *E*, *t*, u_{lf}, u_{sl}, and *D*, are the liquid entrainment rate, measured film thickness, measured film velocity, liquid superficial velocity and pipe internal diameter respectively.

5.2.6 Comparison of entrainment data with literature models

As mentioned earlier, there is generally a dearth of annular two-phase flow correlations developed specifically for large pipes. (Pickering et al. 2001) noted that the existing commercial modelling methods and codes are largely based on data gathered in smaller diameters, typically 2 inches (50 mm) or less, but the predictions they provide are nevertheless used to design larger diameter riser systems in the oil and gas industry. Deepwater fields specifically present

substantial flow assurance challenges which engineers need to tackle. In the case of risers in such fields, there is a huge amount of uncertainty in modelling the complex fluid mixtures. Compounding the problem are the rather questionable extrapolations of correlations developed for smaller diameter pipes to large diameters representative of such deepwater risers typically in the range of 6 inches (150 mm). In this section, it is shown that for the entrained droplet fraction, which is important in determining pressure drop in such pipes (and hence upstream facility design), the commonly used correlations in the literature do not produce good quality and consistent predictions for large pipe flows. This is done by comparing experimental data obtained from 4–5-inch pipes (given in Table 5-3) with the predictions of literature correlations for entrained liquid droplet fraction (given in Table 5-4).

Table 5-4: Summary of literature correlations on entrained droplet fraction

Correlation	Pipe diameter ranges (mm)	Fluids	Pressure (bar)	Re_g range	Re_l range	L/D	Flow direction*	Number of data points
Oliemans et al (1986)	9.3 – 31.8	Air/water, air/ethanol, steam/water, air/genklene	1–100	72–99600	Laminar/ turbulent		↑	727
Ishii & Mishima (1989)	9.5 – 15.6	Air/water	1–2.7		318 - 6350		↑ ↓	n/a
Pan & Hanratty (2002)	10.6 – 57.2	Air/water, Freon/Freon, helium/water, air/genklene	n/a	7580–65340	20 - 12900		↑	n/a
Barbosa et al (2002)	31.8	Air/water	1.3–5	4000–9500	380 - 10500		↑	33
Sawant et al 2008	9.4	Air/water	1.2–4	345 – 2670	110–1140		↑	66
Sawant et al (2009)		Air/water, helium/water, air/genklene, steam/water, Freon	1.2–69	345–29100	110–1140	400	↑	n/a
Cioncolini et al (2012)	9 – 95	Air/water, steam/water, air/ethanol, R113, R12, He/water, air/genklene	1–70	111–266000	8700–14000		↑ ↓→	2293

*Flow direction: ↑ - Upwards; ↓ - Downwards; → - Horizontal

All the models as can be seen in Figure 5-9a–g when compared against this experimental database generally underestimate the entrained droplet fraction. Only a limited number of predicted points fall within the defined 30% error band. It is worth noting that here, most of the correlations gathered involve air–water fluid combination and in some cases, steam–water mixtures, hydrocarbon mixtures or condensing refrigerants. As such, they involve gas/liquid mixtures with physical properties not very different from those used for this study.

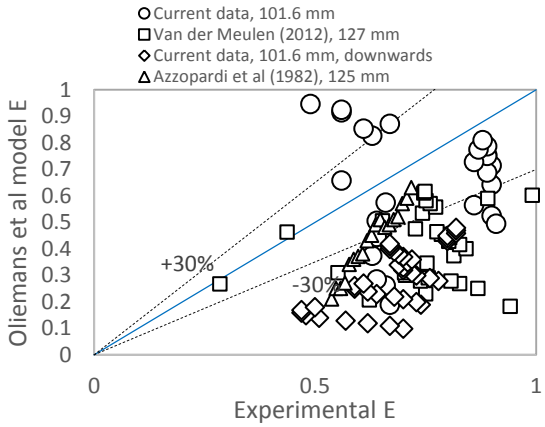

a. Oliemans et al (1986)

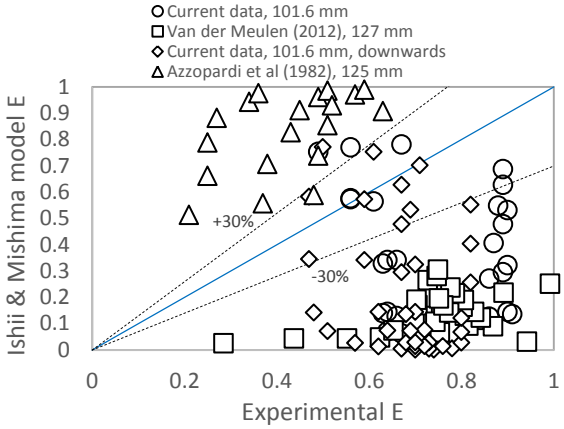

b. Ishii & Mishima (1989)

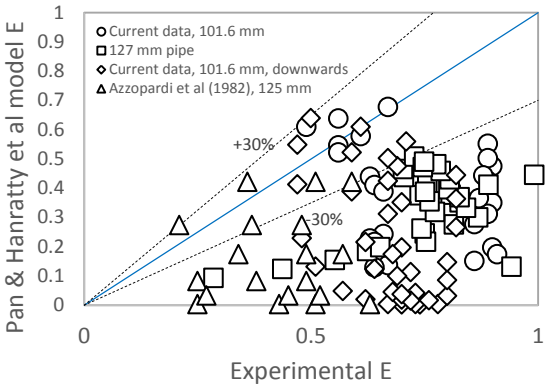

c. Pan & Hanratty (2002)

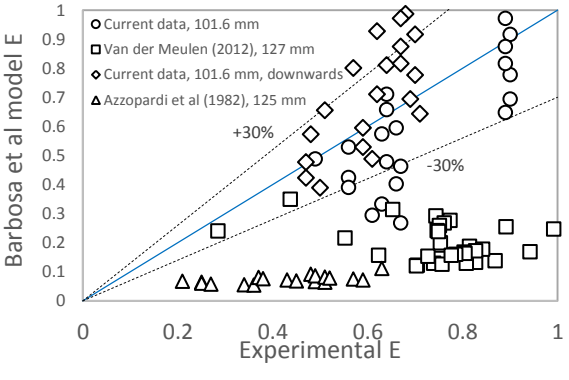

d. Barbosa et al (2002)

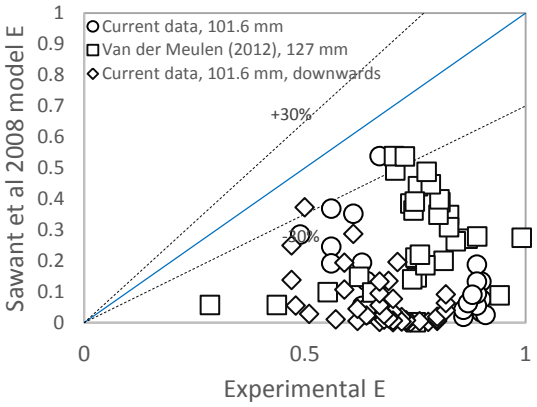

e. Sawant et al 2008

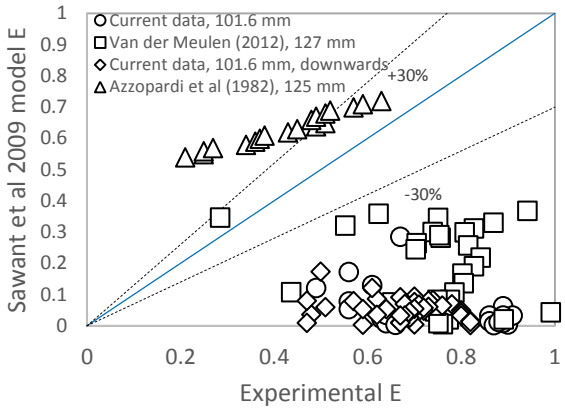

f. Sawant et al (2009)

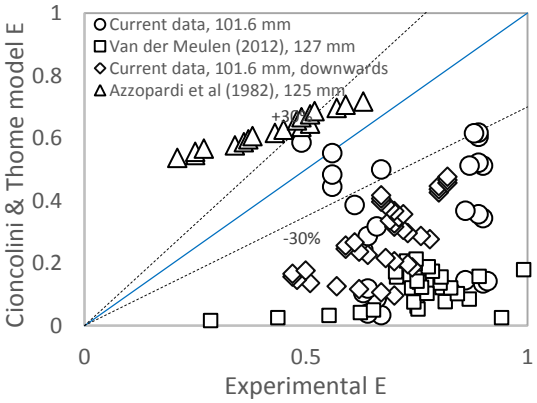

g. Cioncolini et al (2012)

Figure 5-9: Comparison of experimental data with model predictions

5.2.7 Correlation of entrainment data for large diameter pipes

Entrained liquid droplet fraction data has been obtained from 101.6, 125 and 127 mm ID pipes, and in the previous section, it has been shown that conventional entrainment correlations developed using small pipe data do not satisfactorily describe these large experimental pipe data. This may be due to the fact that the large pipes – due to the Rayleigh–Taylor instability – are no longer able to sustain large slug bubbles thereby causing flow regime transition to occur from bubbly to churn hence producing completely different hydrodynamics to smaller pipes. (Kataoka & Ishii 1987) have shown this to be

the case where void fraction is concerned. They compared published small pipe void fraction correlations with a large number of large diameter pipe measurements and reported that these were inadequate in predicting large pipe void fractions.

It has therefore become imperative to correlate entrainment fraction data exclusively using large pipe measurements for such channels. Use of the Reynolds numbers as candidates for correlation is natural as they capture inertia changes resulting from changes in fluid superficial velocities. The weber number is especially used in the investigation of multiphase flows characterised by an interface separating two fluids. It is a particularly important dimensionless number generally used in spray theory. It is used in studying liquid atomisation and in the study of surface tension waves on shear-driven liquid films. In annular two phase flow, the core flow can be considered as a spray interacting with the liquid film, which is shear-driven by the core flow and characterised by surface tension waves appearing at its surface. The crests of such waves are atomised by flowing gas in the core hence producing entrainment. Therefore, the selection of the Weber number here as a correlating group is consistent with the phenomena of annular flow. On the other hand, inclusion of the gas and liquid Froude numbers is intuitive, based on the fact that the Froude number is a ratio of inertial forces of pressure driven gas/liquid flow to the opposing gravitational force, particularly for high velocity gas flow such as is the case in annular two-phase flow where the inertial forces dominate resulting in $Fr_g > 1$. This is termed supercritical flow and the gas Froude number inclusion is reasonable. From the foregoing, it was assumed that the entrained droplet

fraction is a function of the liquid and gas Reynolds numbers, Weber number, and the liquid and gas Froude numbers:

$$e = f(Re_l,\ Re_g, We, Fr_l, Fr_g) \quad \textbf{(5-16)}$$

Therefore, Equation (5-16) can be explicitly rewritten assuming the dimensionless numbers relate to the entrained droplet fraction in a power law form as follows:

$$e = A\, Re_l^a Re_g^b We^c Fr_l^d Fr_g^e \quad \textbf{(5-17)}$$

Where $Re_l = \rho_l u_{sl} D/\mu_l$ is the superficial liquid Reynolds number; $Re_g = \rho_g U_{sg} D/\mu_g$ the superficial gas Reynolds number; $We = \rho_g u_{sg}^2 D/\sigma$ the Weber number; while $Fr_l = u_{sl}/\sqrt{gD}$ and $Fr_g = u_{sg}/\sqrt{gD}$ are the liquid and gas Froude numbers respectively. The coefficient A and the indices a–e are regression constants to be determined by multiple nonlinear least squares regression. It was discovered that the inclusion of Fr_l or otherwise does not markedly change the R^2 value and the following correlation is finally arrived at:

$$e = 4.83 \times 10^{-4}\, Re_l^{0.143} Re_g^{0.64} We^{0.66} Fr_g^{-2.024} \quad \textbf{(5-18)}$$

Rearranging Equation (5-18) such that a straight line relationship can be established between $e\, Fr_g^{2.024}$ and $Re_l^{0.143} Re_g^{0.640} We^{0.660}$ as shown in Figure 5-10 which shows that the new correlation describes 97% of this study's large diameter entrained fraction and those from Azzopardi et al (1982) and Van der Meulen (2012).

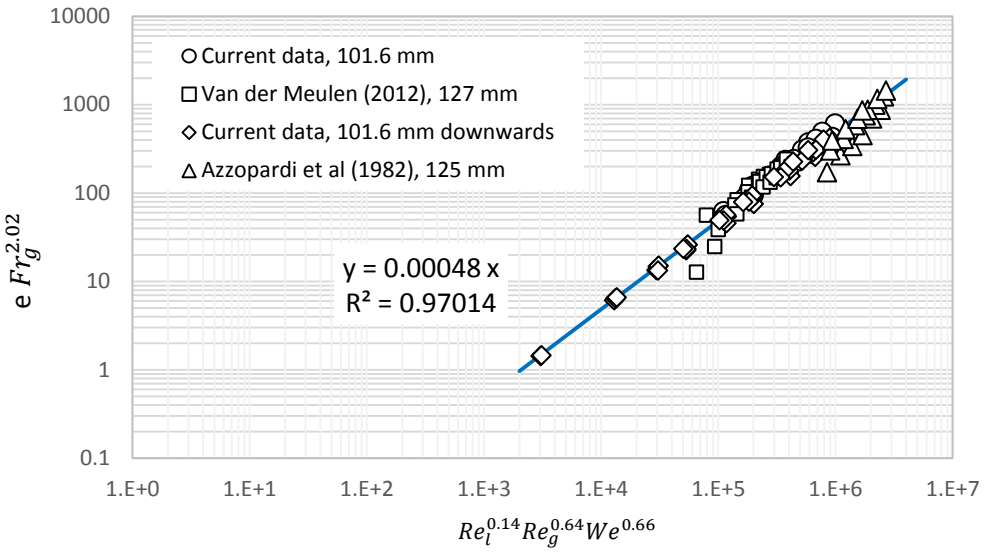

Figure 5-10: New correlation of entrained droplet fraction data

In addition, when compared with the various predictions of previous correlations as shown in Figure 5-9a–g, the new correlation has 89.6% of its predictions within ±30% of experimental data as shown in Figure 5-11. Comparatively, the previous correlations had between 18 and 42% within the ±30% error band (Table 5-5) with the best performing being that of Barbosa et al.

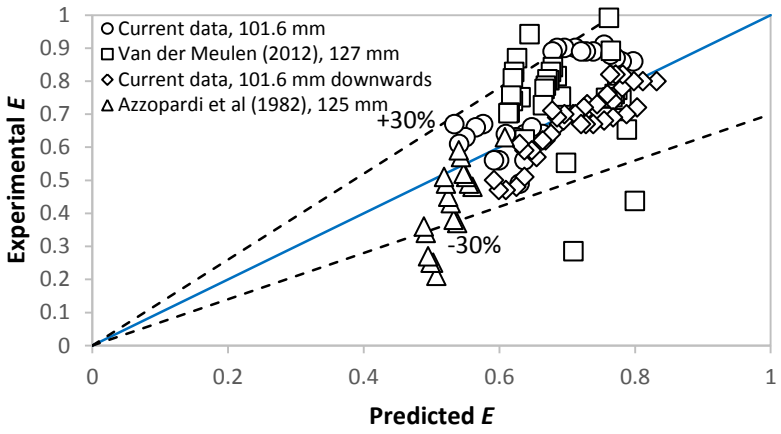

Figure 5-11: Comparison of new empirical model predictions with experimental entrained droplet fraction

However, in the ±60% error band, Oliemans et al's correlation performed best among the existing correlations having 67% of its predictions within a ±30% error band. This is notwithstanding inferior to that of the new correlation which has 91.3% of its predictions in the ±60% error band.

The statistical parameter mean percentage absolute error (PMAE) shows that the new model produces the least overall average deviation from the experimentally measured entrained liquid droplet data. A comparison of the PMAE for the new model and the previous ones is given in Table 5-5. The PMAE values are calculated as follows:

$$PMAE = \frac{1}{n}\sum_{i}^{n}|\epsilon_i| \tag{5-19}$$

$$where\ |\epsilon_i| = \left|\frac{E_{exp} - E_{pred}}{E_{exp}}\right| \times 100\% \tag{5-20}$$

where ϵ_i is the error calculated at each data point i, n is the total number of data points and subscripts *exp* and *pred* denote experimental and predicted values of the entrained droplet fraction respectively.

Table 5-5: Performance evaluation of present and existing correlations

	Model							
Performance Parameter	Oliemans et al (1986)	Ishii & Mishima (1989)	Pan & Hanratty (2002)	Barbosa et al (2002)	Sawant et al (2008)	Sawant et al (2009)	Cioncolini et al (2012)	Present
PMAE*	49.08	74.80	59.86	56.92	77.83	74.97	64.18	24.22
% within ±30% exp. data	37.39	21.74	35.65	42.61	29.57	18.26	30.43	89.57
% within ±60% of exp. data	66.96	29.57	48.70	44.35	35.65	20.87	43.48	91.30

* PMAE is defined in Equation (5-20)

5.2.8 Conclusions and future work

Entrained droplet fraction has been measured in a 101.6 mm large diameter pipe flow rig sing film velocity measurements in the annular flow regime. Together with literature data on droplet entrainment obtained from Azzopardi et al. (1982) and Van der Meulen (2012) in 125 and 127 mm pipes respectively. These produced an experimental database of 115 data points, and comparison was made with predictions of several empirical correlations in the open literature. It was established that there were large deviations between the experimental data and these predictions. A possible reason for these deviations in droplet fraction is the difference in hydrodynamics of small pipe flow (5–95 mm diameter, from which most of existing correlations are based) and large pipe hydrodynamics. In order to cater for these inadequacies of existing correlations, a new prediction method for entrained liquid fraction in annular two phase flow was proposed by assuming its power law relationship with the liquid and gas Reynolds numbers, Weber number, and the gas Froude number. The new correlation is explicit, easy to use, hence enabling its implementation as closure into existing flow simulator codes. It has been shown that this new model reproduces the available data better than existing empirical correlations and can be used for better prediction of pressure drop in gas condensate pipes, and dryout in industrial heat exchanger tubes. However, more data needs to be collected for even larger pipes: 150 mm ID and above and at higher gas velocities of 30–100 m/s. This better replicates conditions within the early life of gas wells when reservoir pressures are highest.

5.3 Chapter summary

This chapter has focused on the pipe diameter effect on vertical upwards annular flow. Firstly, interfacial friction factor which is directly related to the frictional pressure drop in gas–liquid annular two-phase flow was obtained from pressure drop and liquid film thickness measurements with the fluids co-currently flowing upwards through a 4-m long test section. Significant discrepancies were found between the published correlations derived using small pipe measurements and the current experimentally determined interfacial friction. Most of the published correlations are Wallis-type which are only functions of the relative film thickness, while others are not, in that they also correlate the friction factor with the gas and liquid Reynolds numbers for example. Attempts were therefore made to develop a new correlation using a dimensionless liquid film thickness and gas Reynolds number function where the results obtained show that this correlation well fits the large pipe interfacial friction factor data.

Secondly, entrained droplet fraction, also important in determining pressure drop and liquid holdup in many industrial pipes such as wet gas production pipelines was measured in the 101.6 mm pipe. A literature review has revealed that gas/liquid two-phase flow behaviour in large pipes (with diameter >100 mm) is different from that of smaller pipes based on the investigation of many authors in the last 30 years. Correlations derived from such small pipes when used as closures in numerical flow simulator codes may not give accurate predictions for typically large industrial pipes. Trial and error therefore results, which may include model tuning and/or the use of correction factors. Here the

entrained droplet fraction measured using liquid film velocity and gas void fraction measurements. Probability distribution functions of the void fraction measurements from a capacitance Wire Mesh Sensor coupled with visual observations were used for flow regime identification. It was observed that published droplet fraction correlations derived using small pipe data when compared to the present experimentally determined entrained fraction produced large deviations. These can lead to inaccurate holdup and total pressure drop predictions and could have serious consequences for design and operation of oil and gas pipeline systems, particularly wet gas risers where annular flow is the prevailing regime. A new empirical correlation for droplet entrainment has been proposed that fits both the current large pipe measurements and two others of 125 and 127 mm internal diameter.

Chapter Six

CONCLUSIONS AND RECOMMENDATIONS

6.1 Conclusions

This work is an experimental study carried out on gas–liquid two-phase flow in a 4-inch (101.6 mm) large diameter flow loop. The working fluids are air and water at pressures of between 1–1.9 bar. The flow regime of interest is annular in both vertically upwards and downwards flow directions. A capacitance Wire Mesh Sensor was used to obtain the cross-sectional void fraction distribution for air and water superficial velocity ranges of 1.42–28.87 and 0.1–1.0 m/s respectively. A probe operating based on the principle of conductivity difference between the phases was used to measure the thickness of the liquid flowing on the pipe walls.

Conclusions drawn are as follows:

i. Vertical downflow

- Liquid film thickness characteristics in downwards annular flow in large diameter pipes differ from those obtained in small diameter pipes. This is evidenced by the distinctly different slope and intercept obtained when Nusselt's dimensionless film thickness t* for this study together with those of existing correlations are plotted against the liquid film Reynolds number. This may suggest a different local turbulence structure within liquid films flowing in downwards large diameter pipes.
- The ratio of the top and bottom pressure gradients produces a unique and consistent pattern for all liquid flow rates when plotted against the

superficial gas velocity. A pressure gradient reversal characterised by large fluctuations from negative to positive were observed between 5 and 10 m/s gas superficial velocities and may be related a change in flow regime from churn-annular flow to annular two-phase flow

- It was found that the interfacial friction factor in downwards annular flow is a function of $Re_g^{-0.2}\, t_g^+\, (Fr_g \frac{t}{D})^{-1.1}$ for large diameter pipes rather than $Re_g^{-0.2} t_g^+$ as established by earlier researchers for small diameter pipes. The former group was shown to also well correlate small diameter pipe interfacial friction factor.

ii. Vertical upflow

- Most Wallis–type correlations underpredict large pipe interfacial friction factors, signifying that interfacial friction factor in large pipes does not vary with dimensionless film thickness alone. A new correlation was derived exclusively for large pipes from the measurements of this study and those from two others. In doing so, use was made of the dimensionless film thickness, gas and liquid Reynolds numbers, and the gas Froude number. The new correlation improved the prediction of the friction factors and therefore provides better frictional pressure gradient estimation for applications such as industrial scale gas condensate pipes and heat transfer equipment.
- Large deviations were observed between entrained droplet fraction (e) experimental data and empirical model predictions from the open literature. This further reinforces previous observations by other

investigators of the difference in hydrodynamics between small pipe flow (< 100 mm diameter, from which most of existing correlations are based) and larger pipes. In order to cater for these inadequacies, a new prediction method for entrained liquid fraction in annular two phase flow in large pipes was proposed. By assuming a power law relationship exists with the liquid and gas Reynolds numbers, Weber number, and the gas Froude number and it was found that a simple straight line relationship exists between $e\ Fr_g^{2.024}$ and $Re_l^{0.143} Re_g^{0.640} We^{0.660}$.

6.2 Recommendations

The following recommendations are hereby proposed in order to further two-phase flow knowledge in large diameter pipes.

- Use of a straight pipe section without the bends will allow for the collection of data from annular flow region that is more developed. This could also serve for studies quantifying the effect of the bend on flow development and assessment of existing correlations. Appendix C provides some details on work that has commenced on this recommendation.
- Further correlations could be developed for other annular flow parameters in large pipes, such as pressure drop, and void fraction using the available data.
- As stated throughout the thesis, annular flow data for large pipes is very scarce. Therefore, higher gas velocities need to be explored, beyond the 30 m/s of this study. Furthermore, the use of even larger diameter pipes

(6 inch and above) is recommended. These expand the application range of any empirical models derived.

- Mechanistic modelling approaches for large diameter pipes also need to be researched. For example the Two or Three Fluid Model that has been extensively used for smaller channels can also be applied for pressure drop, and holdup predictions in large diameter pipes.

REFERENCES

Alekseenko, S. V, Nakoryakov, V.Y. & Pokusaev, B.G., 1985. Wave formation on a vertical falling liquid film. *AIChE Journal*, 31(9), pp.1446–1460. Available at: http://dx.doi.org/10.1002/aic.690310907.

Ali, S.F., 2009. *TWO PHASE FLOW IN LARGE DIAMETER VERTICAL RISER*. Cranfield University.

Ali, S.F. & Yeung, H., 2014. Two-phase flow patterns in large diameter vertical pipes. *Asia-Pacific Journal of Chemical Engineering*, 9(1), pp.105–116. Available at: http://doi.wiley.com/10.1002/apj.1750 [Accessed August 8, 2015].

Alipchenkov, V.M. et al., 2004. A three-fluid model of two-phase dispersed-annular flow. *International Journal of Heat and Mass Transfer*, 47(24), pp.5323–5338. Available at: http://linkinghub.elsevier.com/retrieve/pii/S0017931004002972 [Accessed August 20, 2015].

Alipchenkov, V.M. et al., 2002. The Development of a Three-Fluid Model of Two-Phase Flow for Dispersed-Annular Mode of Flow in Channels : Deposition and Entrainment of Droplets. , 40(5), pp.772–778.

Almabrok, A.A., 2014. *Gas - Liquid two-phase flow in up and down vertical pipes*. PhD Thesis, Cranfield University.

Alves, I.M. et al., 1991. Modeling Annular Flow Behavior for Gas Wells. *SPE Production Engineering*, 6(04), pp.435–440. Available at: http://www.onepetro.org/doi/10.2118/20384-PA [Accessed August 26, 2015].

Andreussi, P. & Zanelli, S., 1979. Downward annular mist flow of air water mixtures. In Dubrovnik, Yugoslavia: International Seminar.

Armand, A.A., 1964. Resistance with motion of a two-phase system along horizontal tubes. *Tolotekh Inst Journal*, 1, pp.16–23.

Asali, J.C., 1983. *Entrainment in vertical gas-liquid annular flows*. Univ of Illinois, Urbana.

Asali, J.C., Hanratty, T.J. & Andreussi, P., 1985. Interfacial drag and film height for vertical annular flow. *AIChE Journal*, 31(6), pp.895–902. Available at: http://dx.doi.org/10.1002/aic.690310604.

Aziz, K., Govier, G.W. & Forgasi, M., 1972. Pressure Drop In Wells Producing Oil And Gas. *Journal of Canadian Petroleum Technology*, 11(03). Available at: http://www.onepetro.org/doi/10.2118/72-03-04 [Accessed July 31, 2015].

Azzopardi, B.J., Taylor, S. & Gibbons, D.B., 1982. *Annular two phase flow in a large diameter tube*, UKAEA Atomic Energy Research Establishment. Available at: http://books.google.co.uk/books?id=zEfIMgEACAAJ.

Bar, N., Biswas, M.N. & Das, S.K., 2015. Information Systems Design and Intelligent Applications J. K. Mandal et al., eds. , 339. Available at:

http://link.springer.com/10.1007/978-81-322-2250-7 [Accessed August 1, 2015].

Barbosa, J.R. et al., 2002. Liquid entrainment , droplet concentration and pressure gradient at the onset of annular flow in a vertical pipe. , 28, pp.943–961.

Barnea, D., Shoham, O. & Taitel, Y., 1980. Flow pattern characterization in two phase flow by electrical conductance probe. *International Journal of Multiphase Flow*, 6(5), pp.387–397. Available at: http://linkinghub.elsevier.com/retrieve/pii/0301932280900014 [Accessed August 4, 2015].

Beggs, D.H. & Brill, J.P., 1973. A Study of Two-Phase Flow in Inclined Pipes. *Journal of Petroleum Technology*, 25(05), pp.607–617. Available at: http://www.onepetro.org/doi/10.2118/4007-PA [Accessed July 31, 2015].

Bendiksen, K.H. et al., 1991. The Dynamic Two-Fluid Model OLGA: Theory and Application. *SPE Production Engineering*, 6(02), pp.171–180. Available at: http://www.onepetro.org/doi/10.2118/19451-PA [Accessed August 26, 2015].

Bergelin, O.P. et al., 1949. Co-curreint gas liquid flow. II. Flow in vertical tubes. *Heat Transfer and Fluid Mechanics Institute*, pp.19–28.

Bhagwat, S.M. & Ghajar, A.J., 2012. Similarities and differences in the flow patterns and void fraction in vertical upward and downward two phase flow. *Experimental Thermal and Fluid Science*, 39, pp.213–227. Available at: http://www.sciencedirect.com/science/article/pii/S0894177712000374 [Accessed August 6, 2015].

Bhagwat, S.M., Mollamahmutoglu, M. & Ghajar, A.J., 2012. Experimental investigation and empirical analysis of non-boiling gas-liquid two-phase heat transfer in vertical downward pipe orientation. In Rio Grande, Puerto Rico: ASME, pp. 1–11.

Bhagwat, S.M., Mollamahmutoglu, M. & Ghajar, A.J., 2012. Experimental investigation and performance evaluation of isothermal frictional two phase pressure drop correlations in vertical downward gas-liquid two phase flow. In *Proceedings of the ASME 2012 Summer Heat Transfer Conference*. Rio Grande, Puerto Rico: ASME, pp. 1–12. Available at: http://ghajar.ceat.okstate.edu/pub_pdfs/Bhagwat et al_HT2012-58049.pdf.

Bilgesu, H.I. & Ternyik, J., 1994. A New Multi-Phase Flow Model for Horizontal, Inclined, and Vertical Pipes. In *SPE Eastern Regional Meeting*. Society of Petroleum Engineers, pp. 87 – 94. Available at: http://www.onepetro.org/doi/10.2118/29166-MS [Accessed August 24, 2015].

Brauer, H., 1956. *Flow and heat transfer at falling liquid films*, VDI Forschungsh.

Brauner, N., 1987. Roll wave celerity and average film thickness in turbulent wavy film flow. *Chemical Engineering Science*, 42(2), pp.265–273.

Brill, J.P., 1987. Multiphase Flow in Wells. *Journal of Petroleum Technology*, 39(01), pp.15–21. Available at: http://www.onepetro.org/doi/10.2118/16242-

PA [Accessed July 23, 2015].

Brill, J.P. & Mukherjee, H.K., 1999. *Multiphase Flow in Wells*, Henry L. Doherty Memorial Fund of AIME, Society of Petroleum Engineers. Available at: https://books.google.co.uk/books?id=oo4KAQAAMAAJ.

Brotz, W., 1954. Uber die Vorausberedinung der Absorptions geschwineig von Gayen instromenden flussig kectsschichten. *Chem Ing. Tech.*, 26, pp.470–8.

Cai, S. et al., 1994. Neural network based objective flow regime identification in air-water two phase flow. *The Canadian Journal of Chemical Engineering*, 72(3), pp.440–445. Available at: http://dx.doi.org/10.1002/cjce.5450720308 [Accessed August 24, 2015].

Charvonia, D.A., 1959. *A Study of the Mean Thickness of the Liquid Film and the Characteristics of the Interfacial Surface in Annular, Two-Phase Flow in a Vertical Pipe.*, DTIC Document.

Cheng, H., Hills, J.H. & Azzorpardi, B.J., 1998. A study of the bubble-to-slug transition in vertical gas-liquid flow in columns of different diameter. *International Journal of Multiphase Flow*, 24(3), pp.431–452. Available at: http://linkinghub.elsevier.com/retrieve/pii/S0301932297000670.

Chien, S.-F., 1990. Predicting Wet-Steam Flow Regime in Horizontal Pipes. *Journal of Petroleum Technology*, 42(03), pp.356–362. Available at: http://www.onepetro.org/doi/10.2118/17574-PA [Accessed August 24, 2015].

Chien, S.F. & Ibele, W., 1964. Pressure drop and liquid film thickness of two-phase annular and annular-mist flows. *Journal of Heat Transfer*, 86, pp.89–96.

Chung, D.K. & Mills, A.F., 1974. Effect of interfacial shear on gas absorption into a turbulent falling film with co-current gas flow. *Lett. Heat Mass Transfer*, 1, pp.43–48.

Cicchitti, A. et al., 1960. Two-phase cooling experiments - pressure drop, heat transfer and burnout measurements. *Energia Nucleare*, 7(6), pp.407–25.

Cioncolini, A. & Thome, J.R., 2012. Entrained liquid fraction prediction in adiabatic and evaporating annular two-phase flow. *Nuclear Engineering and Design*, 243, pp.200–213. Available at: http://linkinghub.elsevier.com/retrieve/pii/S0029549311009873 [Accessed March 14, 2013].

Cioncolini, A. & Thome, J.R., 2010. Prediction of the entrained liquid fraction in vertical annular gas–liquid two-phase flow. *International Journal of Multiphase Flow*, 36(4), pp.293–302. Available at: http://linkinghub.elsevier.com/retrieve/pii/S0301932209001918 [Accessed April 28, 2013].

Cioncolini, A., Thome, J.R. & Lombardi, C., 2009a. Algebraic turbulence modeling in adiabatic gas–liquid annular two-phase flow. *International Journal of Multiphase Flow*, 35(6), pp.580–596. Available at: http://linkinghub.elsevier.com/retrieve/pii/S0301932209000202 [Accessed

April 28, 2013].

Cioncolini, A., Thome, J.R. & Lombardi, C., 2009b. Unified macro-to-microscale method to predict two-phase frictional pressure drops of annular flows. *International Journal of Multiphase Flow*, 35(12), pp.1138–1148. Available at: http://linkinghub.elsevier.com/retrieve/pii/S030193220900127X [Accessed April 14, 2013].

Collier, J.G. & Hewitt, G.F., 1961. Data on the vertical flow of air-water mixtures in the annular and dispersed flow regions. Part II: Film thickness and entrainment data and analysis of pressure drop measurements. *Transaction of the Institution of Chemical Engineers*, 39, pp.127–136.

Costigan, G. & Whalley, P.B., 1997. Slug flow regime identification from dynamic void fraction measurements in vertical air-water flows. *International Journal of Multiphase Flow*, 23(2), pp.263–282. Available at: http://linkinghub.elsevier.com/retrieve/pii/S030193229600050X [Accessed August 4, 2015].

Cousins, L.B., Dencon, W.H. & Hewitt, G.F., 1965. Liquid mass transfer in allular two-phase flow. In *Smposium on Two-phase Flow*. University of Exeter, pp. C401 – C430.

Dalkilic, a. S., Laohalertdecha, S. & Wongwises, S., 2008. Two-phase friction factor in vertical downward flow in high mass flux region of refrigerant HFC-134a during condensation. *International Communications in Heat and Mass Transfer*, 35(9), pp.1147–1152. Available at: http://linkinghub.elsevier.com/retrieve/pii/S0735193308001292 [Accessed January 24, 2014].

Dukler, A.E., Wicks, M. & Cleveland, R.G., 1962. Pressure drop and hold-up in two-phase flow: Part A comparison of existing correlations; Part B, An approach through similarity analysis. *AIChE Journal*, 10(1), p.38.

Duns, H. & Ros, N.C.J., 1963. Vertical flow of gas and liquid mixtures in wells. In *World Petroleum Congress*. Frankfurt, Germany: World Petroleum Congress.

Fedotkin, I.M. et al., 1979. Pressure drop in downtake turbulent film and gas flows. *Fluid Mech. - Sov. Res.*, 8, pp.85–90.

Fiend, K., 1960. *Stromungsuntersuchungen bei gegenstrom von Riesel-Filmen und Gas in lotrechten Rohren*, VDl-Forsclurngsh.

Fore, L.B., Beus, S.G. & Bauer, R.C., 2000. Interfacial friction in gas-liquid annular flow: analogies to full and transition roughness. *International Journal of Multiphase Flow*, 26.

Fore, L.B. & Dukler, A.E., 1995. Droplet deposition and momentum transfer in annular flow. *AIChE Journal*, 41(9), pp.2040–2046. Available at: http://dx.doi.org/10.1002/aic.690410904.

Frohn, A. & Roth, N., 2000. *Dynamics of droplets*, Springer Science & Business Media.

Fukano, T. et al., 1991. Interfacial shear stress and holdup in an air - water

Annular two-phase flow. In *Proceedings of the ASME-JSME Thermal Engineering Joint Conference: Reno, Nevada, March 17-22, 1991*. Amer Society of Mechanical, p. 217.

Fukano, T. & Furukawa, T., 1998. Prediction of the effects of liquid viscosity on interfacial shear stress and frictional pressure drop in vertical upward gas–liquid annular flow. *International Journal of Multiphase Flow*, 24(4), pp.587–603. Available at: http://www.sciencedirect.com/science/article/pii/S0301932297000700.

Ganchev, B.G., Kozlov, V.M. & Orlov, V. V, 1972. Some results of falling liquid film studies by stroboscopic visualization technique. *Zh. Prik. Mekh. Tekh.*, 2(140).

Garner, F.H., Ellis, S.R.M. & Lacey, J.A., 1954. The size distribution and entrainment of droplets. *Transaction of the Institution of Chemical Engineers*, 32, pp.222–235.

Ghajar, A.J., 2005. Nonboiling heat transfer in gas-liquid flow in pipes - a tutorial. In A. P. Silva Freire, ed. *10th Brazilian Congress of Thermal Sciences and Engineering*. Rio de Janeiro: Scielo, pp. 46–73. Available at: http://www.scielo.br/pdf/jbsmse/v27n1/25375.pdf.

Gill, L.E., Hewitt, G.F. & Lacey, P.M.C., 1964. Sampling probe studies of the gas core in annular two-phase flow: II, studies of the effect of phase flow rates on phase and velocity distribution. *Chemical Engineering Science*, 19(665).

Gomez, L.E. et al., 1999. A Unified Mechanistic Model for Steady-State Two-Phase Flow in Wellbores and Pipelines. In *SPE Annual Technical Conference and Exhibition*. Society of Petroleum Engineers. Available at: http://www.onepetro.org/doi/10.2118/56520-MS [Accessed August 26, 2015].

Govan, A.H. et al., 1991. Flooding and churn flow in vertical pipes. *International Journal of Multiphase Flow*, 17(1), pp.27–44. Available at: http://www.sciencedirect.com/science/article/pii/030193229190068E [Accessed August 10, 2015].

Green, H.L., 1950. Problems in the atomisation of liquids. In *Symposium on some aspects of fluid flow*. Leamington Spa: Institute of Physics, p. 75.

Griffith, P. & Wallis, G.B., 1961. Two-Phase Slug Flow. *Journal of Heat Transfer*, 83(3), pp.307–318. Available at: http://dx.doi.org/10.1115/1.3682268.

Guo, T. & Jeong, J.H., 2014. Experimental study on flooding and flow reversal in small diameter tubes with various inclinations and horizontal lengths. *International Journal of Refrigeration*, 38, pp.290–298. Available at: http://www.sciencedirect.com/science/article/pii/S0140700713002247 [Accessed August 11, 2015].

Hagedorn, A. & Brown, K.E., 1965. Experimental Study of Pressure Gradients Occurring During Continuous Two-Phase Flow in Small-Diameter Vertical Conduits. *Journal of Petroleum Technology*, 17(4), pp.475 – 484. Available

at: https://www.onepetro.org/journal-paper/SPE-940-PA.

Hashemi, A., Kim, J.H. & Sursock, J.P., 1986. Effect of diameter and geometry on two-phase flow regimes and carry-over in a model pwr hot leg. In *Proceedings of the eighth international heat transfer conference*. San Francisco, California: Hemisphere Publishing Corp.

Hewitt, G.F., 1986. Co-current and counter-current two phase annular flow. In *9th Australasian fluid mechanics conference, Auckland*.

Hewitt, G.F. & Govan, A.H., 1990. Phenomenological modelling of non-equilibrium flows with phase change. *International Journal of Heat and Mass Transfer*, 33(2), pp.229–242. Available at: http://www.sciencedirect.com/science/article/pii/001793109090094B.

Hewitt, G.F. & Hall-Taylor, N.S., 1970. *Annular two-phase flow,* Oxford; New York: Pergamon Press.

Hewitt, G.F., Lacey, P.M.C. & Nicholls, B., 1965. Transitions in film flow in a vertical tube. In *Symposium on two-phase flow*. Exeter, p. Vol 2, Paper B4.

Hewitt, G.F., Martin, C.J. & Wilkes, N.S., 1984. Experimental and modelling studies of annular flow in the region between flow reversal and the pressure drop minimum. In *Symposium on two-phase annular and dispersed flow*. Pisa, Italy.

Hewitt, G.F. & Roberts, D.N., 1969. *Studies of Two Phase Patterns by Simultaneous X-Ray and Flash Photography*, Harwell, Berkshire.

Hewitt, G.F. & Wallis, G.B., 1963. Flooding and associated phenomena in falling film in a vertical tube. In *Multiphase flow symposium*. Philadelphia, pp. 62–74.

Hills, J.H., 1976. The operation of a bubble column at high throughputs. *The Chemical Engineering Journal*, 12(2), pp.89–99. Available at: http://www.sciencedirect.com/science/article/pii/0300946776870025 [Accessed January 4, 2016].

Hori, K. et al., 1978. Study of ripple region in annular two-phase flow (Third report, effect of liquid viscosity on gas-liquid interfacial character and friction factor). *Trans. Jap. Soc. Mech. Eng.*, 44(387), pp.3847–3856.

Hujghe, J. & Mondin, H., 1961. Transfert de chaleur par melange de liquide et de gas en convection forcee turbulente aves faible vaporisation de la phase liquide. *Hebd. Seanc. Acad. Sci*, 253, pp.395–397.

Isbin, H.S., Moy, J.E. & Da Cruz, A.J.R., 1957. Two-phase steam - water criticalflow. *AIChE Journal*, 3(361).

Ishii, M., 1975. Thermo-fluid dynamic theory of two-phase flow. *NASA STI/Recon Technical Report A*, 75, p.29657.

Ishii, M. & Grolmes, M.A., 1975. Inception criteria for droplet entrainment in two-phase concurrent film flow. *AIChE Journal*, 21(2), pp.308–318. Available at: http://dx.doi.org/10.1002/aic.690210212.

Ishii, M. & Mishima, K., 1989. Droplet entrainment correlation in annular two-phase flow. *International Journal of Heat and Mass Transfer*, 32(10),

pp.1835–1846. Available at: http://linkinghub.elsevier.com/retrieve/pii/0017931089901555.

Jayanti, S., Tokarz, A. & Hewitt, G.F., 1996. Theoretical investigation of the diameter effect on flooding in countercurrent flow.

Jensen, R.T., 1971. *Inception of liquid entrainment during emergency cooling of pressurized water reactors*,

Jiang, Y. & Rezkallah, K.S., 1993. A STUDY ON VOID FRACTION IN VERTICAL CO-CURRENT UPWARD AND DOWNWARD TWO-PHASE GAS-LIQUID FLOW—I: EXPERIMENTAL RESULTS. *Chemical Engineering Communications*, 126(1), pp.221–243. Available at: http://dx.doi.org/10.1080/00986449308936220 [Accessed August 5, 2015].

Jones, O.C. & Zuber, N., 1975. The interrelation between void fraction fluctuations and flow patterns in two-phase flow. *International Journal of Multiphase Flow*, 2(3), pp.273–306. Available at: http://linkinghub.elsevier.com/retrieve/pii/0301932275900154 [Accessed August 4, 2015].

Kaji, R. & Azzopardi, B.J., 2010. The effect of pipe diameter on the structure of gas/liquid flow in vertical pipes. *International Journal of Multiphase Flow*, 36(4), pp.303–313. Available at: http://linkinghub.elsevier.com/retrieve/pii/S0301932209001906 [Accessed October 26, 2012].

Kaji, R. & Azzopardi, B.J.J., 2010. The effect of pipe diameter on the structure of gas/liquid flow in vertical pipes. *International Journal of Multiphase Flow*, 36(4), pp.303–313. Available at: http://linkinghub.elsevier.com/retrieve/pii/S0301932209001906 [Accessed October 26, 2012].

Kapitza, P.L., 1965. Collected papers of Kapitza 1938-1964. In D. Ter-Harr, ed. *Wave flow of thin layers of a viscous fluid*. New York: Macmillan, pp. 662–709.

Karapantsios, T.D. & Karabelas, A.J., 1995. Longitudinal characteristics of wavy falling films. *International Journal of Multiphase Flow*, 21(I), pp.119–127.

Kataoka, I. & Ishii, M., 1987. Drift flux model for large diameter pipe and new correlation for pool void fraction. *Int. J. Heat Mass Transfer*, 30(9), pp.1927–1939.

Kim, D., 2000. *An experimental and experimental investigation of convective heat transfer for gas liquid two phase flow in vertical and horizontal pipes*. Oklahoma State University, Stillwater.

Klausner, J.F., Chao, B.T. & Soo, S.L., 1991. An improved correlation for two-phase frictional pressure drop in boiling and adiabatic downflow in the annular flow regime. , pp.317–328.

Kobayashi, A. et al., 2004. Void fraction in upward gas-liquid two-phase flow in a large diameter pipe. In *5th Int Conf Multiphase Flow*. Yokohama, Japan.

Kosky, P.G., 1971. Thin liquid films under simultaneous shear and gravity

forces. *International Journal of Heat and Mass Transfer*, 14(8), pp.1220–1224. Available at: http://www.sciencedirect.com/science/article/pii/001793107190216X.

Kuo, K.K. & Cheung, F.B., 1995. *Droplet entrainment of breakup by shear flow*,

Kutateladze, S.S., 1972. Elements of the hydrodynamics of gas-liquid systems. *Fluid Mechanics-Soviet Research*, 1(4), pp.29–50.

Lane, W.R., 1951. Shatter of drops in streams of air. *Ind Eng Chem*, 43, p.1312.

Lao, L., Xing, L. & Yeung, H., 2012. Behaviours of elongated bubbles in a large diameter riser. In *Multiphase 8*. Banff, Canada: BHR Group, pp. 381–392.

Levy, S., 1999. *Two-phase flow in complex systems*, John Wiley & Sons.

Liu, Y. & Zhang, S., 2010. Local flow regime identification for boiling two- phase flow by BP neural networks approach. In *Sixth International Conference on Natural Computation*. pp. 362–366.

Lockhart, R.W. & Martinelli, R.C., 1949. Proposed correlation of data for isothermal two-phase, two component flow in pipes. *Chem Eng Prog*, 45, pp.39–48.

Lopez de Bertodano, M.A., 1998. Entrainment data in vertical flows. *Private communication*.

Magiros, P. & Dukler, A., 1961. Entrainment and pressure drop in concurrent gas-liquid flow. In *Proceedings of the 7th Midwestern Mechanics Conference, Vol 1*. pp. 532–553.

Matsui, G., 1986. Automatic identification of flow regimes in vertical two-phase flow using differential pressure fluctuations. *Nuclear Engineering and Design*, 95, pp.221–231. Available at: http://linkinghub.elsevier.com/retrieve/pii/002954938690049X [Accessed August 4, 2015].

Matsui, G., 1984. Identification of flow regimes in vertical gas-liquid two-phase flow using differential pressure fluctuations. *International Journal of Multiphase Flow*, 10(6), pp.711–719. Available at: http://linkinghub.elsevier.com/retrieve/pii/0301932284900077 [Accessed August 4, 2015].

Van der Meulen, G.P., 2012. *CHURN-ANNULAR GAS-LIQUID FLOWS IN LARGE DIAMETER VERTICAL PIPES*. University of Nottingham.

Mikielewicz, D., Gliński, M. & Wajs, J., 2011. Experimental and theoretical study of dryout in annular flow in small diameter channels. *Archives of Thermodynamics*, 32(1), pp.89–108. Available at: http://www.degruyter.com/view/j/aoter.2011.32.issue-1/v10173-011-0005-5/v10173-011-0005-5.xml [Accessed August 20, 2015].

Moeck, E.O., 1970. *Annular-dispersed two-phase flow and critical heat flux*. McGill University. Available at: http://www.iaea.org/inis/collection/NCLCollectionStore/_Public/01/002/1002083.pdf.

Mudawar, I. & El-Masri, 1988. Boiling Incipience in Plane Rotating Water Films.

Transactions of the ASME, 110(May), pp.126–129.

Newitt, D.M., Dombrowski, N. & Knelman, F.H., 1954. Liquid Entrainment: The Mechanism of Drop Formation from Gas or Vapour Bubbles. *Transaction of the Institution of Chemical Engineers*, 32(244).

No, H.C. & Jeong, J.H., 1996. Flooding correlation based on the concept of hyperbolicity breaking in a vertical annular flow. *Nuclear Engineering and Design*, 166(2), pp.249–258. Available at: http://www.sciencedirect.com/science/article/pii/002954939601271X [Accessed August 11, 2015].

Nusselt, W., 1916. Die oberflachen Kondensation das Wasserdampfes. *VDI-Zeitschrift*, 54, pp.1154–1178.

Ohnuki, A. & Akimoto, H., 2000. Experimental study on transition of flow pattern and phase distribution in upward air–water two-phase flow along a large vertical pipe. *International Journal of Multiphase Flow*, 26(3), pp.367–386. Available at: http://www.sciencedirect.com/science/article/pii/S0301932299000245 [Accessed August 8, 2015].

Ohnuki, A. & Akimoto, H., 2001. Model development for bubble turbulent diffusion and bubble diameter in large vertical pipes. *Journal of Nuclear Science and Technology*, 38(12), pp.1074–1080. Available at: http://www.tandfonline.com/doi/abs/10.1080/18811248.2001.9715138.

Ohnuki, A., Akimoto, H. & Sudo, Y., 1995. Flow pattern and its transitions in gas-liquid two phase flow along as large vertical pipe. In *Proceedings of the 2nd International Conference on Multiphase*.

Oliemans, R.V.A., Pots, B.F.M. & Trompe, N., 1986. Modelling of annular dispersed two-phase flow in vertical pipes. *International Journal of Multiphase Flow*, 12(5), pp.711–732.

Omebere-Iyari, N.K., 2006. *The effect of pipe diameter and pressure in vertical two-phase flow*. University of Nottingham.

Omebere-Iyari, N.K. & Azzopardi, B.J., 2007. A Study of Flow Patterns for Gas/Liquid Flow in Small Diameter Tubes. *Chemical Engineering Research and Design*, 85(2), pp.180–192. Available at: http://linkinghub.elsevier.com/retrieve/pii/S0263876207730356 [Accessed October 31, 2012].

Omebere-Iyari, N.K., Azzopardi, B.J. & Ladam, Y., 2007. Two-phase flow patterns in large diameter vertical pipes at high pressures. *AIChE Journal*, 53(10), pp.2493–2504. Available at: http://doi.wiley.com/10.1002/aic.11288 [Accessed August 7, 2015].

Oshinowo, O., 1971. *Two-phase Flow in a Vertical Tube Coil*. Thesis (Ph.D.)--University of Toronto. Available at: https://books.google.co.uk/books?id=6VermQEACAAJ.

Osman, E.-S.A., 2001. Artificial Neural Networks Models for Identifying Flow Regimes and Predicting Liquid Holdup in Horizontal Multiphase Flow. In *SPE Middle East Oil Show*. Manama, Bahrain: Society of Petroleum

Engineers. Available at: http://www.onepetro.org/doi/10.2118/68219-MS [Accessed August 24, 2015].

Owen, D.G., 1986. *An experimental and theoretical analysis of equilibrium annular flows*. University of Birmingham.

Paleev, I.I. & Filippovich, B.S., 1966. Phenomena of liquid transfer in two-phase dispersed annular flow. *Int. J. Heat and Mass Transfer*, 9, pp.1089–1093.

Pan, L. & Hanratty, T.J., 2002. Correlation of entrainment for annular flow in vertical pipes. *International Journal of Multiphase Flow*, 28(3), pp.363–384. Available at: http://www.sciencedirect.com/science/article/pii/S0301932201000738.

Peng, D.J. et al., 2010. Flow regime transitions in large diameter pipes. In *7th International Conference on Multiphase Flow*. Tampa, FL USA, pp. 1–9.

Petalas, N. & Aziz, K., 2000. A Mechanistic Model for Multiphase Flow in Pipes. *Journal of Canadian Petroleum Technology*, 39(06). Available at: http://www.onepetro.org/doi/10.2118/00-06-04 [Accessed July 31, 2015].

Pickering, P.F. et al., 2001. THE PREDICTION OF FLOWS IN PRODUCTION RISERS - TRUTH & MYTH ? In *IIR Conference*. Aberdeen, pp. 1–16.

Prasser, H.-M. et al., 2003. Influence of the pipe diameter on the structure of the gas-liquid interface in a vertical two-phase pipe flow. In *10th Int Topical Meeting on Nuclear Reactor Thermal Hydraulics*. Seoul.

Sawant, P., Ishii, M. & Mori, M., 2008. Droplet entrainment correlation in vertical upward co-current annular two-phase flow. *Nuclear Engineering and Design*, 238(6), pp.1342–1352. Available at: http://linkinghub.elsevier.com/retrieve/pii/S0029549307005304 [Accessed May 20, 2013].

Sawant, P., Ishii, M. & Mori, M., 2009. Prediction of amount of entrained droplets in vertical annular two-phase flow. *International Journal of Heat and Fluid Flow*, 30(4), pp.715–728. Available at: http://linkinghub.elsevier.com/retrieve/pii/S0142727X09000587 [Accessed May 8, 2013].

Schadel, S.A. et al., 1990. Rates of atomization and deposition in vertical annular flow. , 16(3), pp.363–374.

Schlegel, J.P. et al., 2012. Experimental study of two-phase flow structure in large diameter pipes. *Experimental Thermal and Fluid Science*, 41, pp.12–22. Available at: http://linkinghub.elsevier.com/retrieve/pii/S0894177712000465.

Shearer, C.J. & Nedderman, R.M., 1965. Pressure gradient and liquid film thickness in concurrent upwards flow of gas/liquid mixtures: application to film cooler design. *Chemical Engineering Science*, 20(671).

Shoham, O., 2006. *Mechanistic Modeling of Gas-liquid Two-phase Flow in Pipes*, Society of Petroleum Engineers. Available at: https://books.google.co.uk/books?id=WfxwPgAACAAJ.

Shoukri, M., Hassan, I. & Gerges, I., 2003. Two-Phase Bubbly Flow Structure in

Large-Diameter Vertical Pipes. *The Canadian Journal of Chemical Engineering*, 81(April), pp.205–211.

Da Silva, M.J. et al., 2010. High-resolution gas–oil two-phase flow visualization with a capacitance wire-mesh sensor. *Flow Measurement and Instrumentation*, 21(3), pp.191–197.

Skopich, A. et al., 2015. Pipe-diameter effect on liquid loading in vertical gas wells. *SPE Production and Operations*, 30(2), pp.164–176. Available at: https://www.onepetro.org/download/journal-paper/SPE-164477-PA?id=journal-paper%2FSPE-164477-PA.

Smith, T.R. et al., 2012. Two-phase flow structure in large diameter pipes. *International Journal of Heat and Fluid Flow*, 33(1), pp.156–167. Available at: http://www.sciencedirect.com/science/article/pii/S0142727X11001469.

Stevanovic, V., Prica, S. & Maslovaric, B., 2007. Multi-Fluid Model Predictions of Gas- Liquid Two-Phase Flows in Vertical Tubes. *FME Transactions*, 35, pp.173–181.

Stevanovic, V. & Studovic, M., 1995. A simple model for vertical annular and horizontal stratified two-phase flows with liquid entrainment and phase transitions: one-dimensional steady state conditions. *Nuclear Engineering and Design*, 154(3), pp.357–379. Available at: http://linkinghub.elsevier.com/retrieve/pii/002954939400925O [Accessed August 20, 2015].

Sun, K.H., 1979. Flooding correlations for BWR bundle upper tieplates and bottom side-entry orifices. In *Proceedings of the multi-phase flow and heat transfer symposium-workshop*. Miami Beach, FL, USA: Hemisphere Publishing Corp. Available at: https://inis.iaea.org/search/search.aspx?orig_q=RN:12641609.

Taitel, Y., 1994. Advances in Two-Phase Flow Modeling. In *University of Tulsa Centennial Petroleum Engineering Symposium*. Tulsa, Oklahoma, USA: Society of Petroleum Engineers. Available at: http://www.onepetro.org/doi/10.2118/27959-MS [Accessed August 12, 2015].

Taitel, Y., Bornea, D. & Dukler, A.E., 1980. Modelling flow pattern transitions for steady upward gas-liquid flow in vertical tubes. *AIChE Journal*, 26(3), pp.345–354. Available at: http://dx.doi.org/10.1002/aic.690260304.

Taitel, Y. & Dukler, A.E., 1976. A model for predicting flow regime transitions in horizontal and near horizontal gas-liquid flow. *AIChE Journal*, 22(1), pp.47–55. Available at: http://dx.doi.org/10.1002/aic.690220105.

Taitel, Y. & Dukler, A.E., 1976. A theoretical approach to the Lockhart-Martinelli correlation for stratified flow. *International Journal of Multiphase Flow*, 2(5-6), pp.591–595. Available at: http://www.sciencedirect.com/science/article/pii/0301932276900197 [Accessed August 24, 2015].

Takahama, H. & Kato, S., 1980. LONGITUDINAL FLOW CHARACTERISTICS OF VERTICALLY FALLING LIQUID FILMS WITHOUT COCURRENT GAS

FLOW. *International Journal of Multiphase Flow*, 6, pp.203–215.

Tambouratzis, T. & Pázsit, I., 2009. Non-invasive on-line two-phase flow regime identification employing artificial neural networks. *Annals of Nuclear Energy*, 36(4), pp.464–469. Available at: http://www.sciencedirect.com/science/article/pii/S0306454908003204 [Accessed August 24, 2015].

Tambouratzis, T. & Pàzsit, I., 2010. A general regression artificial neural network for two-phase flow regime identification. *Annals of Nuclear Energy*, 37(5), pp.672–680. Available at: http://www.sciencedirect.com/science/article/pii/S0306454910000587 [Accessed August 24, 2015].

Ternyik, J. et al., 1995. Virtual Measurement in Pipes: Part 1-Flowing Bottom Hole Pressure Under Multi-Phase Flow and Inclined Wellbore Conditions. In *SPE Eastern Regional Meeting*. Society of Petroleum Engineers. Available at: http://www.onepetro.org/doi/10.2118/30975-MS [Accessed August 24, 2015].

Ternyik, J., Bilgesu, H.I. & Mohaghegh, S., 1995. SPE 30976 Virtual Measurement in Pipes , Part 2 : Liquid Holdup and Flow Pattern Correlations. In *SPE Eastern Regional Conference & Exhibition*. Morganstown, WV, USA.

Tishkoff, J.M., Pinchak, A.C. & Ostrach, S., 1979. Turbulent co-current gas-liquid flow in a tube with and without swirl. *J. Fliuids Eng*, 101, pp.61–68.

Tong, L.S. & Tang, Y.S., 1997. *Boiling Heat Transfer And Two-Phase Flow*, CRC Press.

Tsoukalas, L.H., Ishii, M. & Mi, Y., 1997. A neurofuzzy methodology for impedance-based multiphase flow identification. *Engineering Applications of Artificial Intelligence*, 10(6), pp.545–555. Available at: http://linkinghub.elsevier.com/retrieve/pii/S0952197697000377 [Accessed August 4, 2015].

Tutu, N.K., 1982. Pressure fluctuations and flow pattern recognition in vertical two phase gas-liquid flows. *International Journal of Multiphase Flow*, 8(4), pp.443–447. Available at: http://linkinghub.elsevier.com/retrieve/pii/030193228290012X [Accessed August 4, 2015].

Ueda, T. & Tanaka, T., 1974. Studies of Liquid Film Flow in Two-Phase Annular and Annular-Mist Flow Regions : (Part 1, Downflow in a Vertical Tube). *Bulletin of JSME*, 17(107), pp.603–613. Available at: http://joi.jlc.jst.go.jp/JST.Journalarchive/jsme1958/17.603?from=CrossRef [Accessed June 20, 2015].

USUI, K., 1989. Vertically Downward Two-Phase Flow, (II). *Journal of Nuclear Science and Technology*, 26(11), pp.1013–1022. Available at: http://www.tandfonline.com/doi/abs/10.1080/18811248.1989.9734422 [Accessed August 5, 2015].

Usui, K. & Sato, K., 1989. Vertically Downward Two-Phase Flow, (I). *Journal of*

Nuclear Science and Technology, 26(7), pp.670–680. Available at: http://www.tandfonline.com/doi/abs/10.1080/18811248.1989.9734366 [Accessed August 6, 2015].

Verbeek, P.H.J., Mielsn, R. & Schellenkens, C.J., 1993. Liquid entrainment in annular dispersed upflow. In *European Two Phase Flow Group Meeting*. Hanover.

Vieira, R.E. et al., 2015. Experimental characterization of vertical downward two-phase annular flows using Wire-Mesh Sensor. *Chemical Engineering Science*, 134, pp.324–339.

Vince, M.A. & Lahey, R.T., 1982. On the development of an objective flow regime indicator. *International Journal of Multiphase Flow*, 8(2), pp.93–124. Available at: http://linkinghub.elsevier.com/retrieve/pii/030193228290012X [Accessed August 4, 2015].

Wallis, G.B., 1969a. Annular two-phase flow - part II (additional effects). *ASME*, 69.

Wallis, G.B., 1969b. *One Dimensional Two-Phase Flow*, New York: McGraw-Hill.

Wallis, G.B., 1968. Phenomena of liquid transfer in two phase dispersed annular flow. *Int. J. Heat and Mass Transfer*, 11, pp.783–785.

Wallis, G.B., 1962a. *The onset of droplet entrainment in annular gas-liquid flow*, General Electric Co. General Engineering Lab., Schenectady, NY.

Wallis, G.B., 1962b. *The transition from flooding to upwards cocurrent annular flow in a vertical pipe*,

Webb, D.R. & Hewitt, G.F., 1975. Downwards co-current annular flow. , 2, pp.35–49.

Whalley, P.B., 1996. *Two-phase flow and heat transfer*, Oxford University Press. Available at: https://books.google.co.uk/books?id=y5xRAAAAMAAJ.

Wicks, M. & Dukler, A.E., 1960. Entrainment and pressure drop in concurrent gas-liquid flow: air-water in horizontal flow. *AIChE Journal*, 6, p.463.

Wongwises, S. & Kongkiatwanitch, W., 2001. Interfacial friction factor in vertical upward gas-liquid annular two-phase follow. *International Communications in Heat and Mass Transfer*, 28(3), pp.323–336. Available at: http://linkinghub.elsevier.com/retrieve/pii/S073519330100238X [Accessed May 30, 2015].

Wright, D. & Laufenbrenner, D., 1975. Course report. *Chem. E.*, p.379.

Xiao, J.J., Shonham, O. & Brill, J.P., 1990. A Comprehensive Mechanistic Model for Two-Phase Flow in Pipelines. In *SPE Annual Technical Conference and Exhibition*. Society of Petroleum Engineers. Available at: http://www.onepetro.org/doi/10.2118/20631-MS [Accessed August 26, 2015].

Yamazaki, Y. & Yamaguchi, K., 1979. Characteristics of Cocurrent Two-Phase Downflow in Tubes. *Journal of Nuclear Science and Technology*, 16(4), pp.245–255. Available at:

http://www.tandfonline.com/doi/abs/10.1080/18811248.1979.9730898 [Accessed August 5, 2015].

Zadrazil, I. et al., 2012. Shear layers in the turbulent pipe flow of drag reducing polymer solutions. *Chemical Engineering Science*, 72, pp.142–154. Available at: http://linkinghub.elsevier.com/retrieve/pii/S0009250912000024 [Accessed December 19, 2012].

Zangana, M.H.S., 2011. *Film behaviour of vertical gas-Liquid Flow in a large diameter pipe*. University of Nottingham. Available at: http://eprints.nottingham.ac.uk/12782/1/546275.pdf.

Zhao, X., 2005. *Mechanistic based models for slug flow in vertical pipes*. Texas Tech University.

Zuber, N., 1962. On the Atomization and Entrainment of Liquid Films in Shear Flow. *General Electric Company Report*, 62.

Appendix A : Experimental matrix

Table A-1: Flow conditions used throughout this study

U_{sl}, m/s	0.1	0.2	0.3	0.48	0.7	1.0
Qg, Sm^3/h	U_{sg}, m/s	U_{sg}, m/s	U_{sg}, m/s	U_{sg}, m/s	U_{sg}, m/s	U_{sg}, m/s
6	0.16	0.15	0.14	0.14	0.14	0.15
10	0.25	0.25	0.25	0.25	0.25	0.25
20	0.54	0.54	0.52	0.51	0.51	0.52
30	0.83	0.82	0.80	0.78	0.77	0.77
40	1.12	1.12	1.09	1.06	1.03	1.02
50	1.43	1.42	1.39	1.36	1.33	1.32
80	2.38	2.34	2.30	2.25	2.19	2.13
100	3.01	2.96	2.91	2.86	2.76	2.70
150	4.59	4.51	4.43	4.36	4.18	3.99
200	6.23	6.12	5.96	5.81	5.57	5.27
300	9.35	9.10	8.87	8.50	8.10	7.62
400	12.47	12.03	11.62	11.15	10.47	9.80
600	18.36	17.43	16.72	15.58	14.38	13.44
800	23.64	22.30	21.26	19.59	17.80	16.04
1000	28.81	26.57	25.02	22.55	20.78	18.53

Where Q_g, u_{sg} and u_{sl} are respectively the gas (air) flow rate, velocity and superficial liquid (water) velocities

Appendix B : Downwards film thickness correlation attempt

This section provides the details of an initial attempt to correlate the downwards film thickness using multiple nonlinear regression of several dimensionless numbers whose rational for inclusion follows.

Along with the liquid film Reynolds number, in a proposed correlation, the inclusion of the gas Reynolds and the Ohnesorge numbers based on the liquid properties are therefore introduced. While the former accounts for the effect of the flowing gas on the liquid film thickness the latter captures the effect of entrained droplets. Also, the inclusion of the gas Froude number attempts to account for the pipe diameter scale effects owing to the different pipe sizes of the aforementioned literature experimental data which the present correlation will be obtained. The Ohnesorge number is defined as the ratio of viscous forces to inertial and surface tension forces given as:

$$Oh_l = \frac{\mu_l}{\sqrt{\rho_l \sigma D}} \quad \textbf{(B-1)}$$

Smaller Ohnesorge numbers signify decreasing significance of viscosity and a greater proclivity to form droplets. The current experiments have $Oh_l = 0.00033$ which match the large entrainments observed. Additionally, the gas Froude number ($\mathrm{Fr}_g = U_g/\sqrt{gD}$) is the ratio of a characteristic velocity to a gravitational wave velocity and is useful in characterising flow involving different length scales which in this study are the different pipe diameters utilised by Webb & Hewitt and Chien & Ibele (see Table 2) whose data is used to produce the new empirical correlation.

Assuming the dimensionless film thickness is a power law function of the gas and liquid Reynolds numbers, the Froude number and the Ohnesorge number,

$$\frac{t}{D} = A\ \mathrm{Re}_l^a \mathrm{Re}_g^b \mathrm{Fr}_g^c\ \mathrm{Oh}_l^d \qquad \textbf{(B-2)}$$

Multiple Linear Regression was used to obtain the best values of the coefficient *A* and the indices *a*, *b*, *c*, and *d* that minimises the error with experimental data. Application of the regression procedure resulted in the following correlation:

$$\frac{t}{D} = 2315\ \mathrm{Re}_l^{0.37} \mathrm{Re}_g^{-0.6} \mathrm{Fr}_g^{0.5}\ \mathrm{Oh}_l^{1.32} \qquad \textbf{(B-3)}$$

Figure 18 shows that the new correlation well collapses the dimensionless film thicknesses from the current studies covering 4 pipe diameters namely: 31.8, 38.2, 50.8 and 101.6 mm spanning the range of both small and large diameter pipes.

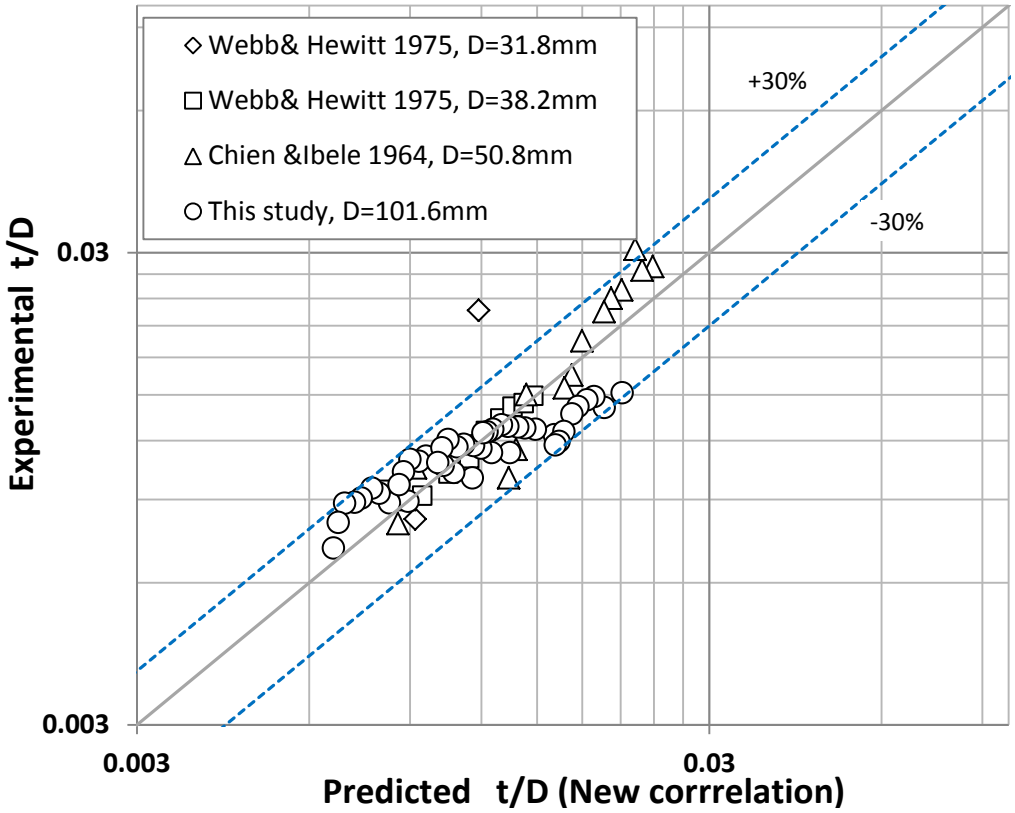

Figure B-1: Comparison between film thickness datasets in downward annular flows in different pipe sizes with prediction using the new proposed correlation

Only two out of 72 data points were out of the 30% error band between the predictions and experimental data. The index of 0.37 for Re_l is close to the 1/3 in Nusselt's theory. In summary, the new model is at a reasonable consistence with previously propounded theories such as the celebrated Nusselt theory and with the current experimental observations.

Appendix C : Serpent Rig modification

In order to quantitatively study the effect of the U-bend on the structure of two phase flow in upwards and downwards annular flow, a modification has been proposed. The modification involves modifying the experimental rig as shown in Figure C-1 so that water is injected, through a porous wall feature, into the upward flow pipe section. Due to practical considerations of space and being able to revert the rig to its original configuration, this has been updated so that the U-bend is completely removed and the air connection is made using the existing flange as shown in the figure.

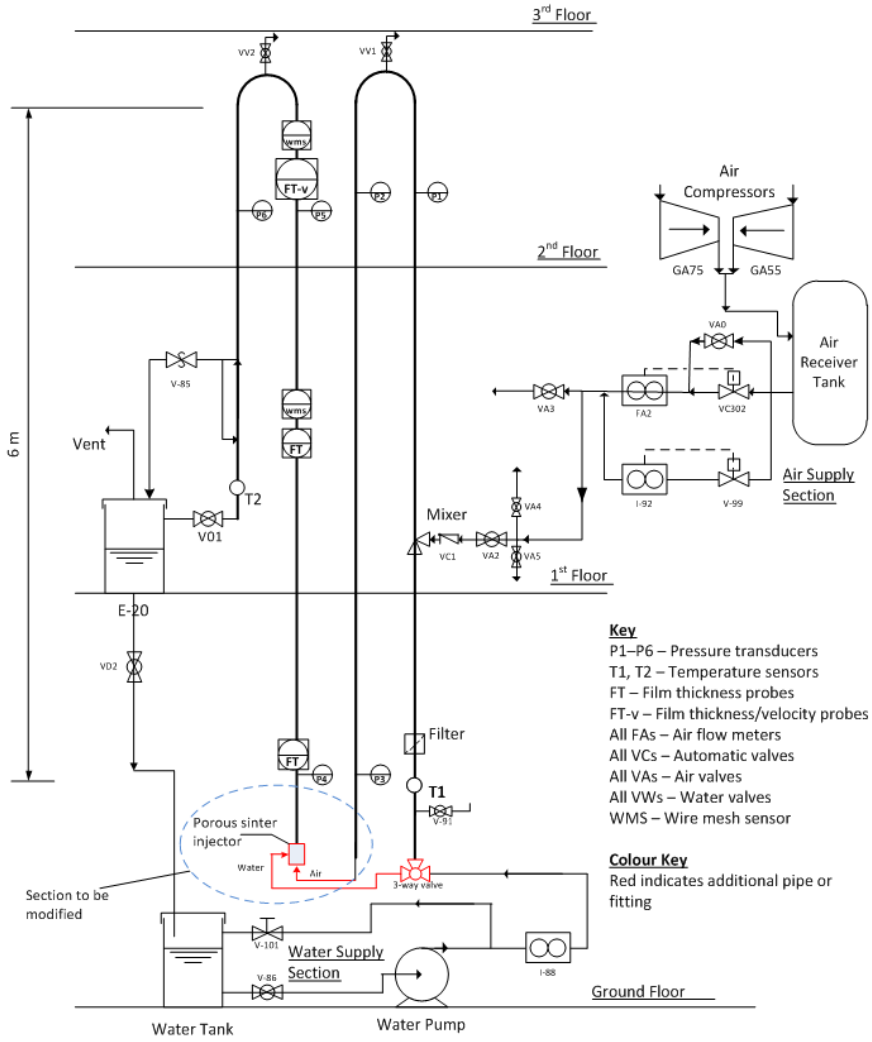

Figure C-1: Proposed rig modification to study bend effect on upwards two-phase flow

C.1 Porous sinter injector design, fabrication and installation

In designing the porous sinter injector to be fitted on the upwards section of the modified rig, various engineering drawings were produced, a sample of which is presented in Figure C-2. The porous sinter injector consists of a 350 mm-long outer T-section casing with an internal diameter of 165.1 mm machined to 171.5 mm for 50.9 mm from the edge to hold the clamping ring shown in Appendix A. The clamping ring serves both as a smooth transition from the 165.1 mm ID to

the 128 mm ID of the porous stainless steel cylinder and a stopper to prevent the porous cylinder buckling under the weight of downstream pipework.

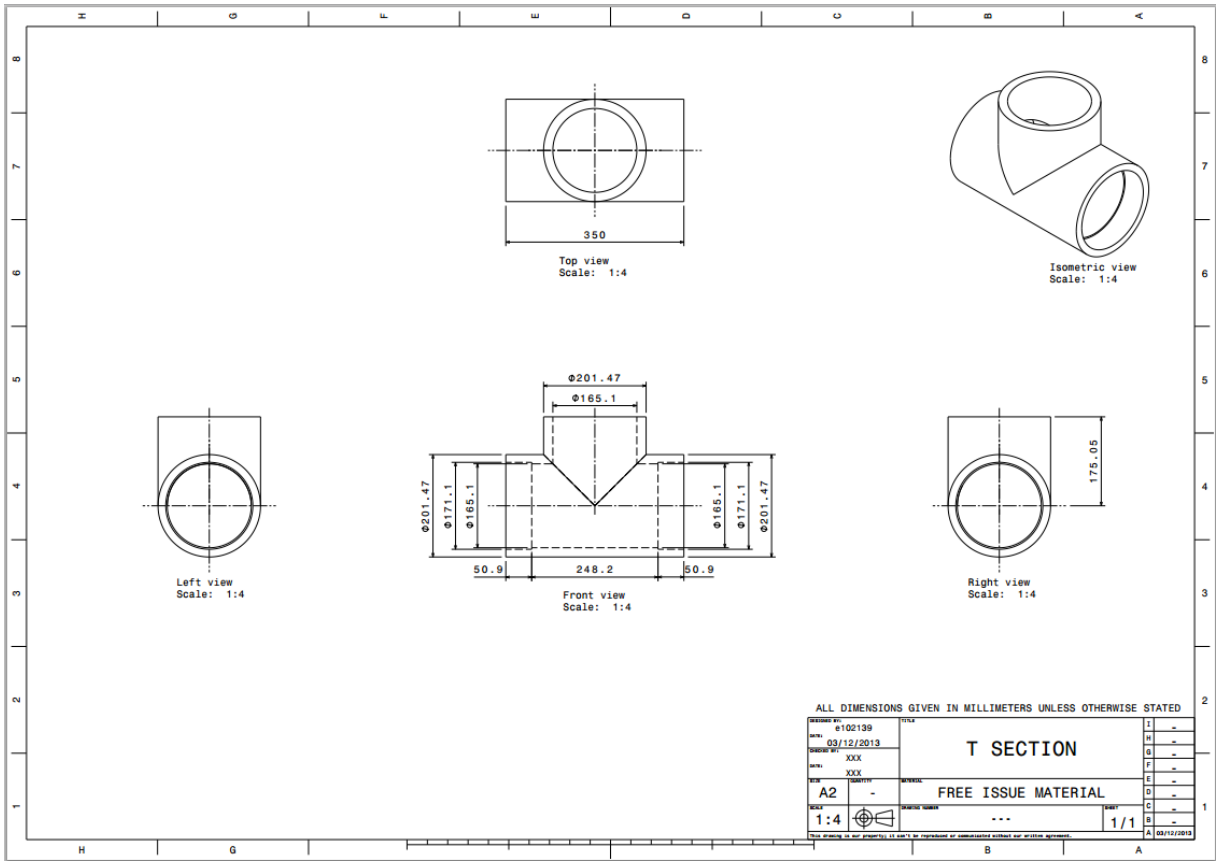

Figure C-2: Sample engineering drawing of the porous sinter injector PVC casing with all dimensions given in mm.

PVC was chosen as the material for the external casing as against stainless steel or other steels due to cost, ease of machining, corrosion damage and weight. Figure C-3 shows the side and top views of the fabricated porous sinter injector. Installation of the injector on the modified rig together with the associated pipework will provide useful data on fully developed annular flow.

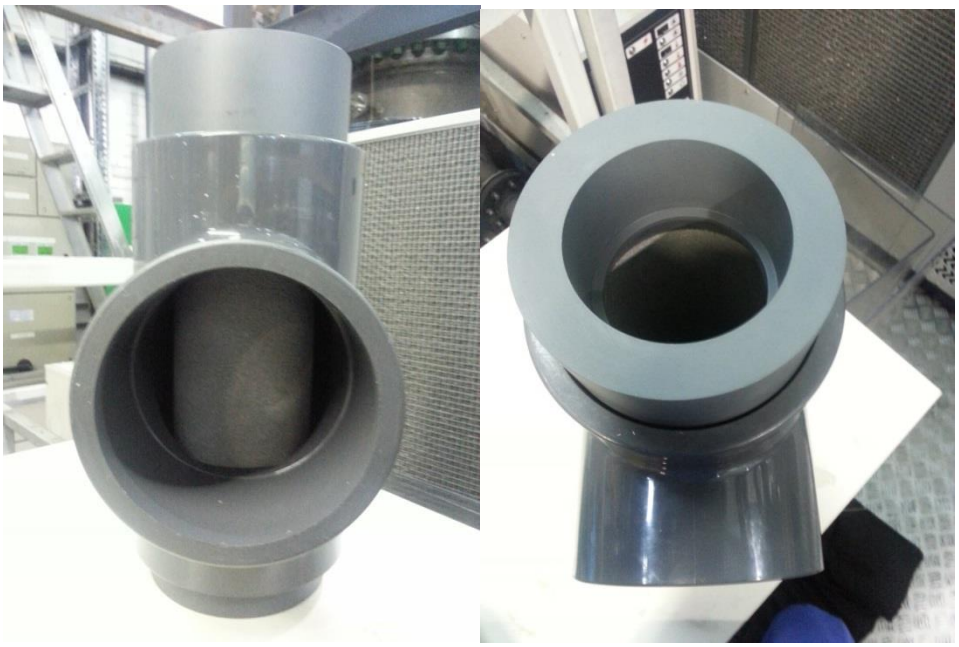

Figure C-3: Fabricated porous sinter injector (a) side view with the porous stainless steel cylinder fitted which can be clearly seen (b) top view.

C.2 Effect of the U-bend

Data was collected in the first two years of the PhD study on upward and downward two-phase flow in the Serpent Rig facility. The theory is that data on film thickness/velocity, instantaneous/differential pressure, and void fraction are one way or the other affected by the bend but by how much is not yet known. It is especially so for upwards flow which unlike downflow does not develop as quickly due to being against gravitational forces. Therefore, it is envisaged that the rig modification proposed which discards the U-bend upstream of the upward section will provide valuable data for large diameter two-phase annular flow from which the effect of the U-bend can be quantitatively studied.